BIO ELECTRO MAGNETICS

Journal of the Bioelectromagnetics Society

Volume 8, Number 1, 1987

Alan R. Liss, Inc., New York

BIO ELECTRO MAGNETICS

Journal of the Bioelectromagnetics Society

Bioelectromagnetics (ISSN 0197-8462) is published quarterly by Alan R. Liss, Inc., 41 East 11th Street, New York, NY 10003. **Subscription Price:** Volume 8, 1987, four issues: $130 in the US; $143 outside the US. All subscriptions outside North America will be sent by air. Payment must be made in US dollars. Payments not drawn on a US bank will be subject to bank collection charges. Exclusive agent in Japan: Igaku Shoin Limited, Foreign Department, 1-28-36 Hongo, Bunkyo-ku, Tokyo 113, Japan. 1987, ¥ 38,300 in Japan (Air Cargo Service only).
Changes of Address: Bioelectromagnetic Society members only: Send changes of address to the Bioelectromagnetics Society, P.O. Box 3729, Gaithersburg, MD 20878. **Non-member Subscribers:** Send changes of address to the publisher. Enclose present mailing label with change of address. **Claims:** All subscribers should send claims directly to the publisher. Claims cannot be honored beyond four months after mailing date. Duplicate copies cannot be sent to replace issues not delivered because of failure to notify publisher or Society of change of address.
Indexed by: BIOSIS Data Base • Chemical Abstracts • Excerpta Medica • Index Medicus • Current Contents/Life Sciences-Science Citation Index • ISI-Soviet Union.
Printed in the United States of America.

Bioelectromagnetics 8:1–7 (1987)

Transcriptional Patterns in the X Chromosome of *Sciara coprophila* Following Exposure to Magnetic Fields

Reba Goodman, Joan Abbott, and Ann S. Henderson

Department of Pathology, Columbia University Health Sciences, New York (R.G.); Electro-Biology, Inc., Fairfield, New Jersey (J.A.); and Biological Sciences, Hunter College, The Graduate Division of the City University of New York, New York (A.S.H.)

We previously demonstrated that exposure of salivary gland cells of the dipteran, *Sciara coprophila*, to either asymmetrical or symmetrical changing magnetic fields results in an increase in the incorporation of radioactive uridine into RNA. The present report is an analysis of the grain count distribution over the X chromosome of Sciara in transcription autoradiograms following exposure of the salivary gland cells to two pulsed magnetic signals and a 72-Hz sine wave signal. The results show augmented uptake of ^{3}H-uridine into nascent RNA chains following short exposures of the cells to magnetic fields. Transcription is augmented in previously active loci, as well as at chromosome regions that are not detectable as active in control cells. The quantitative pattern of RNA synthesis in transcription autoradiograms is hypothesized to be signal specific on the basis of differences in grain counts over significantly labelled chromosome sites.

Key words: magnetic fields, transcriptional increases, polytene chromosomes

INTRODUCTION

Theoretically, the response of cells to magnetic (B) fields could produce a diversity of effects. Exposure of cells to weak magnetic fields has been previously shown to result in changes in many measurable forms of cellular function [Pilla et al, 1983]. On a practical level, little is known of the basis for a given biological response to magnetic fields. The present study has monitored transcriptional changes by transcription autoradiography in the salivary gland cells of the dipteran, Sciara. The critical questions addressed here are whether transcription is augmented, and whether new transcripts are induced when cells are exposed to magnetic fields?

We previously demonstrated that exposure of salivary gland cells to quasi-rectangular asymmetrical pulsed magnetic fields at low frequencies (15–72 Hz) can result in increased incorporation of radioactive uridine into RNA [Goodman et al, 1983; Goodman and Henderson, 1986]. Transcriptional augmentation is also observed in salivary gland cells following exposures to symmetrical sine waves [Goodman and Henderson, 1986]. The position of newly formed RNA in sucrose gradients analyzed

Received for review February 25, 1986; revision received May 23, 1986.

Address reprint requests to Reba Goodman, Department of Pathology, Columbia University Health Sciences, 630 West 168 Street, New York, NY 10032.

following short exposures (15–45 min) of cells to magnetic fields is consistent with that expected for mRNA, irrespective of the signal type employed.

In a previous report, we compared the results of transcription autoradiography on the X chromosome of Sciara following exposure of cells to 72-Hz sine waves (CW) and a 72-Hz repetitive single pulse (SP) signal. A distinct increase in the uptake of ^{3}H-uridine into nascent RNA was observed, but a detailed analysis of the grain distribution was not done [Goodman and Henderson, 1986]. In the present study, an analysis of grain distribution in transcription autoradiographs was done following exposure of the cells to three signals: (a) single repetitive pulse (SP) at 72 Hz; (b) repetitive pulse bursts (PT or pulse train) at 15 Hz, and (c) sine waves at a frequency of 72 Hz. Evidence is presented that supports the hypothesis that different magnetic fields stimulate transcription at specific chromosomal regions.

MATERIALS AND METHODS

Salivary gland cells of fourth instar female larvae (approximately 20 days from hatching) were used in these studies [Gabrusewycz-Garcia, 1964]. The procedures for exposing the cells to the magnetic fields have been described [Goodman et al, 1983; Goodman and Henderson, 1986]. All experiments were repeated in triplicate. Briefly, salivary glands were exposed to magnetic fields immediately after decapitation of the larvae [Zegarelli-Schmidt and Goodman, 1981]; the salivary glands floated outside the larval body while maintaining attachment. We placed 30 decapitated larvae in a 60-mm circular Petri dish containing 0.5 ml Schneider's Drosophila medium (SDM) (Gibco) with 100 μCi/ml ^{3}H-uridine (specific activity, 40.8 Ci/mM; New England Nuclear) for 15, 30, and 45 min incubations. The gland cells were exposed to either the SP, PT, or sinusoidal fields by placing the Petri dish on a plastic form in the center of the coils (see below). The region containing the dish had been previously monitored to have no detectable extraneous magnetic signals or electrical noise above the normal 60-Hz background.

The coils were placed in a 20 °C incubator (the normal growth temperature for Sciara) with the current generator outside the incubator. Control cells were treated in the same manner, but placed in an identical incubator in sham coils. There were no measurable thermal changes (detection sensitivity of 0.1 °C) during the exposure periods. After exposure, the glands were removed from the incubators, flooded with several changes of ice-cold 0.05 M Tris (pH = 7.4), and dissected on ice. The isolated glands were fixed in 45% acetic acid:1% lactic acid for chromosome squashes. Preparation of the squashes and autoradiographic methods have been described [Zegarelli-Schmidt and Goodman, 1981; Goodman et al, 1983].

The signal device and generator for producing asymmetric signals were designed by Electro-Biology, Inc (EBI). Sine waves were produced by a RadioShack amplifier and generator. Helmholtz-aiding coils constructed at EBI were used to deliver the signals. The cells were exposed to each of the fields by placing a petri dish on a plastic form in the center of Helmholtz-aiding coils positioned in a vertical orientation [McLeod et al, 1983], i.e., the magnetic field was generated in a horizontal plane. The coils were constructed of wire bundles approximately 1 cm in diameter wound around a square form with a 10 cm distance between the sides. There was a 7.5 cm radius from the center of the form. The local geomagnetic field at the sample location was 46 μT, at an inclination of 76 °N.

The signals were monitored before and after the incubation of the cells with a Tektronix 2465 (300 MHz) oscilloscope using a calibrated search coil. The characteristics of each signal is as follows: (a) SP (Biosteogen system 204; Electro-Biology, Inc.); the width of the positive portion of the signal was 380 μsec; the negative portion was 4.5 msec, with a pulse rate of 72 Hz; the peak magnetic field was 3.5 mT; the approximate induced electric field was measured at 9.0×10^{-3} V/m; (b) PT (Biosteogen system 204; Electro-Biology, Inc.); the width of the positive portion of the signal was 200 μsec and the negative portion was 28 μsec with a repetition rate within the burst of 4 kHz, and a burst repetition rate of 15 Hz; the peak magnetic field was 1.9 mT; the approximate induced electric field was measured at 9.0×10^{-3} V/m, and (c) sine wave at 72 Hz; the peak magnetic field was measured at 1.1 mT; the approximate induced electric field was measured at 5×10^{-4} V/m. Table 1 describes the waveform characteristics for each of the signals used in this study.

Analysis of transcription autoradiograms of the X-chromosome was made by grain counts over morphologically defined regions as delineated on the basis of the chromosome banding pattern [Gabrusewycz-Garcia, 1964]. Grain counts were made in enlarged photographs (8 × 10 inches). The original designation of regions was based on the pattern observed in transcription autoradiographs of the control preparations. Measurements of the regions were made with a millimeter ruler. The values given here are means of measurements for 11 photographs in the control, 14 photographs for cells exposed to the sine and PT signals, and 15 photographs for the SP signal.

RESULTS

The present study focused on the X chromosome as a well characterized chromosome in the Sciara chromosome complement [Crouse, 1977; Crouse et al, 1977], although all four polytene chromosomes of Sciara salivary gland cells had a higher grain density in preparations from exposed cells. This was true of all exposure periods of 15, 30, and 45 min. At the level of detection in transcription autoradiography, there were quantitative, and possible qualitative differences, between patterns seen in cells exposed to different fields. The majority of the label was in interband regions, as would be expected for transcripts that will contribute to the mRNA population. A heavy grain density was observed following exposure to each of the magnetic fields (Fig. 1). Chromosomes of control cells were lightly labelled in the same regions. Thus, augmented transcription occurred at chromosomal loci that were normally active at this developmental stage in Sciara.

An analysis of grain counts over the X-chromosome is given in Fig. 2. Normally active chromosome regions were defined on the basis of banding morphology associated with the grain distribution present in transcriptional autoradiograms of unexposed cells. Eight major chromosome regions showed augmented transcription. Three additional regions (Xc, B″, and Xf) were labeled in cells exposed to each of the magnetic signals. These represent transcriptively active regions that were below detection in control autoradiograms.

The chromosome regions analyzed did not respond quantitatively in the same manner to each of the signals (Fig. 2). The sine signal at 72 Hz and the SP signal were the most effective in transcriptional augmentation. Exposure of cells to the PT signal resulted in a less intense transcriptional response.

TABLE 1. Characteristics of EM Signals

Signal	Rate (Hz)	Positive induced amplitude[a] (mV)	Positive duration (μsec)	Burst width (msec)	Negative space (μsec)	Negative spike (μsec)	Peak (B) magnetic field (mT)	Positive dB/dT (T/sec)	Negative dB/dT (T/sec)	Negative induced amplitude (mV)	Electric (E) field (typical in liquid layer) (V/m)
SP	72	15	380			45,00	3.5	9	0.8	1.33	9.0×10^{-3}
PT	15	14.5	200	5	28	24	1.9	9	75	125	9.0×10^{-3}
Sine	72	0.8					1.1	0.5			5.0×10^{-4}

[a]Electro-Biology Inc., standard probe.

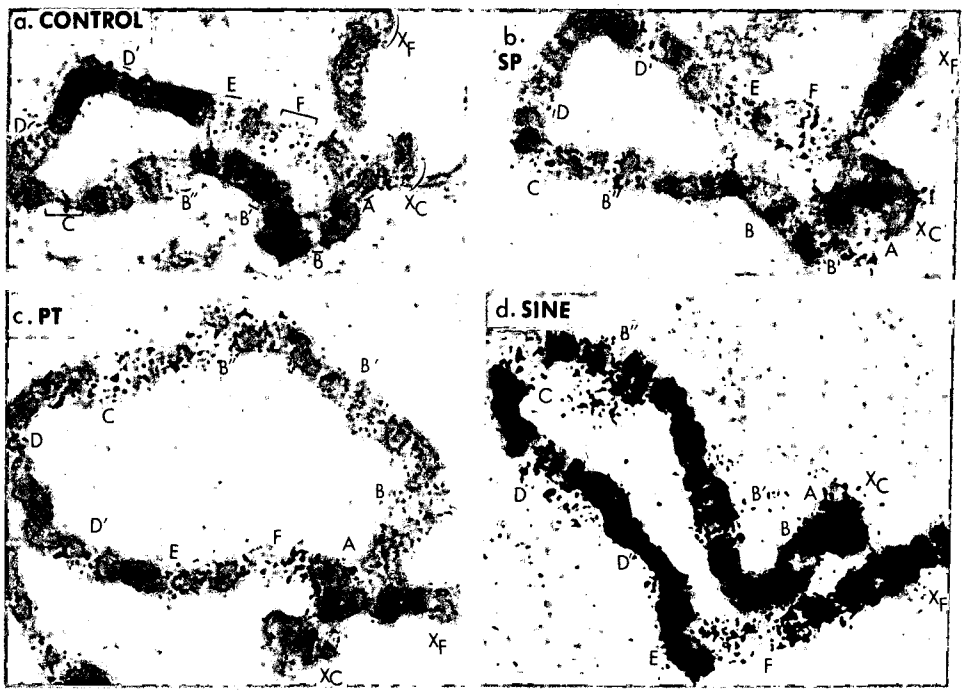

Fig. 1. Transcription autoradiograms of the X chromosome from salivary gland cells following 45-min incubations in the presence of ^{3}H-uridine (see Methods). These are representative of patterns seen at incubations of 15, 30, or 45 min. The regions A–F are compared with respect to grain density in chromosomes exposed to magnetic fields (**b–d**), or isolated from magnetic fields (**a**). The letters represent approximate map regions as follows (according to Gabrusewycz-Garcia [1964], and Crouse et al, [1977]): A, 2B–2C; B, 3C–4B; B′, 4C; B″, 6A; C, 6C–7A; D, 8A–8B; D′, 9C; E, 12A–12B, and F, 13B–14A. Xc designates the centromeric end of the chromosome and Xf the free end. Note the increase in label over regions B″ and Xc in chromosomes from cells exposed to magnetic fields. All incubations and signal exposures were at 20 °C. Autoradiographic exposure times were identical at 24 h. (a) Chromosome X from control cells. (b) X chromosome from cells exposed to the SP signal at 72 Hz for 45 min. (c) X chromosome from cells exposed to the PT signal for 45 min. (d) X chromosome from cells exposed to the 72-Hz sine signal for 45 min. Magnification, ×500.

DISCUSSION

This study has investigated the question of whether exposure to magnetic fields can alter transcriptional patterns in cells. Increased uptake of ^{3}H-uridine occurred in salivary gland cells exposed to magnetic fields that could be seen as augmentation of pre-existing transcripts and activation of new transcripts, or transcripts that were not detectable in unexposed cells. The general pattern of transcription, however, is similar in chromosomes of cells exposed to magnetic fields and those of control cells. The major difference lies in the degree of transcriptive activity. The most obvious interpretation of our data is that transcription, albeit augmented in cells exposed to the signals, is primarily taking place at chromosomal loci that are normally active at this developmental period. The activation of previously inactive genes or gene sets is also strongly suggested by the data. At least three X-chromosome regions are labeled in transcription autoradiograms of exposed cells that are not detectable in chromosomes of control preparations.

X Chromosome: Analysis of Transcription Autoradiograms

Chromosome regions	X_C	A	B	B′	B″	C	D	D′	E	F	X_F	number of plates	mean grs/ plate
% Length	4	2.6	2	1.2	1.7	3.2	1.1	1	4.1	13	10		
Control: $\bar{x}$ grains/plate	NS	3	3	3	NS	6	3	1	7	18	NS	11	65
Exposed cells: $\bar{x}$ grains/plate													
SP	92	27	33	37	28	*61	46	22	48	100	56	15	721
Sine	92	24	20	*53	*47	31	54	14	*85	*177	39	14	763
PT	30	12	23	23	28	34	20	23	33	62	34	14	540

Fig. 2. Analysis of the relative grain distribution by grain counts. Specified autoradiographically labelled regions of the X chromosome of Sciara were counted to determine grain distribution following incubation for 45 min in the presence of the three magnetic fields used in this study (see Fig. 1). In control data, the grain distribution over the regions Xc, Xf, and B″ was not significantly different from a random distribution of grains (abbreviated NS). The asterisk indicates values that deviated strongly from the other signals.

This data supports our previous studies in which RNA synthesis was significantly increased by exposure of cells to magnetic fields [Goodman et al, 1983; Goodman and Henderson, 1986]. Increased transcription was most notable in exposed cells in transcripts that will contribute to the mRNA population as judged on the basis of oligo (dT) column chromatography, and on the basis of sedimentation coefficients in analyses of sucrose gradients. In the present study, transcription was most pronounced in the interband regions of the X chromosome, as would be expected for transcripts contributing to mRNA classes. Related data from our laboratory has shown the presence of both new and augmented polypeptide groups in autoradiograms from one and two dimensional gel electrophoresis of protein preparations from cells exposed to magnetic fields, including the fields used in the present study [manuscript in preparation]. The presence of new polypeptide synthesis supports the present data.

In other studies, magnetic fields have been shown to cause changes in cell surface membrane adhesion [Rein and Pilla, 1985], collagen and glycosamino glycans synthesis [Fitton-Jackson and Bassett, 1980; Farndale and Murray, 1985] and the differentiative state of cells [Chiabrera et al, 1979]. Inhibition of lysosomal release has also been demonstrated [Murray et al, 1985]. Sinusoidal waves have been studied primarily in terms of environmental safety, but signals with frequencies between 15 and 4000 Hz have been experimentally associated with induction of DNA synthesis in human fibroblasts [Liboff et al, 1984]. Sensitivity to induced voltage has also been implicated in affecting DNA synthetic activity [Cadossi et al, 1985].

The mechanism of response of cells to magnetic fields with respect to transcriptional changes remains to be determined. There are potentially many means by which this could occur. Some of these would include direct influence at the DNA level, modulation of uptake of radioactive label into the cells, and changes in the levels of "second messengers," such as cyclic adenosine monophosphate (cAMP), within the cell. We are also unable to explain at the present time the apparent differential response of the regions measured for transcriptional activity to different magnetic signals. Further study is obviously necessary to understand this phenomenon.

ACKNOWLEDGMENTS

Allan Krim, Marisa Figueiredo, and Alun Uluc provided excellent technical assistance for these experiments. We thank Dr. Carl Blackman for making the geomagnetic field measurements and for excellent editorial assistance. This research was supported by Electro-Biology, Inc., Fairfield, NJ, grants from the ONR (NR 665-047), NSF (PCM-83-40513), and PSC-CUNY award 665113 from the City University of New York. A.S.H. is a Leukemia Society of America Scholar.

REFERENCES

Cadossi R, Ceccherelli G, Ruggeri MP, Emilia G, Torelli GM (1985): Effect of low frequency pulsing electromagnetic fields (PEMFS) on the response of human lymphocytes to phytohaemagglutinen (PHA) stimulation and on the release of B-cell growth factors. Trans 5th Ann Bioelectric Repair and Growth Society 5:43.

Chiabrera A, Hinsenkamp M, Pilla A, Ryaby J, Ponta D, Belmont F, Beltrame M, Grattarola M, Nicolini C (1979): Cytofluorometry of electromagnetically controlled cell dedifferentiation. J Histochem Cytochem 27:375–381.

Crouse HV (1977): X heterochromatin subdivision and cytogenetic analysis in *Sciara coprophila* (Diptera, Sciaridae). I. Centromere localization. Chromosoma 63:39–55.

Crouse HV, Gerbi SA, Liang CM, Magnus L (1977): Localization of ribosomal DNA within the proximal X heterochromatin of *Sciara coprophila* (Diptera, Sciaridae). Chromosoma 64:305–318.

Farndale RW, Murray JC (1985): Pulsed electromagnetic fields promote collagen production in bone marrow fibroblasts via athermal mechanisms. Calcif Tissue Int 37:178–182.

Fitton-Jackson S, Basset CAL (1980): The response of skeletal tissues to pulsed electromagnetic fields. In Richards RJ, Rajan KT (eds): "Tissue Culture in Medical Research." New York: Pergamon Press, pp 21–28.

Gabrusewycz-Garcia N (1964): Cytological and autoradiographic studies in *Sciara coprophila* salivary gland chromosomes. Chromosoma 15:312–344.

Goodman R, Bassett CAL, Henderson A (1983): Pulsing electromagnetic fields induce cellular transcription. Science 220:1283–1285.

Goodman R, Henderson A (1986): Sine waves induce cellular transcription. Bioelectromagnetics 7:23–30.

Liboff A, Williams T, Strong D, Wister R (1984): Time-varying magnetic fields: Effect on DNA synthesis. Science 223:818–820.

McLeod B, Pilla AA, Sampsel MW (1983): Electromagnetic fields induced by Helmholtz-aiding coils inside saline filled boundaries. Bioelectromagnetics 4:357–370.

Murray JC, Lacy M, Fitton-Jackson S (1985): The effect of pulsed electromagnetic fields on degradative pathways in cultures of synovial fibroblasts. Trans 5th Ann Bioelectric Repair and Growth Society 5:36.

Pilla AA, Sechaud P, McLeod B (1983): Electrochemical and electrical aspect of low frequency electromagnetic current induction in biological systems. J Biol Physics 11:51–58.

Rein G, Pilla AA (1985): Biological and physical mechanisms of electromagnetic modulation of cell surface membrane adhesion. Trans 5th Bioelectric Repair and Growth Society 5:15.

Zegarelli-Schmidt EC, Goodman R (1981): The Diptera as a model system in cell and molecular biology. In Bourne J, Danielli J (eds): "International Review of Cytology." Vol. 71. New York: Academic Press, pp 245–363.

Bioelectromagnetics 8:9–21 (1987)

Reproduction of Japanese Quail After Microwave Irradiation (2.45 GHz CW) During Embryogeny

R.P. Gildersleeve, M.J. Galvin, D.I. McRee, J.P. Thaxton, and C.R. Parkhurst

Department of Poultry Science, North Carolina State University, Raleigh (R.P.G., J.P.T., C.R.P.); Laboratory of Behavioral and Neurological Toxicology, National Institute of Environmental Health Sciences, Research Triangle Park, North Carolina (M.J.G., D.I.M.)

Japanese quail (*Coturnix coturnix japonica*) embryos were irradiated continuously in ovo with 2.45-GHz continuous wave radiation during the first 12 days of embryogenesis at an incident power of 5 mW/cm^2 and a specific absorption rate of 4.03 mW/g. The internal temperature of irradiated and nonirradiated (sham) eggs was 37.5 ± 0.3 °C, which is the optimum temperature for incubating quail eggs. At 35 days after hatching irradiated and sham-irradiated males were paired with irradiated or sham-irradiated females and daily records of reproductive performance were collected through 224 days of age. Progeny were hatched from each of the male-female pairs, and progeny reproductive performance was measured from 35 through 168 days of age. Hatchability was not affected by irradiation during embryogeny. Mortality after hatching, egg production, egg weight, fertility, hatchability of eggs produced, and reproductive performance of the progeny were not affected by irradiation during embryogeny. These observations indicate that irradiation of quail embryos with low-level microwave radiation does not affect the reproductive capacity of the hatchlings or of progeny produced from quail irradiated during incubation.

Key words: avian embryogeny, quail eggs, radiation, progeny reproductive performance, birds

INTRODUCTION

Birds are nearly ubiquitous in the biosphere. Many avian species are highly mobile and capable of traveling great distances to remote geographical areas. Because of these behaviors, birds have received attention in published reports on the biological effects of environmental contaminants. Avian reproduction has been studied extensively and particular emphasis has been given to avian reproductive capacity after exposure to pesticides. However, the reproductive capacity of birds exposed to microwave radiation has not been studied extensively. Microwave radiation is found throughout the environment. This results in a high probability of birds being exposed

Received for review May 1, 1986; revision received June 30, 1986.

This is paper No. 10480 of the Journal Series of the North Carolina Agricultural Research Service, North Carolina State University, Raleigh.

The use of trade names in this publication does not constitute endorsement by the North Carolina Agricultural Research Service of the products mentioned or criticism of similar ones not mentioned.

Address reprint requests to Dr. R.P. Gildersleeve, Poultry Science Department, Box 7608, North Carolina State University, Raleigh, NC 27695-7608.

to microwaves. Because birds may nest on or near microwave antennas, incubating eggs may be exposed to microwaves and avian reproduction may be affected by microwave irradiation. The rationale for the present study was to evaluate the potential effects of microwave radiation on the reproductive system of Japanese quail when exposure occurs during embryonic development.

The avian embryo has been used to evaluate the biological consequences of microwave irradiaton in ovo. Avian embryos serve as a unique model to measure the bioeffects of microwave exposure on embryos because maternal influences on development are essentially eliminated. Carpenter et al [1960] reported teratogenic effects of 2.45 GHz continuous wave (CW) microwave exposure at estimated specific absorption rates (SAR) of 70, 98, and 140 W/kg [Durney et al, 1978] in chicken (*Gallus domesticus*) embryos. Hills et al [1974] exposed chicken and turkey (*Meleagris gallopavo*) embryos in ovo to either 6-GHz microwaves at 0.05 and 0.2 mW/cm^2 or 2.45-GHz CW microwaves at an incident power density of 0.246–1.02 W/cm^2 with an estimated SAR of 86–357 W/kg and reported that exposure to high densities resulted in embryo mortality. The effects of microwave exposure in these reports and others [Van Ummersen, 1963] can be tentatively attributed to marked increases in egg temperature and thermal gradients and subsequent hyperthermia of exposed embryos [Baranski and Czerski, 1976; Clarke and Justesen, 1983]. Recent reports on avian [McRee and Hamrick, 1977; Byman et al, 1985] and mammalian [Berman et al, 1981; Jensh et al, 1982; Schmidt et al, 1984] embryos have shown no morphologically teratogenic effects of exposure to microwave radiation at intensities that do not induce hyperthermia. However, other authors have indicated that nonthermal effects of microwave exposure in ovo may be important during embryonic development [Fisher et al, 1979] and posthatch [McRee and Hamrick, 1977; Galvin et al, 1981].

In a series of experiments designed to evaluate the potential effects of microwave irradiation in vivo on the growth and reproduction of female chickens, Kondra et al [1970, 1972] reported no adverse effects of 6-GHz CW exposure at incident power densities of 0.02–400 pW/cm^2 [see also Krueger et al, 1975]. A pulsed wave density of 360 mW/cm^2 also produced no detrimental effects on the egg production of chickens [Romero-Sierra and Tanner, 1970]. Brief but intense exposure of neonatal female chickens to 2.45-GHz CW radiation (estimated SAR of 2,770 W/kg) resulted in no latent effects on reproduction [Davidson et al, 1976]. Rugh and McManaway [1978] exposed mice to 2.45-GHz microwave radiation in utero or postnatally and observed no effect of exposure on reproductive capacity. With rats, Jensh et al [1982] also observed no effect of prenatal exposure to 915-MHz microwave radiation at a density of 10 mW/cm^2 on reproductive capacity. In summary, the efficiency of female reproduction in the studies described above was not affected by exposure.

Mammalian reproduction may be affected by microwave exposure of the testes [Imig et al, 1948; Gunn et al, 1961; Varma and Traboulay, 1975; Saunders and Kowalczuk, 1981]. This effect may be associated with microwave-radiation-induced temperature changes in the testes that might have adversely altered spermatogenesis. In studies in which testicular temperature was not significantly affected by irradiation, the results have been inconclusive [Varma and Traboulay, 1975; Rugh and McManaway, 1978; Mainkowska et al, 1979; Cairnie and Harding, 1981]. In avian male studies, exposure of Japanese quail in ovo at an SAR of 4 mW/g resulted in a reduced reproductive capacity [McRee et al, 1983]. In a similar preliminary investigation

in the same laboratory, males were also affected by in ovo exposure, but females were not.

The present study was designed to evaluate reproductive parameters in Japanese quail after exposure to microwave radiation during embryogeny. The study extended the work of McRee et al [1983] into an experiment in which a large number of birds could be evaluated over a long duration of their reproductively active lives. To evaluate further the long-term effects of exposure, the progeny of quail that had been irradiated as embryos were also evaluated over a significant interval of their lives.

MATERIALS AND METHODS

In each of six trials, fertile Japanese quail eggs were obtained from a flock of Athens Randombred breeders that is maintained by the Department of Poultry Science at North Carolina State University. The normal incubation time is 17 days, and the optimum incubation temperature and relative humidity are 37.5 ± 0.3 °C and 60 ± 5%, respectively. The proper incubating conditions were maintained during the irradiation period. The irradiation area was located inside an environmental chamber lined with microwave absorber. This material provided a reflectivity of −45 dB at 2.45 GHz. The eggs were rotated every 2 hr to prevent adherence of embryos to the shells through an angle of approximately 90° from 45° to 135° with the long axis of the egg perpendicular to the floor at 90°. The equiment that was constructed to ensure rotation of the eggs has been described previously [Hamrick et al, 1977].

Fertilized quail eggs were exposed in the far field to 2.45-GHz CW microwave radiation at 5 mW/cm^2. When looking down the absorber-lined horn irradiator toward the eggs, the electric field vector is upward, perpendicular to the floor, and the magnetic field vector points to the right, horizontal to the floor. The specific absorption rate (SAR) in the center of the egg was determined using time-temperature profiles measured by a Vitek noninteracting temperature probe [Bowman, 1976] and was found to be 4.03 mW/g. Because of the properties of the different layers of the egg and the curved shape of the egg, which induces a focusing effect, the center of the egg is 0.4 °C warmer than the front. The temperature along the major axis (top to bottom) was almost constant. The details of this exposure system and the dosimetric technique have been described at length in previous publications [Hamrick and McRee, 1975; Hamrick et al, 1977]. The temperature of the environmental chamber used for irradiation was 35.5 °C. This temperature maintained the eggs at the optimum incubation temperature (37.5 °C) during microwave exposure [McRee et al, 1983]. The control nonirradiated eggs (sham-irradiated) were incubated at 37.5 °C in a similar incubation environment but did not receive microwave radiation.

The eggs were irradiated continuously for the first 12 days of development. At 14 days, all the eggs were transferred to an egg incubator (Jamesway Model 252 B; Jamesway Incubator Co., Gettysburg, PA) for the remainder of the incubation period. The process of incubation was completed on six groups of 78 irradiated and 78 sham-irradiated eggs, producing a total of 468 irradiated and 468 sham-irradiated eggs.

After each of the six hatches, hatchability was measured and the chicks were identified individually as irradiated or sham-irradiated chicks and moved into metal brooders, where the temperature was maintained at 35 ± 1.0 °C during the first week, 32 ± 1.0 °C during the second week, 29 ± 1.0 °C during the third week, and 25 ± 2.0 °C during the fourth week of age. At 35 days of age, the quail were

weighed and transferred as male and female pairs into 17 × 18 × 19-cm stainless steel mating cages with 1.3 × 2.5-cm wire mesh floors. Irradiated and sham-irradiated males were paired with either irradiated or sham-irradiated females, yielding a total of four treatment combinations (Table 1). There were 10 caged pairs of quail from each treatment combination distributed randomly over 40 cages in each of the six hatches. After the quail from the sixth hatch were caged, there were a total of 240 caged pairs of quail with each of the four treatment combinations represented in 60 of the caged pairs (Table 1). The quail were maintained as mated pairs through 224 days of age and then weighed. During that interval, they were maintained at a room temperature of 25 ± 2.9 °C, a relative humidity of 40–60% (range), and a photoperiod of 16 hr/day with lights on from 0600 to 2200 hours EST or EDT. Both feed and water were available ad libitum. The quail layer ration contained 24% protein, 11,700 kJ of metabolizable energy/kg, and 2.55% Ca.

Each day the following data were collected from each pair of quail: egg production, egg weight, egg type (eg, normal, cracked, or soft-shelled), egg fertility determined after incubation for 3 days, morbidity, and mortality. Every 28 days, beginning at 56 days of age, eggs collected from each pair over a 10-day period were incubated in an egg incubator under optimum conditions described herein to assess developmental abnormalities, embryonic mortality, and hatchability. These data were collected until the parent population was 224 days of age. The eggs collected from parents that were 84 and 168 days of age from Trials 1–3 were incubated and hatched, and the progeny were grown under the same conditions as the parents and caged at 35 days of age as nonsibling male-female pairs. The pairings were made within parent treatment groups (Table 1). The data collected from the progeny were from the same variables that were measured in the parents. These data were collected through 168 days of age, and then each bird was weighed.

From the data collected each day, the following parameters were calculated in each parent and progeny treatment group: 1) total mortality number and percentage; 2) age at which first egg was laid; 3) number and percentage of eggs laid that were: fertile, infertile, soft-shell or shelless, and cracked-shell; 4) number of consecutive days an egg was or was not laid; 5) number and percentage of total, fertile, and infertile eggs laid; 6) total egg weight and average egg weight every 7 and 28 days; 7) total number of percentage of eggs incubated to assess hatchability; 8) total number and percentage of hatched eggs; 9) total number and percentage of embryonic mortality from 0 to 3 (early), 4 to 14 (middle), and 15 to 18 (late) days of incubation; 10) total number and percentage of embryonic mortality resulting from malformation

TABLE 1. Experimental Pair Assignments To Measure Reproductive Efficiency of Progeny From Japanese Quail Parents That Were Irradiated With Microwaves During Embryogeny

Parent pairings			Progeny pairings			Progeny
♂	♀	n	♂	♀	n	group
I[a]	I	60	I × I[c]	I × I	60	1
I	S[b]	60	I × S	I × S	60	2
S	S	60	S × S	S × S	60	3
S	I	60	S × I	S × I	60	4

[a]I, irradiated during embryogeny.
[b]S, nonirradiated (sham).
[c]I × I, I × S, S × S, S × I = Experimental treatment of parents.

of the cranial, abdominal, or other anatomical region; and 11) total number and percentage of embryonic mortality resulting from malpositioning of the embryo (ie, wrong orientation within the shell).

At 224 days of age, the females in Trials 1 and 2 were weighed and killed by decapitation and ovary weights were measured. Additionally, in Trials 1 and 2, from 224 to 238 days of age, all irradiated and sham-irradiated males were caged individually and trained to ejaculate upon manual manipulation [Marks and Lepore, 1965]. Then at least three semen samples were collected from each male. The three semen samples from each quail were evaluated for percentage spermatocrit and spermatozoal motility, viability, and morphology. Spermatocrit percentages were measured in microcapillary tubes after centrifugation. Motility was measured using a hanging drop slide preparation from each male immediately after semen collection [Herman and Swanson, 1941]. Motility was subjectively scored using a scale of 1 to 5 with 5 representing maximum ($\approx$ 100%) motility. Viability and morphology of the spermatozoa were determined using the nigrosin-eosin staining method of Edens et al [1973] by classifying 200 consecutive cells in each semen sample. The spermatozoa were classified as number live, dead, and abnormal (ie, coiled tails, bent heads, broken tails, balloon heads, or swollen acrosomes). The quail were weighed and killed by decapitation after the third semen sample was collected and testes weights were measured.

In Trials 5 and 6, reproductive behavior, egg production, and mortality were observed through 364 days of age. Reproductive behaviors were recorded over a 10-day period from 224 through 234 days of age. During the last 2 hr before the lights were extinguished in the room, the pairs were observed for the frequencies of five reproductively oriented behavioral responses [Gildersleeve et al, 1985]. Two pairs from each treatment group were observed for two 15-min periods during the 2-hr period. The recorded behaviors were 1) male initiated head grabbing (male grabs the nape of the neck of the female with his beak), 2) mounting (male stands with both feet on the back of the female while head grabbing), and 3) cloacal contact. Females were observed for frequency of 1) nonreceptivity (constant locomotion while the male attempted to mount or escape without cloacal contact) and 2) pecking by the female toward the male.

The parameters described herein were calculated to assess reproductive capacity after the parent and progeny data were sorted by sex, experimental treatment, sex within experimental treatment, and parent age for the progeny. Percentage measurements were subjected to log, square root, and arcsin transformations and were also analyzed without transformation when scatter plots revealed nonlinearity of the data.

The statistical analyses for effects of treatments, sex, and interactions were conducted across all trials using the general linear models [SAS, 1982] procedure for the analysis of variance of completely randomized designs with a probability level of .01 for rejection of the null hypotheses. The experimental treatment and sex within treatment means were partitioned by Duncan's new multiple range tests and t tests [Steel and Torrie, 1980] with $P < .01$. For the parameters that were measured over time, linear regression analyses were conducted to determine slope of response lines. Nominal data were analyzed for significance using χ^2 tests [Siegel, 1956].

RESULTS

Microwave irradiation did not affect hatchability of irradiated eggs (75 $\pm$ 5%) as compared to the sham-irradiated eggs (72 $\pm$ 8%). The effects of irradiation on

mortality, egg weight, and egg production in parents and progeny are shown in Tables 2 and 3 and Figure 1. Since no effect of irradiation on mortality, egg weight, or egg production was found, the data are represented by parent treatment pair type and progeny group to condense the data to a tabular form. Similarly, the data presented in Tables 4–6 and Figure 2 were condensed to facilitate presentation because irradiation during embryogeny did not affect the reproduction parameters measured in either the parents or their progeny. Fertility was not affected by irradiation of the parents during embryogeny (Table 4, Fig. 1). The progeny of the irradiated parents were not different from sham-irradiated progeny in fertility (Table 5, Fig. 2). Both sham-irradiated and irradiated parents and progeny produced eggs at the same rate as indicated by the regression analysis (Figs. 1, 2). Both sham-irradiated and irradiated parents and all progeny groups produced fertile eggs at the same rate as indicated by the regression analysis (Figs. 1, 2). No difference in any of the parameters was found between progeny hatched from 84-day-old and 168-day-old parents among any of the parent experimental pairings. The pattern of distribution of embryonic mortality in either the parents or the progeny eggs was not affected by irradiation (Tables 6, 7). When the data were sorted and analyzed for irradiation effects within each sex, no differences were found between the irradiated and sham-irradiated groups for any of the reproductive parameters measured. To summarize the results, the ANOVAs revealed no significant main effect (sex or irradiation) differences or significant interactions of sex and irradiation treatment. The slopes of the linear regression lines

TABLE 2. Effect of Microwave Irradiation During Embryogeny on Mortality and Egg Production Parameters From 40 Through 224 Days of Age in Japanese Quail

Experimental mating pairs			Mortality		Mean ± SD			
♂	♀	n	♂	♀	Onset of egg production (day)	Egg weight (g)	Total eggs produced	Percentage egg production
I[a]	I	51	2	7	47.3 ± 0.9	9.7 ± 0.6	152 ± 20	81.6 ± 10.7
I	S[b]	54	1	5	49.1 ± 0.9	9.6 ± 0.7	153 ± 17	82.1 ± 9.3
S	S	56	0	4	48.6 ± 0.8	9.5 ± 0.6	157 ± 15	84.3 ± 8.2
S	I	53	1	6	47.0 ± 0.9	9.6 ± 0.8	150 ± 23	80.3 ± 12.1

[a]I, irradiated during embryogeny.
[b]S, nonirradiated (sham).

TABLE 3. Mortality and Egg Production Parameters From 37 Through 168 Days of Age in Progeny of Japanese Quail Parents That Were Irradiated With Microwaves During Embryogeny

Parent pairs		Progeny pairs[a]		Mortality		Mean ± SD			
♂	♀	Group	n	♂	♀	Onset of egg production (day)	Egg weight (g)	Total eggs produced	Percentage egg production
I[b]	I	1	48	5	7	47.1 ± 5.1	9.3 ± 0.5	101 ± 20	78.1 ± 15.3
I	S[c]	2	50	5	5	47.9 ± 5.6	9.3 ± 0.7	100 ± 18	77.3 ± 14.1
S	S	3	51	2	7	46.7 ± 4.0	9.3 ± 0.7	106 ± 15	81.3 ± 11.3
S	I	4	55	2	3	45.8 ± 3.9	9.5 ± 0.8	105 ± 17	80.6 ± 13.3

[a]Progeny groups were male-female pairs produced from the designated parent pairs.
[b]I, irradiated during embryogeny.
[c]S, nonirradiated (sham).

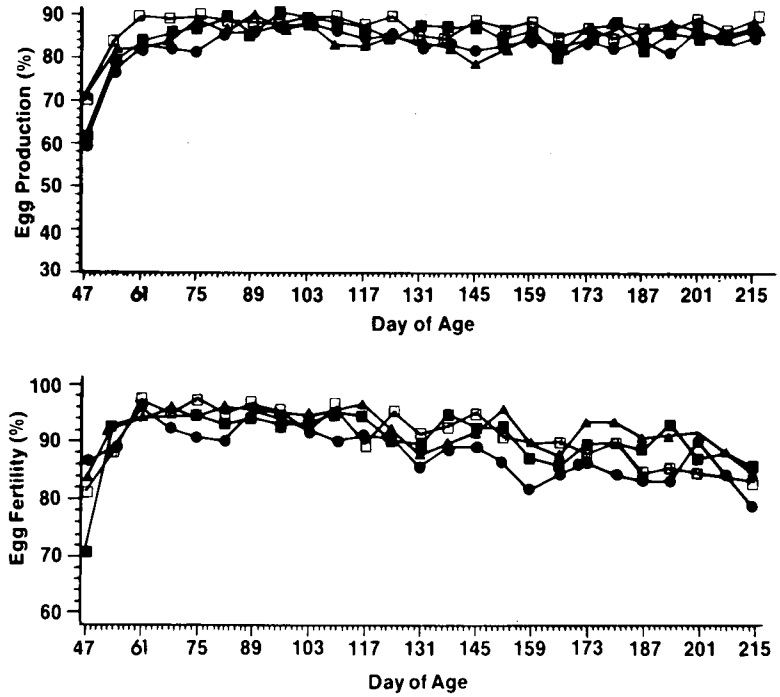

Fig. 1. Egg production and fertility in Japanese quail after 2.45-GHz CW microwave irradiation during embryogeny. Egg production was calculated as a percentage by dividing the number of eggs laid by the number of days the eggs were collected and then multiplying that quotient by 100. Fertility was calculated as the percentage of eggs laid that were fertile. Each point is the mean of 7 days of egg production ($51 \leqslant n \leqslant 56$). Open squares represent irradiated male-female pairs. Solid squares represent nonirradiated (sham-irradiated) male-female pairs. Solid circles represent irradiated male-sham female pairs. Solid triangles represent sham irradiated male-irradiated female pairs. Standard deviations do not appear for reasons of clarity. No significant ($P < .01$) differences were found among the pairs in any 7-day interval.

TABLE 4. Effect of Microwave Irradiation During Embryogeny on Fertile and Defective Egg Production From 40 Through 224 Days of Age in Japanese Quail

Experimental mating pairs			Mean ± SD			
♂	♀	n	Total fertile eggs	Percentage fertile eggs	Total soft-shelled eggs	Total cracked-shelled eggs
I[a]	I	51	140 ± 22	92.5 ± 7.1	1 ± 2	3 ± 3
I	S[b]	54	139 ± 27	90.7 ± 13.5	1 ± 3	3 ± 3
S	S	56	142 ± 22	90.5 ± 11.0	2 ± 6	3 ± 2
S	I	53	133 ± 30	88.4 ± 13.6	2 ± 5	3 ± 4

[a]I, irradiated during embryogeny.
[b]S, nonirradiated (sham).

TABLE 5. Fertile and Defective Egg Production From 37 Through 168 Days of Age in Progeny of Japanese Quail Parents That Were Irradiated With Microwaves During Embryogeny

Progeny parent pairs		Progeny pairs[a]		Mean ± SD			
♂	♀	Group	n	Total fertile eggs	Percentage fertile eggs	Total soft-shelled eggs	Total cracked-shelled eggs
I[b]	I	1	48	93 ± 24	90.9 ± 12.9	1 ± 1	2 ± 1
I	S[c]	2	50	95 ± 19	94.2 ± 4.7	1 ± 1	2 ± 2
S	S	3	51	90 ± 23	85.2 ± 19.2	1 ± 2	2 ± 3
S	I	4	55	94 ± 22	89.7 ± 13.8	1 ± 1	2 ± 4

[a]Progeny groups were male-female pairs produced from the designated parent pairs.
[b]I, irradiated during embryogeny.
[c]S, nonirradiated (sham).

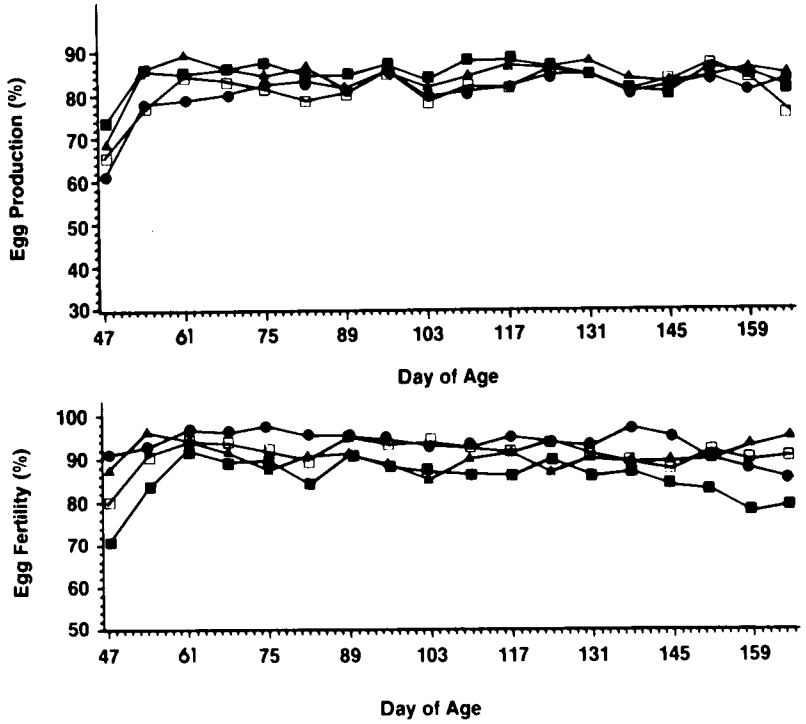

Fig. 2. Egg production and fertility in progeny of Japanese quail parents that were irradiated with 2.45-GHz CW microwave radiation during embryogeny. Egg production was calculated as a percentage by dividing the number of eggs laid by the number of days the eggs were collected and then multiplying that quotient by 100. Fertility was calculated as the percentage of eggs laid that were fertile. Each point is the mean of 7 days of egg production ($48 \leqslant n \leqslant 55$). Open squares represent male-female progeny pairs whose parents were irradiated. Solid squares represent male-female progeny pairs whose parents were not irradiated (sham-irradiated). Solid circles represent male-female progeny pairs from irradiated male-sham irradiated female parent pairs. Solid triangles represent male-female progeny pairs from sham irradiated male-irradiated female parent pairs. Standard deviations do not appear for reasons of clarity. No significant ($P < .01$) differences were found among the progeny pairs in any 7-day interval.

TABLE 6. Effect of Microwave Irradiation During Embryogeny on Hatchability and Embryonic Mortality of Eggs Produced From 40 Through 224 Days of Age in Japanese Quail

Experimental mating pairs			Total[a] No. eggs incubated	Mean (%) ± SD					
					Embryonic mortality				
							Late		
♂	♀	n		Hatchability	Early	Mid	Total	Malposition	Malformed
I[b]	I	54	2,683	88.3 ± 8.6	5.7 ± 6.0	1.3 ± 2.1	4.7 ± 2.3	0.7 ± 0.8	1.0 ± 1.2
I	S[c]	54	2,765	88.7 ± 9.6	5.5 ± 7.9	0.8 ± 1.6	5.0 ± 2.1	1.3 ± 1.0	0.2 ± 0.3
S	S	56	2,725	88.4 ± 11.7	6.1 ± 8.8	1.3 ± 2.1	4.1 ± 1.9	1.5 ± 1.8	1.0 ± 1.3
S	I	53	2,828	85.7 ± 13.0	5.9 ± 7.0	1.5 ± 2.9	6.9 ± 4.3	1.9 ± 2.2	1.4 ± 1.7

[a]Total number of eggs incubated in seven incubations.
[b]I, irradiated during embryogeny.
[c]S, nonirradiated (shams).

TABLE 7. Hatchability and Embryonic Mortality of Eggs Produced from 37 Through 168 Days of Age by Progeny of Japanese Quail Parents That Were Irradiated With Microwaves During Embryogeny

Parent pairs		Progeny[a] pairs		Total[b] no. eggs incubated	Mean (%) ± SD					
						Embryonic mortality				
								Late		
♂	♀	Group	n		Hatchability	Early	Mid	Total	Malposition	Malformed
I[c]	I	1	48	1,673	88.9 ± 14.2	6.4 ± 12.3	0.9 ± 1.8	3.8 ± 2.2	0.6 ± 0.9	0.1 ± 0.2
I	S[d]	2	50	1,776	88.0 ± 10.6	6.0 ± 7.1	2.0 ± 4.0	4.0 ± 2.2	0.8 ± 1.0	0.3 ± 0.4
S	S	3	51	1,808	88.8 ± 13.3	6.1 ± 10.4	1.3 ± 2.5	3.8 ± 2.2	0.9 ± 1.2	0.2 ± 0.3
S	I	4	55	1,859	86.7 ± 11.5	6.5 ± 7.5	1.9 ± 2.9	4.9 ± 3.0	0.9 ± 1.2	0.4 ± 0.4

[a]Progeny groups were male-female pairs produced from the designated parent pairs.
[b]Total number of eggs incubated in five incubations.
[c]I, irradiated during embryogeny.
[d]S, nonirradiated (shams).

of parameters measured over time did not differ among treatment groups. Irradiation of male or female embryos did not result in sex-related alterations in fertility or hatchability. The progeny of either irradiated males or females reproduced in a manner that was not different from shams.

In Trials 1, and 2, no significant differences were found between irradiated and sham-irradiated body or gonadal weights (Table 8). Similarly, no significant differences were found between irradiated and sham-irradiated males in percentage spermatocrit or spermatozoal viability, morphology, and motility (Table 9).

In Trials 5 and 6, no significant differences were found among the experimental pair groups from 224 through 364 days of age in rate of egg production, mortality, or reproductive behaviors (data not shown).

DISCUSSION

This study may represent the first investigation of low-level effect of microwave irradiation on the reproduction of more than one generation of birds. Furthermore, this study is primary in its practical approach to the question of potential long-term, and therefore, genetic effects of exposure to microwave radiation on multiple generations of animals.

The results of the present study clearly indicate that irradiation of Japanese quail embryos in ovo with 2.45-GHz CW microwave radiation at an SAR of 4.03 mW/g does not affect the reproductive efficiency of the hatchlings. The results from the progeny of quail that were irradiated during embryogeny indicate that a long-term genetic effect of irradiation does not exist when assessed by measuring the reproduc-

TABLE 8. Effect of Microwave Irradiation During Embryogeny on Body and Gonad Weight in Japanese Quail

Experimental treatment	n ♂	n ♀	Mean body weight (g) ± SD: Males by age (days) 38	Males by age (days) 238	Testes weight (g)	Females by age (days) 35	Females by age (days) 224	Ovary weight (g)
I[a]	38	36	98 ± 8	121 ± 11	4.09 ± 0.76	106 ± 10	145 ± 9	5.76 ± 1.28
S[b]	40	37	98 ± 7	122 ± 11	3.72 ± 0.62	102 ± 9	145 ± 14	5.50 ± 1.38

[a]I, irradiated during embryogeny.
[b]S, nonirradiated (sham).

TABLE 9. Effect of Microwave Irradiation During Embryogeny on Spermatozoal Parameters in Japanese Quail

Experimental treatment	n	Mean ± SD: Spermatocrit (%)	Viability (%): Live	Viability (%): Dead	Abnormal[a] (%)	Motility score[b]
I[c]	38	35.0 ± 5.0	93.7 ± 6.3	0.1 ± 0.2	6.2 ± 7.9	4.6 ± 0.5
S[d]	38	32.6 ± 4.8	94.9 ± 4.4	0.2 ± 0.4	4.9 ± 3.9	4.6 ± 0.5

[a]Abnormal, pooled percentages of spermatozoa with coiled tails, bent heads, broken tails, balloon heads, or swollen acrosomes.
[b]Motility of spermatozoa based on subjective scores of 1 (poor) to 5 (excellent).
[c]I, irradiated during embryogeny.
[d]S, nonirradiated (sham).

tive parameters typically monitored in avian species or from other studies in mammals [Jensh et al, 1982; Rugh and McManaway, 1978].

Little is known of the long-acting nonthermal effects of embryonic irradiation over multiple generations [Rugh and McManaway, 1978], and very little research has been conducted on the potential effect of in vivo exposure on the genome. In the present study, the data collected from the progeny of parents that had been exposed in ovo suggest that nonthermal effects of microwave irradiation do not include long-acting effects on portions of the genome that influence reproduction in subsequent generations.

A promising experimental approach to study the nonthermal effects of microwave irradiation on reproductive efficiency may include in vivo exposure of sexually mature male animals. During spermatogenesis, mice were irradiated with 2.45-GHz CW at an SAR of 5 mW/g, and an increased incidence of chromosomal chain translocations was found in spermatocytes [Manikowska-Czerska et al, 1985]. Furthermore, it has been reported that low-level microwave radiation interacts with DNA by resonant absorption depending on molecular length [Swicord et al, 1983], which may explain the apparent effects observed by Manikowska-Czerska et al [1985].

In embryos, spermatogonia and oogonia may not be as sensitive to nonthermal levels of irradiation because of the absence of gametogenesis and meiotic divisions. This may in part explain the results from the present study and may also indicate that the effects of irradiation reported by Manikowska-Czerska et al [1985] were on late spermatogonia and/or spermatocytes. Investigations are needed that include irradiation of testes in vivo without thermal insult before and after sexual maturation to further these studies. In addition, the most plausible effects of low-level irradiation in ovo or in utero may be measurable in cells or tissues that continue to differentiate postnatally, such as hematopoietic stem cells, immunological tissues, nervous tissues, and endocrine cells.

McRee et al [1983] reported no increase in relative percentages of spermatozoal abnormalities in 154–161-day-old quail that had been irradiated in ovo. However, they also reported that spermatozoal numbers were reduced and that fertility of eggs produced from matings of irradiated males with nonirradiated females was decreased. This led to the hypothesis that spermatogonia were affected adversely during exposure or maturation. The results of the present study do not extend this male effect to other ages of quail. Only small numerical but nonsignificant fertility effects were noted in the present study. However, from 145 through 168 days of age, a numerical tendency towards decreased female (SXI) fertility was noted (Fig. 1). Clearly, no long-acting effect of in ovo exposure on fertility can be inferred from these data. Other reports on mammals have come to similar conclusions [Rugh and McManaway, 1978; Jensh et al, 1982].

Recently, Byman et al [1985] exposed fertile Japanese quail eggs twice daily for 30 min to 2.45-GHz CW microwave radiation at power densities of 25 or 50 mW/cm^2 and reported that hatchability was decreased by the higher power density. They attributed the decreased hatchability to increased internal egg temperatures during exposure. Hatchability was not affected in the present study or in a past study [McRee et al, 1975] when eggs were exposed continuously during the first 12 days of incubation to 2.45-GHz CW microwave radiation and internal egg temperature was maintained at 37.5 °C. Byman et al [1985] also reported that the growth of chicks hatched from eggs exposed to 25 mW/cm^2 microwave radiation was not different

from nonirradiated controls. Similarly, no effect of irradiation on growth was found by McRee et al [1975] or in the present study. Byman et al [1985] hypothesized that embryos from birds nesting in or about rectennae may be adversely affected by exposure to microwaves from a proposed satelite power system that would collect microwave energy. The present study extends their observations to the potential impact of low-level microwaves from rectennae on the reproductive ability of quail. Apparently, nonthermal or athermal effects of irradiation in ovo do not include adverse alterations in reproductive efficacy. Perhaps the best indication that long-term effects of in ovo exposure to low-level microwave radiation on reproduction do not exist was the well documented lack of effects on the hatchability of irradiated avian embryos by McRee et al [1975].

ACKNOWLEDGMENTS

The authors thank H. Davis, P. Phelps, R. Wiard, T. Bryan, G. Swann, D. Sugg, and C. Smith for their excellent assistance during the course of this study. This study was supported in part by NIEHS contract NO1-ES-2-5019.

REFERENCES

Baranski S, Czerski P (1976): "Biological Effects of Microwaves." Stroudsburg, PA: Dowden, Hutchinson and Ross.

Berman E, Carter HB, House D (1981): Observations of rat fetuses after irradiation with 2450-MHz (CW) microwaves. J Microwave Power 16:9–13.

Bowman RR (1976): A probe for measuring temperature in radio-frequency-heated material. IEEE Trans Microwave Theory Tech MIT-24:43–45.

Byman D, Battista SP, Wasserman FE, Kunz TH (1985): Effect of microwave irradiation (2.45 GHz, CW) on egg weight loss, egg hatchability and hatchling growth of the Coturnix quail. Bioelectromagnetics 6:271–282.

Cairnie AR, Harding RK (1981): Cytological studies in mouse testis irradiated with 2.45-GHz continuous-wave microwaves. Radiat Res 87:100–108.

Carpenter RL, Biddle DK, Van Ummersen CA (1960): Biological effects of microwave radiation with particular reference to the eye. Proc 3rd International Conf Med Electronics, London. "Medical Electronics, Part III." Springfield, IL: Charles C. Thomas, pp 401–48.

Clarke RL, Justesen DR (1983): Temperature gradients in the microwave irradiated egg: implications for avian teratogenesis. J Microwave Power 18:169–180.

Davidson JA, Kondra PA, Hamid MAK (1976): Effects of microwave radiation on eggs, embryos and chickens. Can J Anim Sci 56:709–713.

Durney CH, Johnson CC, Barber PW, Massoudi H, Iskander MF, Lords JL, Ryser DK, Allen SJ, Mitchell JC (1978): "Radiofrequency Radiation Dosimetry Handbook, 2nd ed." Report SAM-TR-78-22. Brooks Airforce Base, TX: USAF School of Medicine.

Edens FW, Van Krey HP, Siegel PB (1973): Selection for body weight at eight weeks of age. 10. Spermatozoal morphology. Poultry Sci 52:2287–2289.

Fisher PD, Lauber JK, Voss WAG (1979): The effect of low-level 2450-MHz CW microwave radiation and body temperature on early embryonic development in chickens. Radio Sci 14/65:159–163.

Galvin MJ, McRee DI, Hall CA, Thaxton JP, Parkhurst CR (1981): Humoral and cell-mediated immune function in adult Japanese quail following exposure to 2.45-GHz microwave radiation during embryogeny. Bioelectromagnetics 2:269–278.

Gildersleeve RP, Tilson HA, Mitchell CL (1985): Injection of diethylstilbestrol on the first day of incubation affects morphology of sex glands and reproductive behavior of Japanese quail. Teratology 31:101–109.

Gunn SA, Gould TC, Anderson WAD (1961): The effect of microwave radiation on morphology and function of rat testis. Lab Invest 10:301–314.

Hamrick PE, McRee DI (1975): Exposure of the Japanese quail embryo to 2.45-GHz microwave radiation during the second day of development. J Microwave Power 10:211–215.

Hamrick PE, McRee DI, Thaxton JP, Parkhurst CR (1977): Humoral immunity of Japanese quail subjected to microwave radiation during embryogeny. Health Phys 33:23–33.

Herman HA, Swanson EW (1941): "Variations in Dairy Bull Semen With Respect to Its Use in Artificial Insemination." Univ Missouri Res Bull 326.

Hills GA, Kondra PA, Hamid MAK (1974): Effects of microwave radiations on hatchability and growth in chickens and turkeys. Can J Anim Sci 54:573–578.

Imig CJ, Thomson JD, Hines HM (1948): Testicular degeneration as a result of microwave irradiation. Proc Soc Exp Biol Med 69:382–386.

Jensh RP, Weinberg I, Brent RL (1982): Teratologic studies of prenatal exposure of rats to 915-MHz microwave radiation. Radiat Res 92:160–171.

Kondra PA, Hamid MA, Hodgson GC (1972): Effects of microwave radiation on growth and reproduction of two stocks of chickens. Can J Anim Sci 52:317–320.

Kondra PA, Smith WK, Hodgson GC, Bragg DB, Gavora J, Hamid MAK, Boulanger RJ (1970): Growth and reproduction of chickens subjected to microwave radiation. Can J Anim Sci 50:639–644.

Krueger WF, Giarola AJ, Bradley JW, Shrekenhamer A (1975): Effects of electromagnetic fields on fecundity in the chicken. Ann NY Acad Sci 247:391–407.

Manikowska E, Luciani JM, Servantie B, Czerski P, Obrenovitch J, Stahl A (1979): Effects of 9.4 GHz microwave exposure on meiosis in mice. Experientia 35:388–390.

Manikowska-Czerska E, Czerski P, Leach WM (1985): Effects of 2.45 GHz microwaves on meiotic chromosomes of male CBA/CAY mice. J Hered 76:71–73.

Marks, HL, Lepore PD (1965): A procedure for artificial insemination of Japanese quail. Poultry Sci 44:1001–1003.

McRee DI, Hamrick PE (1977): Exposure of Japanese quail embryos to 2.45-GHz microwave radiation during development. Radiat Res 71:355–366.

McRee DI, Thaxton JP, Parkhurst CR (1983): Reproduction of Japanese quail exposed to microwave radiation during embryogeny. Radiat Res 96:51–58.

McRee DI, Zinkl J, Thaxton P, Parkhurst CR (1975): Some effects of exposure of the Japanese quail embryo to 2.45-GHz microwave radiation. Ann NY Acad Sci 247:377–390.

Romero-Sierra C, Tanner JA (1970): Microwave radiation and egg production in chickens. Proc 5th Int Symp International Microwave Institute, Scheveningen, the Netherlands.

Rugh R, McManaway M (1978): Does pre- or post-natal microwave radiation sterilize mice? Cong Anom 18:69–74.

SAS (1982): "SAS User's Guide." Cary, NC: SAS Institute, Inc.

Saunders RD, Kowalczuk CI (1981): Effects of 2.45 GHz microwave radiation and heat on mouse spermatogenic epithelium. Int J Radiat Biol 40:623–632.

Schmidt RE, Merritt JH, Hardy KH (1984): In utero exposure to low-level microwaves does not affect rat foetal development. Int J Radiat Biol 46:383–386.

Siegel S (1956): "Non-Parametric Statistics." New York: McGraw-Hill.

Steel RGD, Torrie JH (1980): "Principles and Procedures of Statistics." New York: McGraw-Hill.

Swicord ML, Edwards GS, Sagripanti JL, Davis CC (1983): Chain length dependent microwave absorption of DNA. Biopolymers 22:2513–2516.

Van Ummersen CA (1963): "An Experimental Study of Developmental Abnormalities Induced in the Chick Embryo by Exposure to Radio Frequency Waves." PhD Dissertation, Tufts University.

Varma MM, Traboulay EA (1975): Biological effects of microwave radiation on the testes of Swiss mice. Experientia 31:301–302.

Bioelectromagnetics 8:23–27 (1987)

Comparison of the Dielectric Properties of Normal and Wounded Human Skin Material

C. Gabriel, R.H. Bentall, and E.H. Grant

Physics Department, King's College, London Strand (C.G., E.H.G.), and Institute of Bioelectrical Research, Romanno Bridge, West Linton, Peebleshire (R.H.B.), England

Measurements have been made of the permittivity and conductivity of normal and wounded human skin material over the frequency range 10 MHz–10 GHz. The permittivity of the wounded tissue was found to be about 12% higher than that of the normal tissue. A similar percentage increase was observed for the conductivity. These differences are attributed to the presence of a higher proportion of bulk water in the wounded material.

Key words: permittivity, conductivity, normal vs wounded skin

INTRODUCTION

As far as we are aware, no work has been reported in the literature on the use of dielectric methods to observe differences between wounded and normal tissue. With respect to human tissue, there have been very few dielectric measurements in the microwave region on skin material except for the early work at isolated frequencies of England [1950] and Cook [1951] and the measurements of Tanabe and Joines [1976].

There is currently much interest in the use of electric and magnetic fields to promote wound healing and bone regeneration [Nicolle and Bentall, 1982; Frank and Szeto, 1983; Binder et al, 1984]. It is very important to understand the mechanism underlying such processes, and one step in any line of investigation would be to measure and compare the dielectric properties of normal and pathological material. In the present paper, we report measurements of permittivity and conductivity of human skin in the normal and wounded state over three decades of frequency. The determinations, which were carried out at one temperature only, were made specifically for the purpose of comparison. No attempt is made to interpret the data in terms of cellular and molecular processes. To do this, it is necessary to take measurements over a wide temperature range and it is also of value to have data on frozen tissue material [Gabriel and Grant, 1985] as well as at higher temperatures. We are currently investigating the differences between wounded and normal tissue using these kinds of techniques, and the results will form the subject of a future publication.

EXPERIMENTAL METHODS

The samples were obtained as follows. The donor was a living human subject, and four samples each of normal skin and wounded skin were removed from the

Received for review April 29, 1985; revision received December 3, 1985.

Address reprint request to Dr. C. Gabriel, Physics Department, King's College, London Strand WC2R 2LS, England.

lower outer calf region. A number of full-thickness incisions were made after suitable local infiltration of lignocaine 1%. These incisions were 2 cm in length and were closed with 4/0 prolene sutures. After 48 hr a further lignocaine infiltration was made and a 5 mm biopsy removed from the incision site. At the same time a similar quantity of lignocaine was infiltrated at a distance of 3 in. from the incision and a 5 mm punch biopsy of this unwounded "normal" skin removed. These then constituted the samples. With respect to the wounded material, two samples were taken 48 hr after wounding and two samples 72 hr after wounding. The permittivity and the conductivity of all skin samples were measured within 3 hr of removal.

The dielectric measurements were carried out using an HP 140 Time Domain Spectrometer on line to a PDP 11/10 computer. Full details of the equipment and the experimental technique have been described previously [Dawkins et al, 1979, 1981a,b], and examples of its use in measuring the dielectric properties of biological material also appear elsewhere [Gabriel et al, 1983]. The data were taken at 1 °C, this temperature being chosen in order to cover as large a fraction of the water dispersion as possible with the available measuring frequency range (10 MHz–10 GHz).

RESULTS AND DISCUSSION

The dielectric parameters of four samples each of normal and wounded skin material were determined. For both types of skin the total spread in the values of relative permittivity (ϵ) and conductivity (σ) was around 8% at any given frequency point. Figures 1 and 2 show, respectively, the values of ϵ and σ for wounded and non-wounded skin over the complete frequency range of measurement. For wounded material, the values of ϵ and σ were on average about 12% higher than for normal skin.

It is well known [Schwan, 1957; Grant et al, 1978] that several distinct processes can contribute to the observed dielectric dispersion in biological material between 10 MHz and 10 GHz. However, although unambiguous interpretation of the dielectric data at the low-frequency end of this region may be difficult, it is generally agreed that any dispersion occurring above around 1 GHz is due to the water component. Consequently, measurements carried out at one temperature on two biological materials are unlikely to produce much precise comparative information on the properties of the cells and macromolecules that are present, unless there are gross differences between the two tissues being compared. Conversely, any differences in the water content might be reflected clearly in the dielectric properties of the two tissues.

Following Schwan [1957] and numerous other investigators since then, it will be assumed that the present dielectric data on human skin can be characterised by three dispersion regions; the β dispersion resulting from the charging of cell membranes and the rotation of individual macromolecules; the δ dispersion resulting from the relaxation of bound water, side chains, and perhaps proton fluctuations; and γ dispersion resulting from the bulk water in the system. Since the β dispersion has a complex origin, and the present measurements cover only the high-frequency tail, any fitted dielectric parameters must refer to a high-frequency portion of the β

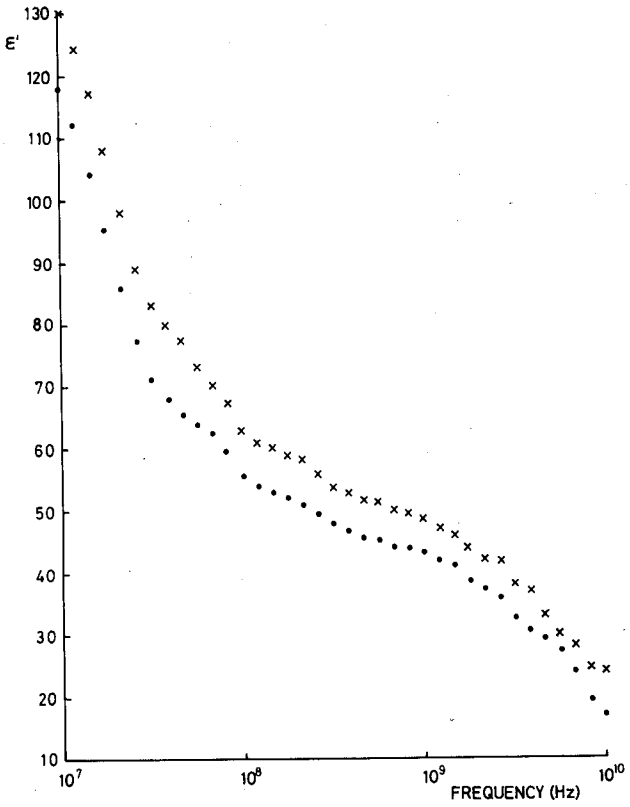

Fig. 1. Relative permittivity of normal and wounded human skin material at 1 °C. x, Wounded skin material; ●, normal skin material.

dispersion and will have no particular physical significance. Representing the dielectric behaviour by

$$\epsilon(f) = \epsilon_\infty + \frac{\Delta\beta}{1 + jf/f_{R\beta}} + \frac{\Delta\delta}{1 + jf/f_{R\delta}} + \frac{\Delta\gamma}{1 + jf/f_{R\gamma}}$$

where Δ and f_R are respective dielectric increments and relaxation frequencies for the three processes, the fitted values of Δ and f_R are obtained (Table 1).

Examination of the data shown in Table 1 reveals no significant differences in the dispersion parameters of the β and δ dispersions for the normal and wounded skin. The dielectric increment of the γ dispersion is, however, appreciably higher for the wounded material, the increase being 10–15%. The values of the relaxation frequency are in agreement to within experimental error for the γ dispersion. The significance of these observations is twofold.

It is well established that the γ dispersion in a biological tissue may be attributed to the bulk water present. Since the dielectric increment is, within a very good approximation, proportional to the amount of substance giving rise to it, it follows that the bulk water content of wound biopsy is 10–15% higher than for normal skin. Although this enhancement of water content in wound material is well known [Ryan and Majno, 1977], this is the first time, as far as we are aware, that the increase has

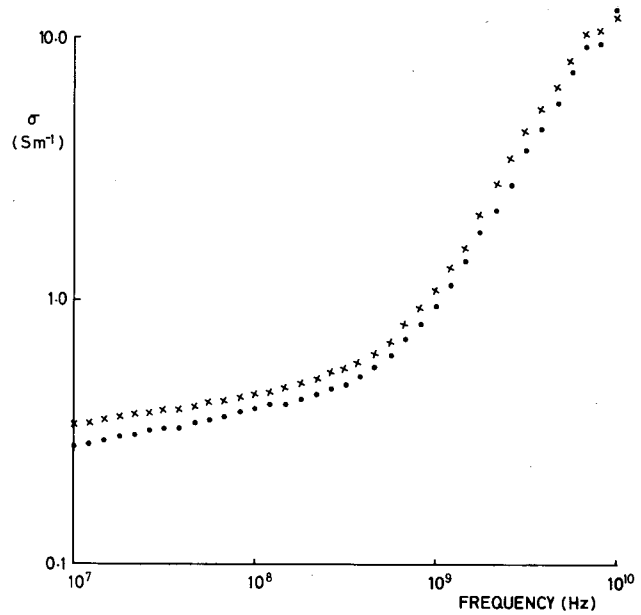

Fig. 2. Electrical conductivity of normal and wounded human skin material at 1 °C. x, Wounded skin material; ●, normal skin material.

TABLE 1. Dielectric Parameters of Normal Human Skin and Human Wound Biopsy at 1 °C

Parameter	Normal skin	Wound biopsy
$\Delta\beta$	91.8 (9.8)[a]	93.0 (10.4)
$f_{R\delta}$ (MHz)	14.7 (1.9)	16.3 (2.3)
Δ_β	14.2 (1.8)	15.2 (2.5)
$f_{R\delta}$ (MHz)	248 (48)	229 (50)
Δ_γ	37.2 (0.6)	42.2 (0.6)
$f_{R\gamma}$ (GHz)	5.9 (0.3)	6.1 (0.3)

[a]The figures in parentheses are the 95% confidence limits.

been quantified using dielectric methods. The second point that emerges from Table 1 is that the relaxation frequency of the skin, normal or wounded, is considerably less than that for pure water (9.1 GHz at 1 °C). The best explanation for this is that an appreciable fraction of the water in tissue has a rotational mobility less than pure water.

REFERENCES

Binder A, Parr G, Hazleman B, Fitton-Jackson S (1984): Pulsed electromagnetic field therapy for persistent rotator cuff tendonitis. Lancet i:695–698.

Cook HF (1951): The dielectric behaviour of some type of human tissues at microwave frequencies. Br J Appl Phys 2:295–300.

Dawkins AWJ, Grant EH, Sheppard RJ (1981a): An on-line computer based system for performing time domain spectroscopy II: Analysis of the errors in total reflection TDS. J Phys E 14:1269–1265.

Dawkins AWJ, Grant EH, Sheppard RJ (1981b): An on-line computer based system for performing time domain spectroscopy III: Presentation of results for total reflection TDS. J Phys E 14:1429–1434.

Dawkins AWJ, Sheppard RJ, Grant EH (1979): An on-line computer based system for performing a time domain spectroscopy I: Description of the main features of the basic system. J Phys E 12:1091–1099.

England TS (1950): Dielectric properties of the human body for wave lengths in the 1–10cm range. Nature 166:480–481.

Frank CB, Szeto AYJ (1983): A review of electromagnetically enhanced soft tissue healing. IEEE Eng Med Biol 12:27–32.

Gabriel C, Grant EH (1985): Dielectric behaviour of ocular tissues in the supercooled and frozen state. Phys Med Biol 30:975–983.

Gabriel C, Sheppard RJ, Grant EH (1983): Dielectric properties of ocular tissues at 37°C. Phys Med Biol 28:43–49.

Grant EH, Sheppard EJ, South GP (1978): "Dielectric Behaviour of Biological Molecules in Solution." London: Oxford University Press.

Nicolle FV, Bentall RHC (1982): Use of radio-frequency pulsed energy in the control of postoperative reaction in blepharosplasty. Aesth Plast Surg 6:169–171.

Ryan GB, Majno G (1977): Acute inflammation—A review. Am J Pathol 86:185–276.

Schwan HP (1957): Electrical properties of tissue and all suspensions. Adv Biol Med Phys 5:147–209.

Tanabe E, Joines WT (1976): A non-destructive method for measuring the complex permittivity of dielectric materials at microwave frequencies. IEEE Trans Instrumentation Measurements 25:222–226.

Bioelectromagnetics 8:29–36 (1987)

Simulated Biological Materials for Electromagnetic Radiation Absorption Studies

G. Hartsgrove, A. Kraszewski, and A. Surowiec

University of Ottawa, Department of Electrical Engineering, Ottawa, Ontario, Canada

For the study of electromagnetic dosimetry and hyperthermia, it is necessary to simulate human biological materials. This can be done by chemical mixtures that are described in this paper. Formulas are presented for simulating bone, lung, brain, and muscle tissue in the frequency range of 100 MHz to 1 GHz. By using these preparations a realistic equivalent to the human body can be constructed.

Key words: simulated biological materials, electromagnetic dosimetry, tissue equivalent materials

INTRODUCTION

Recently, electromagnetic dosimetry and hyperthermia have required more and more complex models of biological materials to investigate the electric field (SAR, temperature) distributions induced inside a real body. Experimental verification of calculations based on these more complex structures needs a more realistic model of the biological object constructed from materials that simulate the permittivity and conductivity of various tissues in the frequency range of interest. Most of the tissue equivalent materials developed to date simulate skeletal muscle. The majority of these materials lose their properties after a short time, because of sedimentation, chemical reactions, and bacterial action. The purpose of this paper is to present recipes for materials at room temperature that simulate the permittivity and conductivity of muscle, brain, lung, and bone tissues at body temperature (37°C) in the frequency range of 100–1000 MHz. These materials are all easy to prepare, inexpensive, and retain their properties for an extended period of time. Muscle simulating materials that have been prepared have retained these properties for over 1 year.

SIMULATED MATERIALS

Muscle Tissue

Our initial attempt was to simulate the properties of skeletal muscle [Hurt, 1985] because this is one of the major components of man. Previous formulas [Chou et al, 1984; Guy, 1971] have been developed for muscle material but they were found to have problems. The major problems were lumping of the gelling agent during mixing,

Received for review January 28, 1986; revision received June 6, 1986.

Address reprint requests to G. W. Hartsgrove, University of Ottawa, Department of Electrical Engineering, 770 King Edward Avenue, Ottawa, Ontario, Canada K1A 6N5.

separation of the components of the mixture, and a short lifetime before the onset of bacteria growth. The problems with the previous mixtures appeared to be mostly associated with the gelling agent; therefore, a substitute was sought. A compound used commercially for increasing the viscosity of many water based compounds was found to be a excellent material for our application. This material is a nonionic water-soluble polymerizing agent called hydroxyetheylcellulose (HEC), also known as Natrosol®. This material is available in a wide range of viscosities and is easily mixed with water. Because of the particular requirements of our project (immersion of a fragile probe into the material to measure the electric field), we needed a liquid or semi-liquid form of tissue equivalent materials. All recipes presented here are for semi-liquid materials (except for castable bone) which have viscosities in the range of 15,000–25,000 mPa. However, by increasing the amount of HEC one can obtain a more solid form of the materials with the same electrical properties.

The other components of the muscle material were sodium chloride (NaCl), to increase conductivity, and sucrose to lower the dielectric constant. One other component, a bacteriacide, was also added to prevent breakdown of the polymer by bacterial agents. The bacteriacide used was Dowicil 75®[1-(3-chloroallyl)-3, 5, 7-triaza-1-azoniaadamantane chloride]. Sucrose is available in the form of cane sugar and is much cheaper than polyethelene powder used in previous formulas. See the Appendix for a list of suppliers. Table 1A gives the proportions by weight for each of the materials, and Table 2 lists the dielectric constants and the conductivities in mS/cm at several selected frequencies. Figure 1 shows the dielectric constant and the conductivity for simulated muscle material as well as expected values based on data from several sources [Hurt, 1985; Stuchly and Stuchly, 1980; Foster et al, 1985; Pethig, 1984; Durney et al, 1978]. The measured dielectric constants are shown as circles, crosses depict the measured conductivities, solid lines present the expected dielectric constant, and dashed lines the conductivity.

Brain Tissue

The properties of brain tissue [Foster et al, 1979] are similar to those of skeletal muscle and the same components are used to produce brain equivalent material. Most of the brain consists of both grey and white matter with grey material having a higher dielectric constant and conductivity than white matter. The formula that is presented here will give properties averaged between those of white and grey matter. The recipe is presented in Table 1A, and frequency characteristics are shown in Figure 2 and in Table 2.

Lung Tissue

The lungs also have been identified as a part of the human body that has properties significantly different from skeletal muscle. It is, however, a complex structure that has different properties depending upon whether the lungs are inflated or deflated [Surowiec et al, in press]. In order to provide the best simulation an average was taken of these two states.

The basis of the lung simulation is the same as the skeletal muscle, as described above, but with the addition of hollow silica microspheres that range in diameter from 30–180 μm with a wall thickness of about 1.5 μm. This size is of the same order as the aveoli in the human lung, which is in the range of 100–200 μm in diameter. The skeletal muscle material is mixed with the microspheres by volume in a ratio of 47%

TABLE 1. (A) Composition by Weight of Muscle and Brain Equivalent Material. (B) Percentage by Volume of Filler Used in Lung Material. (C) Castable Bone Material Components. (D) Liquid Bone Material Components.

A. Muscle and brain material	Percentage by weight	
Material	Muscle	Brain
Water	52.4	40.4
Salt (NaCl)	1.4	2.5
Sugar	45.0	56.0
HEC	1.0	1.0
Bacteriacide	0.1	0.1

B. Lung material	
Material	Percentage by volume
Muscle material (above)	47
Microspheres	53

C. Bone material (castable)	
Material	Percentage by weight
Two ton epoxy	
Epoxy	35.0
Hardener	35.0
KCl Solution	28.0

D. Bone material (liquid)	
Material	Percentage by weight
TWEEN	57.0
n-Amyl alcohol	28.5
Paraffin oil	9.5
Water	4.5
Salt (NaCl)	0.5

TABLE 2. Dielectric Constant and Conductivity of Tissue Equivalent Materials at Selected Frequencies

	Frequency (MHz)					
	100		400		900	
Material	ϵ'	σ	ϵ'	σ	ϵ'	σ
Muscle	70.5	6.8	62.5	9.0	54.7	13.8
Brain	63.0	4.7	50.3	7.5	41.2	12.2
Lung	37.0	3.4	32.6	4.3	28.0	6.6
Bone cast	13.6	0.08	9.3	1.1	7.4	1.6
Bone liquid	10.8	0.35	9.1	0.66	7.2	1.2

muscle equivalent material to 53% microspheres. The properties of the simulated lung material are shown in Figure 3 and in Table 2.

Bone Tissue

Bone material is a very inhomogeneous structure, containing parts of different dielectric properties. The data found in literature [Foster and Schwan, 1985; Pethig,

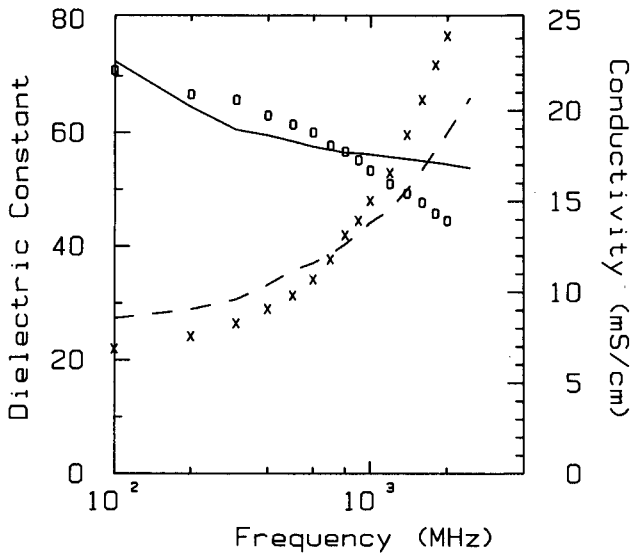

Fig. 1. Dielectric constant (0) and conductivity (X) of muscle equivalent material from 10 MHz to 2.45 GHz. Solid and dashed lines represent expected values of dielectric constant and conductivity, respectively.

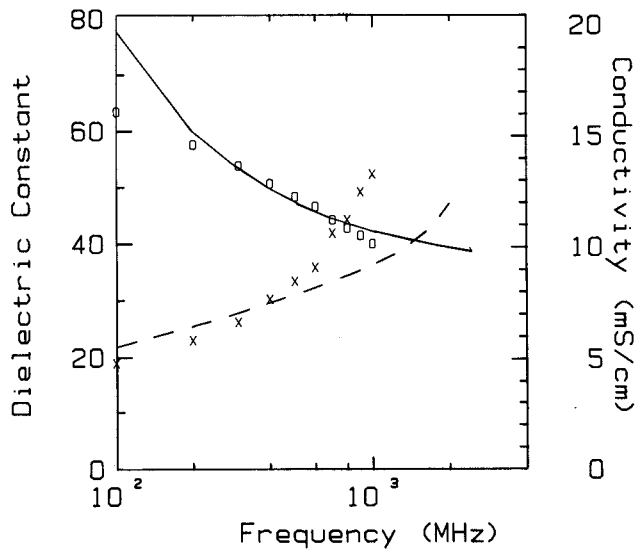

Fig. 2. Properties of simulated brain material compared to expected values (average of white and grey matter). Symbols for Figures 2–5 as in Fig. 1.

1984; Stuchly and Stuchly, 1980] differ significantly. The expected values plotted in Figure 4 and 5 are based on an average of the existing data. In order to simulate bone properties a different approach was necessary because of the relatively low dielectric constant and the desire to have a material that can be cast into the shape of a real bone. There are also experimental situations where it would also be desirable to have a liquid form of bone material so that the interior of the bone may be investigated. To this end we have devised two formulas for bone, one liquid, and the other castable.

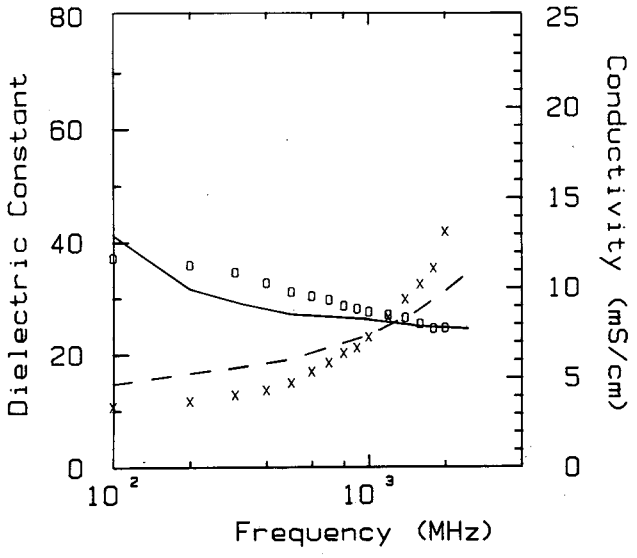

Fig. 3. Simulated lung material dielectric constant and conductivity compared to average properties of inflated and deflated lung.

The castable version is simply made from Devcon two-ton epoxy with a highly conductive potassium chloride (KCl) solution added. The concentration of the salt solution can be adjusted to vary the conductivity of the material and the dielectric constant. The desired conductivity may be achieved when the electrolyte is incorporated into the epoxy, thus forming ionic conductance carriers in the bone equivalent material. The composition of this material is given in Table 1C.

Due to the exothermic reaction some of the water evaporates and the resulting material contains about 0.5% less water than in the original case. The specific density of the resulting material is 0.98 g/cm^{-3}.

This preparation has been found to be easy and fast to produce and it provides reproducible results. The most important aspect of this material is that the dielectric properties of bone material are simulated over a wide frequency range, as shown in Figure 4.

The liquid form of the bone material is made from several chemicals forming a microemulsion. This microemulsion is the same as presented by Foster et al [1982]. Saline solution is added to the microemulsion in order to increase the conductivity.

The amount of NaCl solution and other components of the microemulsion are given in Table 1D. Properties for the liquid bone material are given in Figure 5 and Table 2.

PREPARATION METHODS

The procedure for preparing the tissue equivalent materials are presented here. It is important that the instructions are followed carefully and the material is weighed accurately to obtain reproducible results.

Muscle, Brain, and Lung Tissue Equivalent Material

The following procedure was used to prepare muscle, brain, and lung tissue

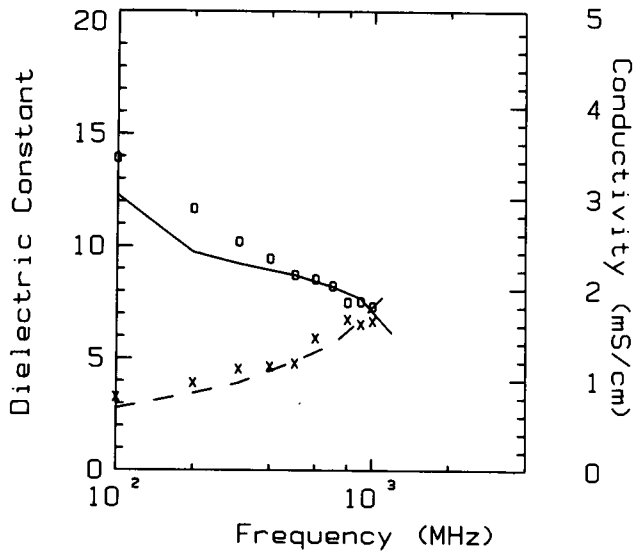

Fig. 4. Electric properties of castable bone-equivalent material.

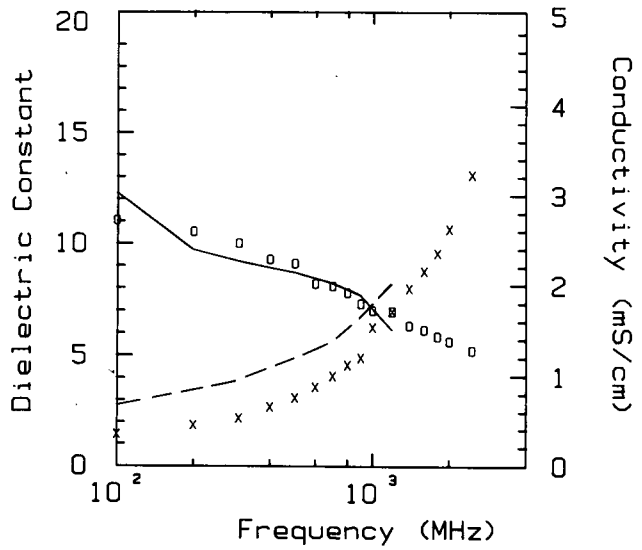

Fig. 5. Electric properties of liquid bone-equivalent material.

equivalent material: (1) Weigh all ingredients accurately. (2) Heat water to 40°C. (3) Add salt and bactericide while stirring. (4) Add sugar (and microspheres in case of lung). (5) Continue to stir at low speed to minimize the amount of air bubbles in the solution. (6) Add the hydroxyethylcellulose (HEC). (7) Remove from heat. (8) Continue to stir until mixture thickens. (9) Let cool to room temperature.

When not in use the material should be stored in a covered container to prevent evaporation of water. If, however, the material does lose some water the original properties can usually be restored by the addition of a small amount of water that is simply stirred into the existing material.

Bone Tissue Equivalent Material

The procedure for preparing the bone equivalent material is as follows: (1) Mix the KCl solution in the proportions given in Table 1C. (2) Add one-quarter of the total amount of KCl solution to the epoxy resin and mix until a homogeneous paste is obtained. (3) Add another 25% of the KCl solution and mix until the material is homogeneous, white, and no water appears on the surface. (4) Add the hardener and mix carefully for about 1 min. (5) Add 25% more KCl and mix using an electric mixer until homogeneous (less than 1 min). (6) Add the remainder of the KCl and continue to mix for 1–2 min. (7) Pour the mixture into molds to set. (8) The material will then slowly begin to solidify producing an exothermic reaction. (9) The material will harden in about 4 h.

The material should then be kept in a moist environment to prevent evaporation of water.

MEASURING TECHNIQUES

The dielectric properties of the tissue simulating materials were measured using an open-ended coaxial-line sensor and a computer-controlled automatic network analyser [Kraszewski et al, 1983]. The system was calibrated with the sensor open-circuited, short-circuited, and immersed in a saline solution to minimize the errors related to the system imperfections. The sensor was then immersed into the material under test (being a liquid or semi-liquid) or was firmly pressed into the flat smooth surface of the cast bone sample. The uncertainty of the measurement was evaluated as being less than 3% for the dielectric constant and 2% for the conductivity of muscle, brain, and lung materials, and less than 5 and 10%, respectively, for bone simulating material.

A summary of the properties of all the materials that have been described are presented in Table 2. This table gives dielectric constants and conductivities at frequencies of 100, 400, and 900 MHz.

SUMMARY

Formulas have been presented along with mixing instructions for the preparation of simulated bone, lung, brain, and muscle material in the frequency range of 100 MHz to 1GHz. These materials are easy to prepare, inexpensive, reproducible, and retain their properties for a long period of time.

The dielectric properties of each of the described materials can easily be changed to match the particular need of an experiment. In general the amount of sodium chloride (or KCl) is responsible for the material's conductivity, and the amount of water influences mainly the value of its dielectric constant. In a limited range these two parameters can be changed almost independent of each other, thus allowing precise simulation of tissue properties at a particular frequency.

With this information it is possible to construct a more realistic model of man for electromagnetic dosimetry studies.

ACKNOWLEDGMENTS

This work was supported by grants from the U.S. Environmental Protection Agency, Health and Welfare Canada, and from the Natural Science and Engineering

Research Council of Canada. The guidance of Dr. S. Stuchly, who proposed this project, is gratefully acknowledged. The authors also wish to thank S. Symons, C. Sibbald, D. M. Bui, J. Dadkhah, and P. Kratchanov for their help in preparing the samples and measuring their dielectric properties.

APPENDIX

List of suppliers for this project includes: Two Ton Epoxy (Devcon Corp., Danvers, MA 01923; NaCl (any grocery store); sucrose (granulated cane sugar, any grocery store); HEC (100,000 A; BP Chemicals) or Natrosol 250 HHR (Hercules Inc., Wilmington, DE 19899); Dowicil 75 (Dow Chemical, Midland, MI 46840); Microspheres (Ecospheres SI, Emerson and Cuming, Canton, MA 02021); KCl, TWEEN, n-amyl alcohol, paraffin oil (Sargent-Welch, Skokie, IL 60077).

REFERENCES

Chou CK, Chen GW, Guy AW, Luk KH (1984): Formulas for preparing phantom muscle tissue at various radiofrequencies. Bioelectromagnetics 5:435–441.

Durney CH, Johnson CC, Barber PW, Massoudi H , Iskander MF, Lords JL, Ryer DK, Allen SJ, Mitchell JC (1978): "Radiofrequency Radiation Dosimetry Handbook, second ed." Brooks AFB, TX: Air Force School of Aerospace Medicine Report, SAM-TR-78-22, pp 50–59.

Foster KR, Epstein BR, Jenin PC, Mackay RA (1982): Dielectric studies on nonionic microemulsions. J Colloid Interface Sci 88:233–246.

Foster KR, Schepps JL, Stoy RD, and Schwan HP (1979): Dielectric properties of brain tissue between 0.01 and 10 GHz. Phys Med Biol 24:1177–1187.

Foster KR, Schwan HP (1986): "Dielectric Properties of Tissue—A Review, Handbook of Biological Effects of Electromagnetic Radiation." Cleveland: CRC Press.

Guy AW (1971): Analysis of electromagnetic fields induced in biological tissues on equivalent phantom models. IEEE Trans Microwave Theory Tech MMT-19:205–214.

Hurt WD (1985): Multiterm Debye dispersion relations for permittivity of muscle. IEEE Trans Biomed Eng BME-32:60–64.

Kraszewski A, Stuchly SS, Stuchly MA, Symons SA (1983): On the measurement accuracy of the tissue permittivity in vivo. IEEE Trans Instrum Meas IM-32:37–42.

Pethig R (1984): Dielectric properties of biological material: Biophysical and medical applications. IEEE Trans Elect Insulation EI-19:453–475.

Stuchly MA, Stuchly SS (1980): Dielectric properties of biological substances—tabulated. J Microwave Power 15:19–26.

Surowiec A, Stuchly SS, Keaney M, Swarup A (in press) Dielectric spectroscopy of inflated and deflated lung. IEEE Trans Biomed Eng.

Bioelectromagnetics 8:37–43 (1987)

Acute, Whole-Body Microwave Exposure and Testicular Function of Rats

R.M. Lebovitz and L. Johnson

Departments of Cell Biology (L.J.) and Physiology (R.M.L.), University of Texas Health Science Center, Dallas

Male Sprague-Dawley rats were exposed for 8 h to continuous-wave microwave radiation (MWR, 1.3 Ghz) at a mean specific absorbed dose rate of 9 mW/g. MWR exposure and sham-irradiation took place in unidirectionally energized cylindrical waveguide sections, within which the animals were essentially unrestrained. The MWR treatment in this setting was determined to yield an elevation of deep rectal temperature to 4.5 °C. The animals were taken for analysis at 6.5, 13, 26, and 52 days following treatment, which corresponded to .5, 1, 2, and 4 cycles of the seminiferous epithelium. Net mass of testes, epididymides, and seminal vesicles; daily sperm production (DSP) per testis and per gram of testis; and the number of epididymal sperm were determined. The levels of circulating follicle-stimulating hormone (FSH) and leutinizing hormone (LH) were derived via radioimmunoassay of plasma samples taken at the time of sacrifice. Despite the evident acute thermogenesis of the MWR at 9 mW/g, no substantial decrement in testicular function was found. We conclude that, in the unrestrained rat, whole body irradiation at 9 mW/g, while sufficient to induce evident hyperthermia, is not a sufficient condition for disruption of any of these key measures of testicular function.

Key words: neurohormones, testis

INTRODUCTION

In previous reports, we indicated that repeated daily exposure to microwave radiation (MWR, 1.3 GHz) at a dose rate of 6.3 mW/g, 6 h per day for 9 days did not significantly perturb testicular function in the adult male rat [Lebovitz and Johnson, 1983; Johnson et al, 1984]. At no stage in the development of the male germ cells could a significant physiologic or morphologic deficit be found. Our approach was to examine testicular function following irradiation at intervals that corresponded to multiples of the 13-day cycle of the seminiferous epithelium of the Sprague-Dawley rat [Clermont, 1962; Clermont and Harvey, 1965; Leblond and Clermont, 1952]. It would thus be possible to test, if a deficit in spermatogenesis were detected at all, at which stage(s) of germ cell maturation maximal sensitivity was evident, and whether this agreed with the results of conventional heating [Setchell and Waites, 1972].

Since, in the previous series of experiments, a moderately thermogenic level of MWR was used (1 to 1.5 °C elevation in rectal temperature), a prolonged course of exposure was felt to be necessary in order to demonstrate any change in testicular

Received for review February 10, 1986; revision received June 27, 1986.

Address reprint requests to Dr. Robert Lebovitz, Department of Physiology, University of Texas Health Science Center, 5323 Harry Hines Blvd., Dallas, TX 75235.

function. Exposure extending over a 9-day period conflicted, however, with the timed sample approach to detecting germ cell differential sensitivity. It was possible, therefore, that a significant stage-specific decrement was missed because of the extended time course of the irradiation. The experiments described here were undertaken, therefore, using a more intense but acute exposure protocol.

METHODS

A total of 32 Sprague-Dawley male rats between 4–5 g initial mass were divided equally into irradiation and sham-irradiation (control) subgroups. Two rats (both irradiated) died several weeks after treatment but prior to their scheduled termination date; the causes of death were undetermined but felt not to be related to the MWR exposure per se.

The animals were kept on a 12/12h light/dark schedule (lights off at 0600 h) and placed in the microwave apparatus during the dark phase. During irradiation, the ambient temperature (23 $\pm$ 1.5 °C) and relative humidity (37% mean, 32 to 45% range) were maintained in the normal range for these animals. The irradiated subgroup was exposed to continuous wave (CW) MWR at 1.3 GHz in cylindrical waveguide sections operating as circularly polarized, unidirectional exposure chambers [Lebovitz and Seaman, 1980] during a single session lasting 8 h. Animals of the control group were handled the same as the irradiated animals and placed in unenergized waveguide chambers for the duration of the irradiation session.

The mean specific absorption rate (SAR) for the irradiated subgroup was 9 mW/g, as determined from previous input/output calibrations at our facility [Lebovitz and Seaman, 1980]. A separate group of body-weight-matched animals was used for the purpose of documenting changes in whole body temperature during exposure at this SAR.

Except for the MWR treatment phase, the animals were randomly grouped and provided with food and water ad lib. Subgroups of treatment and control animals were taken for physiologic and histologic study at either 6.5, 13, 26, or 52 days following irradiation, corresponding to .5, 1, 2, and 4 cycles of spermatogenesis in seminiferous epithelium. At that time, each rat was weighed and decapitated, and trunk blood was taken for subsequent hormonal assay. Testis mass (right and left) and mass of the epididymis and seminal vesicles were individually noted. The right testis was decapsulated and homogenized for 2 min in 1 ml of homogenizing fluid containing 15 mM NaCl, .5% (v/v) Trition X-1, and 3.8 nM NaN_3 [Johnson et al, 1980]. Testicular homogenates were stored at 5 °C and evaluated within 28 h. Only spermatid heads with a shape characteristic of steps 17 through 19 found in stages IV and VIII [Leblond and Clermont, 1952] are resistant to such homogenization; these were enumerated by phase-contrast cytometry. Daily sperm production (DSP) per testis was calculated by dividing the number of homogenization-resistant spermatids by the life span of 6.3 days [Amann et al, 1976; Johnson et al, 1980]. DSP per gram parenchyma (DSP/g) was calculated by dividing the DSP/testis by the difference between testis and tunic mass. The number of sperm in the right epididymis was determined from epididymal homogenates prepared and evaluated as were those for the testes.

Circulating levels of leutinizing hormone (LH) and follicle-stimulating hormone (FSH) were determined from the trunk blood sample using established radioimmu-

noassay techniques [Samson and McCann, 1979] and materials supplied by NIADDK. The results are expressed in terms of the RP reference standards. All of the above determinations were carried out in the "blind" using encoded samples.

RESULTS

The primary aim of these studies was to determine if acute, thermogenic MWR exposure was sufficient to influence the process of spermatogenesis in the unrestrained rat. Calculated DSP /g, presented in terms of cycle periods of the seminiferous epithelium, is shown in Figure 1 for the total of 3 surviving rats. One full spermatogenic cycle takes 52 days in these animals, comprising four 13-day cycles of the seminiferous epithelium [Clermont and Harvey, 1965]. A two-way analysis of variance (ANOVA, unweighted means correction for unequal cell counts using the method of Winer [1971]) revealed no significant treatment effect ($F(1,22) = .09$; $P = .764$). Potential DSP calculated on a per testis basis was similarly unaffected by the exposure ($F(1,22) = 1.059$; $P = .316$). The number of epididymal sperm did appear to be reduced at 26 days following treatment (Fig. 2). However, ANOVA indicated that no treatment effect could be substantiated overall ($F(1,22) = .104$; $P = .748$). There was, however, a marginal indication of interaction between irradiation and post-irradiation sample period ($F(3,22) = 2.676$; $P = .0713$). The isolated subgroup mean epididymal sperm count at 26 days following treatment was, in fact, significantly lower (t-test, $P < .05$) for the irradiated animals. Since confirmation of such a weak interaction was not found in other aspects of these data, we cannot rule out that this was a purely aberrant result. All other subgroup mean differences were not significant. A summary of key physiological data for all treatment groups is presented in Table 1.

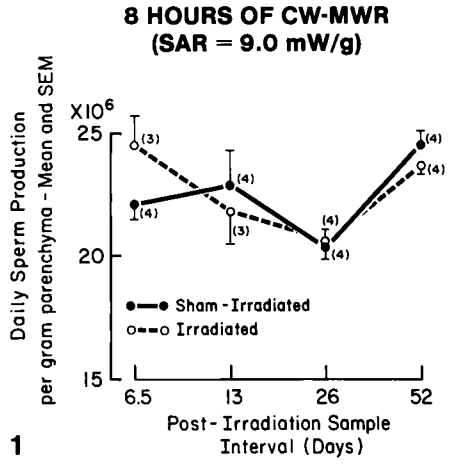

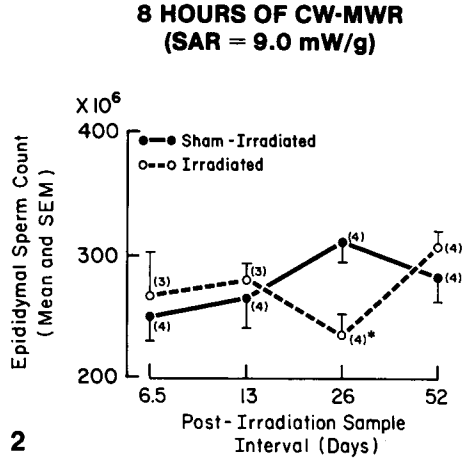

Fig. 1. Calculated DSP/g obtained at four discrete intervals following MWR exposure in a single 8-h session at 9 mW/g (CW). Here, as in Figures 2–4, the number of animals in the specific sample subgroups are indicated in parentheses.

Fig. 2. Epididymal sperm count for the same animals as in Figure 1. The differences between group means at the 26-day post-treatment sample interval were significant in isolation; however, ANOVA applied to the entire experimental group did not reveal a significant difference due to treatment (see text).

TABLE 1. Physiological Parameters Following CW MWR at 9 mW/g†

	Spermatogenic cycle							
	0.5		1		2		4	
	Sham	Irrad	Sham	Irrad	Sham	Irrad	Sham	Irrad
N	4	3	4	3	4	4	4	4
Variable								
Body mass	487.4	479.0	511.8	498.9	519.9	512.4	563.5	552.1
(g)	4.3	12.9	4.2	13.0	12.1	12.0	7.5	19.1
Total testis mass	3.01	3.20	3.13	3.09	3.33	3.24	3.06	3.38
(g)	.03	.17	.14	.02	.14	.16	.12	.17
Right tunic	70.7	72.8	61.8	55.2	69.7	74.6	75.8	80.5
(mg)	4.9	8.2	7.7	4.7	3.7	4.4	3.4	7.3
Left epididymis	.534	.543	.523	.400	.582	.537	.557	.566
(g)	.019	.026	.009	.127	.037	.018	.014	.020
DSP/testis	31.0	37.0	34.1	31.7	31.5	31.1	34.7	37.9
($\times 10^6$)	1.0	3.5	2.9	2.0	0.7	2.4	2.2	1.9
DSP/g	22.1	24.5	22.9	21.8	20.4	20.6	24.5	23.8
($\times 10^6$)	0.6	1.3	1.5	1.2	0.5	.5	0.6	0.2
Right epididymal	250.5	267.0	265.7	281.2	311.2	234.8*	283.2	308.6
sperm count	19.7	36.3	24.8	13.0	16.5	19.7	20.1	10.3
($\times 10^6$)								
Seminal vesicle	1.66	1.69	1.74	1.75	1.53	1.83*	1.56	1.73
(g)	.11	.20	.15	.06	.08	.05	.04	.18

*Difference in subgroup mean significant (Student t) at $P < .05$.

†Data shown are for a single group of 14 irradiated and 16 irradiated-control animals treated simultaneously and taken for analysis at intervals corresponding to .5, 1, 2, and 4 times the cycle period of seminiferous epithelium. The latter corresponds to one full cycle of spermatogenesis. Figures represent mean ± SE.

Seminal vesicle weight would reflect a change in testosterone levels (cf Table 1) and showed no significant difference due to irradiation, although there was a single instance of a significant difference in subgroup means, again at the 26-day post-treatment latency. This measure reflected the response to collective circulating testosterone over a period of time. However, if a reduction in testosterone levels were a result of irradiation, one would expect to observe a relative decrease rather than the increase in seminal vesicle mass that was marginally suggested by these data. Again, two-way ANOVA did not support the conclusion that there were any significant treatment-dependent main ($F(1,22) = 2.178$; $P = .151$) or interaction ($F(3,22) = .638$; $P = .602$) effects for the irradiated group as a whole. More to the point, direct measurement of circulating FSH and LH in the trunk blood taken at the time of termination (Fig. 3) did not show any effect of irradiation. We must conclude from the above data that no substantial neuroendocrine effect was produced by the MWR treatment.

The time course of rectal temperature during irradiation at the 9-mW/g dose rate is shown in Figure 4. Surrogate animals, of the same strain and body mass as that used to obtain the data given above, were used to obtain this thermal profile. Animals were irradiated using identical procedures, and body temperatures were sampled periodically with a rectal probe thermistor. The data indicated that equilibration at an elevated core temperature of 40–41 °C was achieved within 1 h of irradiation and remained stable thereafter. Since the animals were removed from the waveguide periodically for insertion of the rectal probe, and since a slight decline in temperature of the sham-irradiated animals was evident, the MWR-induced whole-body thermal effects shown in Figure 4 must be construed as a conservative underestimate of the actual temperature rise experienced by the animals in the primary experimental group. There was no doubt, therefore, of the significant thermogenic potential for the unrestrained rat of the MWR dose rate utilized in these experiments.

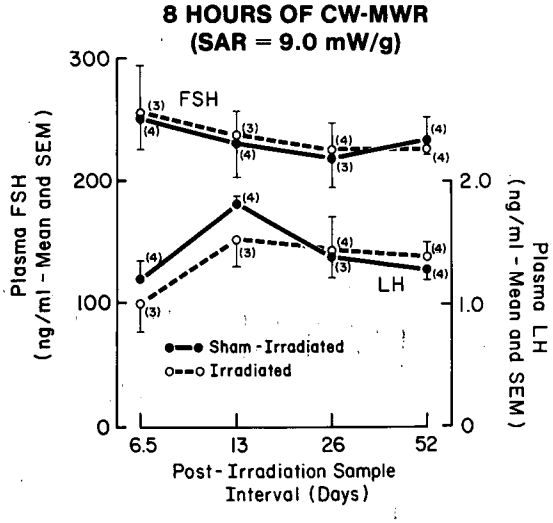

Fig. 3. Circulating FSH and LH levels in plasma taken at the time of sacrifice for testicular examination. The data are within the expected range for normal animals of this age.

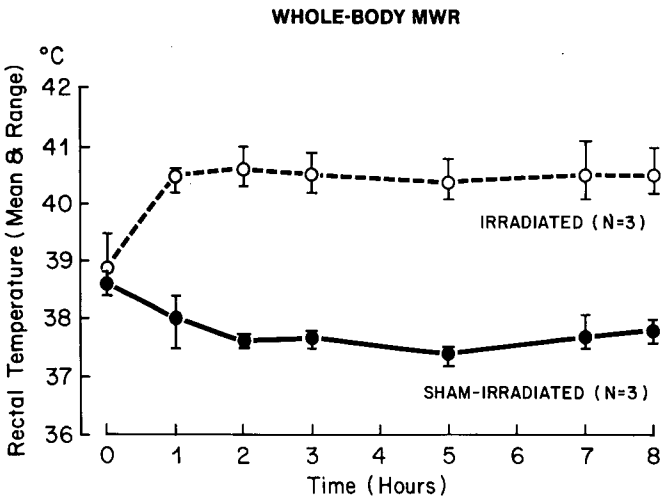

Fig. 4. Rectal temperature in a group of three irradiated and three sham-irradiated animals under the exposure conditions of the primary treatment group whose data appear in Figure 1-3. Temperature data was obtained via insertion of a lubricated rectal probe during brief (less than 2 min) removal of the animal from the waveguide.

DISCUSSION

In previous experiments, whole-body exposure at 6.3 mW/g over several hours did not yield any significant alteration in testicular parameters in the freely mobile rat [Johnson et al, 1984; Lebovitz and Johnson, 1983]. It was of interest, therefore, to consider the effect of an acute dose rate (9 mW/g) at or above the lethal level for chronic exposure using the rat. The expected rise in deep core temperature (Fig. 4) was considerable, yet no notable alteration in testicular parameters could be detected.

The suggestive decline in epididymal sperm count at 26 days would reflect, if real, a threshold decrement on primary spermatogenesis induced the MWR. A differential sensitivity of germ cells at this stage of maturation has been reported with conventional heating of the testes [Chowdhury and Steinberger, 1970]. However, we did not confirm a significant effect of MWR on testicular function by other measures.

In view of the large number of variables measured in this study, the reduction in epididymal sperm count at 26 days after treatment is highly questionable. Further, in view of the unarguable heat-sensitivity of the testis [Chowdhury and Steinberger, 1970; Setchell and Waites, 1972], we must conclude that the clearly thermogenic dose was not sufficient to induce a critical temperature rise in the testes of unrestrained rats. In this respect, our results are in essential agreement with those of Berman et al [1980]. We can, of course, offer no support for macroscopically athermal effects on the testes.

There still remains the question of whether conventional and microwave-induced heating will yield equivalent deficits in testicular function. With all physiologic and/or behavioral thermoregulatory mechanisms intact, it appears that the testis temperature will remain below the critical threshold for damage even with acutely thermogenic levels of whole-body MWR exposure. The next step is to better define the relationship between conventional and MWR-induced heating of the testis. This requires a more controlled preparation, such as immobilized or anesthetized, wherein

testicular dose rate and intratesticular temperature rise can be directly quantified [Lebovitz et al, 1987].

ACKNOWLEDGMENTS

This work was supported by NIH research grant ES-275 and Air Force contract C-616 (to R.M.L.) and NIH research grant HD-16773 (to L.J). We greatly appreciate the courtesy and assistance of Dr. W.K. Samson in performing the plasma FSH and LH radioimmunoassays.

REFERENCES

Amann RP, Johnson L, Thompson DL, Jr, Pickett BW (1976): Daily spermatozoal production, epididymal spermatozoal reserves and transit time of spermatozoa through the epididymis of the rhesus monkey. Biol Reprod 15:586–592.

Berman E, Carter HB, House D (1980): Tests of mutagenesis and reproduction in male rats exposed to 2,45 MHz (CW) microwaves. Bioelectromagnetics 1:65–76.

Chowdhury AK, Steinberger E (1970): Early changes in the germinal epithelium of rat testes following exposure to heat. J Reprod Fert 22:205–212.

Clermont Y (1962): Quantitative analysis of spermatogenesis of the rat: A revised model for the renewal of spermatogonia. Am J Anat 111:111–129.

Clermont Y, Harvey SC (1965): Duration of the cycle of the seminferous epithelium of normal, hypophysectomized and hypophysectomized-hormone treated albino rats. Endocrinology 76:80–89.

Johnson L, Lebovitz RM, Samson WK (1984): Germ cell degeneration in normal and microwave-irradiated rats: Potential sperm production rates at different developmental steps in spermatogenesis. Anat Record 209:501–507.

Johnson L, Petty CS, Neaves WB (1980): A comparative study of daily sperm production and testicular composition in humans and rats. Biol Reprod 22:1233–1243.

Leblond CP, Clermont Y (1952): Definition of the stages of the cycle of the seminiferous epithelium in the rat. Ann NY Acad Sci 55:548–573.

Lebovitz RM, Johnson L (1983): Testicular function of rats following exposure to microwave radiation. Bioelectromagnetics 4:107–114.

Lebovitz RM, Johnson L, Samson WK (1987): Effects of pulse modulated microwave radiation and conventional heating on sperm production in the rat. J Appl Physiol (In press).

Lebovitz RM, Seaman RL (1980): Microwave irradiation and instrumental behavior in rats: Unitized irradiation and behavioral evaluation facility. Bioelectromagnetics 1:415–428.

Samson WK, McCann SM (1979): Effects of lesions in the organum vasculosum lamina terminalis on the hypothalamic distribution of LHRH and gonadotropin secretion in the ovariectomized female rat. Endocrinology 105:939–946.

Setchell BP, Waites GMH (1972): The effects of local heating of the testis on the flow and composition of rete testis fluid in the rat, with some observations on the effects of age and unilateral castration. J Reprod Fert 30:225–233.

Winer BJ (1971): "Statistical Principles in Experimental Design." New York: McGraw-Hill, 907 pp.

Bioelectromagnetics 8:45–55 (1987)

Microwave Facilitation of Domperidone Antagonism of Apomorphine-Induced Stereotypic Climbing in Mice

R.M. Quock, F.J. Kouchich, T.K. Ishii, and D.G. Lange

Toxicology Research Laboratory, Research Service, Clement J. Zablocki Veterans Administration Medical Center, Milwaukee (R.M.Q., F.J.K.); Department of Basic Sciences, Marquette University School of Dentistry (R.M.Q., F.J.K.), and Department of Electrical Engineering and Computer Science, Marquette University School of Engineering (T.K.I.), Milwaukee; Department of Anesthesiology and Critical Care Medicine, The Johns Hopkins Medical Institute, Baltimore (D.G.L.)

The dopaminergic agonist apomorphine produced dose-dependent stereotypic climbing behavior in mice housed in cages with vertical bars. This drug effect was competitively inhibited by systemic pretreatment with the centrally acting dopaminergic antagonist haloperidol but not by microwave irradiation (2.45 GHz, 20 mW/cm^2, CW, 10 min) nor by systemic pretreatment with domperidone, a dopaminergic antagonist that only poorly penetrates the blood–brain barrier (BBB). Yet when mice were systemically pretreated with domperidone and then subjected to microwave irradiation (as above), the apomorphine effect was significantly reduced. Microwave irradiation also facilitated antagonism of the apomorphine effect by low and otherwise ineffective systemic pretreatment doses of haloperidol. Apomorphine-induced stereotypic climbing behavior was also reduced by domperidone administered intracerebrally, which bypassed the BBB. Exposure of intracerebral domperidone-pretreated animals to microwave irradiation failed to increase the degree of antagonism. These findings indicate that microwave irradiation can facilitate central effects of domperidone, a drug which acts mainly in the periphery. One possible explanation for these findings is that microwave irradiation alters the permeability of the BBB and increases the entry of domperidone to central sites of action.

Key words: blood–brain barrier, haloperidol, central vs peripheral actions

INTRODUCTION

In recent years, much interest has emerged in the possible interaction of microwave radiation with biological systems. Our attention was initially drawn to this issue by reports of both microwave-induced alterations in blood–brain barrier (BBB) permeability characteristics to inert radiolabelled markers [Frey et al, 1975; Albert, 1979; Albert and Kerns, 1981] as well as alterations in central nervous system (CNS) effects of a variety of pharmacologic agents [Baranski and Edelwejn, 1968; Thomas

Received for review October 11, 1985; revision received July 18, 1986.

F.J. Kouchich is now at Indiana University School of Optometry, Bloomington, IN 47405.

Address reprint requests to Dr. Raymond M. Quock, Department of Basic Sciences, Marquette University School of Dentistry, 604 North Sixteenth Street, Milwaukee, WI 53233.

and Maitland, 1979; Thomas et al, 1979, 1980; Lai et al, 1983, 1984a,b, 1986]. Unfortunately, there has been little evidence from other groups employing similar techniques to confirm either that the reported change in BBB permeability was a demonstrable phenomenon or that the reported changes in CNS activity of the pharmacologic agents were indeed due to microwave-induced alterations in BBB function [Merritt et al, 1978; Preston et al, 1979; Preston and Préfontaine, 1980].

It is highly probable that differences in animal models and microwave exposure techniques contribute to the lack of agreement on microwave-induced alterations in BBB function. However, we also felt that a more important source of disagreement lies in the relative sensitivities and specificities of the methods employed to evaluate BBB function. Two major techniques are currently employed to evaluate microwave-induced alterations of BBB function: One is histological/ultrastructural [Sutton and Nunnally, 1973; Sutton and Carroll, 1979; Albert, 1977], and the other is physiological [Crone, 1963; Oldendorf, 1970; Rapoport et al, 1978, 1979]. Both types of studies have their relative strengths and weaknesses. The histological/ultrastructural approach is highly site-specific yet lacks sensitivity, and results from such studies are difficult to quantitate. Conversely, physiological methods, although potentially extremely sensitive, usually require changes distributed over large sections of tissue to demonstrate this sensitivity.

In an effort to exploit the strengths of both techniques, we developed a pharmacological assay system, using a CNS agonist that produced a predictable behavioral response, and attempted to employ microwave radiation to alter the CNS availability of an antagonist that was normally excluded from the CNS (based on physicochemical properties). This pharmacological approach enjoyed the advantages of both sensitivity (since it was relatively easy to alter drug dose-response relationships) as well as site specificity (since the agonist/antagonist interaction had been shown to occur in a specific region of the CNS). The technique had an additional advantage in that it permitted a time-dependent evaluation of a microwave-induced response without requiring sacrifice of the test animal. Thus this report describes the influence of microwave radiation on the ability of a non-CNS-acting dopaminergic antagonist, domperidone [Laduron and Leyson, 1979], to block a drug effect of the dopaminergic agonist apomorphine, previously demonstrated to originate from a site-specific action of apomorphine on dopamine receptors in the corpus striatum of the CNS [Protais et al, 1976].

MATERIALS AND METHODS

Over 400 male ICR mice, weighing 20–30 g, were purchased from King Animal Laboratories (Oregon, WI) for these experiments. On the day of the study, animals were acclimated for no less than 60 min to housing in individual circular cages, 12 cm in diameter and 14 cm in height, with 1 mm vertically mounted metal bars spaced 1 cm apart. These cages were additionally separated by cardboard screens to prevent any behavioral interaction between test animals. After conditioning, the animals were challenged with various doses of apomorphine and returned to their individual cages. Assessment of apomorphine-induced stereotypic climbing activity was made according to a previously published method [Quock and Lucas, 1981; Quock et al, 1983]: 0 points, the animals sits with all four paws on the cage floor; 1 point, the animal persistently stands against the cage wall with forepaws grasping the metal bars; and 2

points, the animal persistently climbs on the cage wall with all four paws grasping the metal bars. Scores were assigned by a trained observer who was not blind to the drug or apomorphine treatments; preliminary studies showed that each activity level was quite clear-cut and that prior knowledge of the treatment group did not influence the behavioral scoring. Climbing scores were assigned for two 5 min intervals ending 10 and 20 min following the apomorphine challenge, and the scores were then averaged to yield a stereotypic climbing score for each mouse. The score was determined by the most predominant behavior demonstrated during the 5 min observation period.

In experimental trials, the mice were acclimated to the circular cages, then removed for pretreatment injections followed by either microwave or sham irradiation. Animals were typically run in pairs with both mice receiving injections of the 0.9% saline solvent, haloperidol, or domperidone, then one mouse was subjected to microwave irradiation for 10 min while the other was sham irradiated at the same time. Following the exposure period, the mice were returned to their circular cages for another 20 min before the apomorphine challenge. The protocol for these systemic pretreatment experiments is illustrated in Figure 1. Each animal was used only once and then discarded.

For the purpose of microwave irradiation, we utilized a near-field waveguide microwave exposure system, constructed according to previously published specifications [Ho et al, 1973; Christman et al, 1974]. Conscious and unrestrained test animals were placed individually into a styrofoam containment chamber (5H × 9W × 11L cm) with 6 mm diameter lucite rods traversing the top and bottom of the chamber; the rods were aligned parallel to the vector of the incident electric field to permit adequate ventilation of the animals during exposure. However, unlike with the apparatus of Ho et al [1973], no attempt was made to provide forced ventilation through the exposure chamber. The styrofoam containment chamber was placed into an R-band waveguide (5.4H × 10.9W × 29L cm) modified with hinged screen doors to allow access to the interior. The waveguide was attached by coaxial cable to a 650-W microwave generator (2.45 GHz, continuous wave; CW) operating in a TE_{10} mode. The microwave energy was attenuated by a model 4-5414-30 π-line attenuator

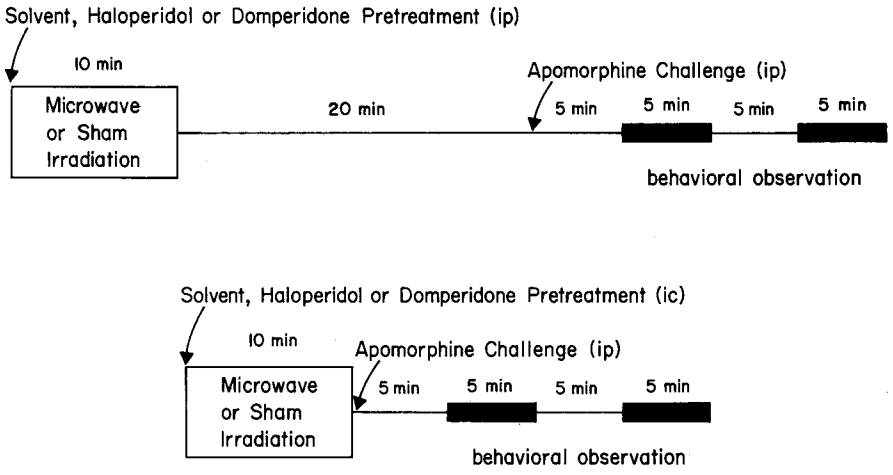

Fig. 1. Time course of experimental protocol for systemic (top) and intracerebral (bottom) pretreatment experiments.

(Arra, Bay Shore, NY), and impedence matching was accomplished using double-stub S2-15N tuners (Microlab/FXR, Livingston, NJ). Transition of the coaxial cable to the R-band waveguide exposure system was accomplished by two model R601C waveguide coaxial adaptors (Microlab/FXR). CB-67N directional couplers (Microlab/FXR) were employed to monitor incident, reflected, and transmitted power using either crystal or bolometer detectors in appropriate detector mounts in conjunction with a model 423A Hewlett-Packard power meter. The maximal power density located at the center of the containment chamber was periodically checked using a model 380m microwave leakage detector (Simpson, Elgin, IL). A specific absorption rate (SAR) of 45.5 W/kg at the nominal incidence flux of 20 mW/cm^2 was calculated in accordance with the Dewar-flask calorimetric technique [Blackman and Black, 1977; Durney et al, 1980] using mouse cadavers aligned parallel to the vector of the incident field. All exposures occurred at an ambient temperature of $22 \pm 1^{\circ}C$ with a relative humidity of approximately 30% in accordance with the observations of Berman et al [1985].

A separate experiment was conducted to determine if the effects of haloperidol might also be potentiated by microwave irradiation. Mice were here pretreated with 0.03 mg/kg of haloperidol, which we had determined in preliminary studies to be a subthreshold dose for antagonism of apomorphine. Animals were then exposed to microwave irradiation, and the influence on apomorphine-induced stereotypic climbing activity was assessed as described above.

Another experiment was conducted to determine if the failure of systemically administered domperidone to antagonize apomorphine was actually due to an inability to penetrate the BBB rather than reduced pharmacological activity compared to haloperidol. The 1 M lactic acid solvent (slightly acidified with glacial acetic acid), haloperidol, and domperidone were administered intracerebrally at a site approximating the lateral cerebral ventricle, thus bypassing the BBB [Haley and McCormick, 1957]. Mice were individually exposed to halothane (Fluothane; Ayerst) on small gauze pads in a large covered beaker; consciousness was lost in 15–20 sec and not regained for 2–3 min. The anesthetized mouse was removed from the beaker and a midline incision made with a scalpel to permit identification of anatomical landmarks on the calvarium. The central microinjection was made at an intracerebral depth of 2.4 mm in a volume of 4 μl slowly infused over 15–20 sec. The method was verified in nontest animals by microinjection of dye marker in similar fashion and central localization of the dye. After 10 min of either microwave or sham irradiation, mice were challenged with apomorphine and evaluated for stereotypic climbing activity (as previously described). The protocol for these intracerebral pretreatment experiments is illustrated in Figure 1.

Drugs used in this study included apomorphine HCl (Merck), haloperidol (Haldol; McNeil), and domperidone (Janssen). Apomorphine was prepared in 0.9% saline solution with one drop of 0.1 N hydrochloric acid per 10 ml of drug solution to stabilize the drug. Haloperidol was diluted to appropriate strength for injection in saline. Domperidone was prepared in 1 M lactic acid rendered slightly more acidic with glacial acetic acid; the final drug solution was titrated to pH 6–7 using 3 M sodium hydroxide. The systemic solvent, haloperidol, and domperidone pretreatments and the apomorphine challenges were all made by intraperitoneal injection in volumes of 0.01 ml/g. Intracerebral solvent, haloperidol, and domperidone pretreatments were made in a volume of 4 μl per animal.

The climbing scores of variously treated groups of animals were analyzed by the Kruskal-Wallis one-way analysis of variance by ranks and the Mann-Whitney U test [Siegel, 1956].

RESULTS

Mice initially placed into the circular cages exhibited exploratory activity of the new environment, including varying degrees of transient cage climbing activity. However, such behavior generally subsided and disappeared after 20–30 min of acclimation. In preliminary experiments, systemic administration of solvent, haloperidol, or domperidone failed to evoke any response resembling apomorphine-induced stereotypic climbing activity in acclimated animals.

Figure 2 shows dose-response curves constructed from the systemic pretreatment experimental data. Groups of control animals challenged with three doses of apomorphine showed progressively greater mean stereotypic climbing scores: 1.0 mg/kg, 0.42 mean $\pm$ 0.10 SEM, n = 20; 2.0 mg/kg, 1.35 $\pm$ 0.08, n = 20; 3.0 mg/kg, 1.68 $\pm$ 0.12, n = 20. Each mean stereotypic climbing score was significantly different from the others ($P < 0.05$, Mann-Whitney U test). Microwave irradiation 20 min prior to apomorphine challenge had no appreciable influence on either the mean stereotypic climbing scores or the apomorphine dose-reponse curve. To demonstrate the sensitivity of this assay system to drug antagonism, the centrally acting dopaminergic antagonist haloperidol was administered at a systemic pretreatment dose of 0.1 mg/kg; this pretreatment significantly lowered the mean stereotypic climbing scores at all three challenge doses of apomorphine. In contrast, the peripherally acting dopaminergic antagonist domperidone at a systemic pretreatment dose of 1.0 mg/kg exerted no significant influence on apomorphine stereotypic climbing scores. How-

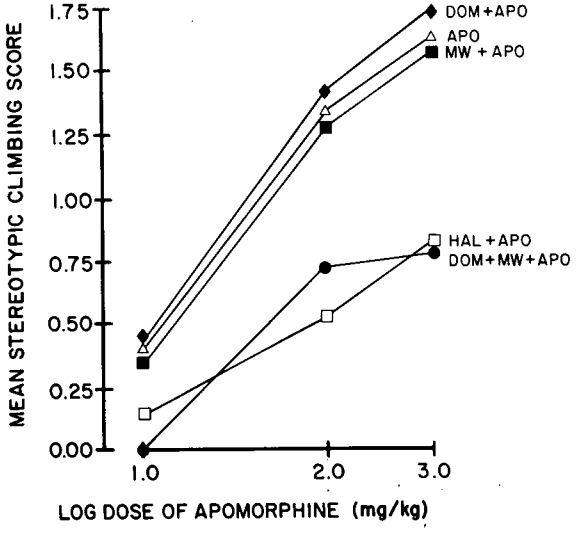

Fig. 2. Dose-response curves for apomorphine-induced stereotypic climbing activity in mice: △, control; ■, microwave-irradiated; □, haloperidol-pretreated; ♦, domperidone-pretreated mice; and ●, domperidone-pretreated and microwave-irradiated. Specific drug pretreatment doses and times and microwave exposure power densities and times can be found in the text. Points indicate the mean stereotypic climbing scores of groups of 20–28 mice each.

ever, the combination of domperidone pretreatment plus microwave irradiation, each of which alone had no effect on apomorphine, significantly reduced the mean stereotypic climbing scores at all three challenge doses of apomorphine. Although there were insufficient data to generate pA_2 [Arunlakshana and Schild, 1959] or even double reciprocal plots [Webb, 1963], it appeared that microwave irradiation had altered the potency of domperidone.

Table 1 shows the mean stereotypic climbing scores evoked by a single challenge dose of apomorphine (2.0 mg/kg) in mice following low-dose systemic haloperidol pretreatment with and without microwave irradiation. The data show that haloperidol at a subthreshold dose of 0.03 mg/kg produced no appreciable influence on the mean stereotypic climbing score. However, in mice pretreated with this low dose of haloperidol, then exposed to microwave irradiation for 10 min, the mean apomorphine-induced climbing score was significantly reduced. This experiment suggests that microwave irradiation can also facilitate central effects of low and otherwise inactive doses of haloperidol.

Table 2 shows the mean stereotypic climbing scores evoked by a single challenge dose of apomorphine (2.0 mg/kg) in control and intracerebrally drug-pretreated and/or microwave-irradiated mice. The data show that haloperidol at an intracerebral pretreatment dose of 1 μg significantly reduced the mean stereotypic climbing score. In comparison, domperidone at an intracerebral pretreatment dose of 3 μg also significantly reduced the mean stereotypic climbing score. Microwave irradiation of animals pretreated intracerebrally with domperidone did not alter the results obtained in the absence of microwave irradiation. Thus it did not appear that microwave exposure altered dopaminergic receptor function.

TABLE 1. Influence of Microwave Irradiation on Haloperidol Antagonism of Apomorphine-Induced Stereotypic Climbing Behavior in Mice

Treatment group	N	Challenge dose of apomorphine (2.0 mg/kg)
Apomorphine control	20	1.35
Haloperidol (0.1 mg/kg, IP) + apomorphine	25	0.53*
Haloperidol (0.03 mg/kg, IP) + apomorphine	19	1.24
Haloperidol (0.03 mg/kg, IP) + microwave irradiation + apomorphine	20	0.85*,**
Kruskal-Wallis ANOVA		0.001

*Significantly different from apomorphine control group at $P < 0.05$ (Mann-Whitney U test).
**Significantly different from haloperidol (0.03 mg/kg) pretreatment group at $P < 0.05$.

TABLE 2. Influence of Microwave Irradiation and/or Intracerebral Pretreament With Dopaminergic Antagonists on Apomorphine-Induced Stereotypic Climbing Behavior in Mice

Treatment group	N	Challenge dose of apomorphine (2.0 mg/kg)
Apomorphine control	20	1.35
Haloperidol (1 μg, IC) + apomorphine	20	0.15*
Domperidone (3 μg, IC) + apomorphine	23	1.03*,**
Domperidone (3 μg, IC) + microwave irradiation + apomorphine	23	1.08*,**
Kruskal-Wallis ANOVA		0.001

*Significantly different from apomorphine control group at $P < 0.05$ (Mann-Whitney U test).
**Significantly different from haloperidol pretreatment group at $P < 0.05$.

DISCUSSION

Previous reports describing the effects of microwave irradiation on BBB function and permeability characteristics have been equivocal. Findings suggestive of microwave-induced alterations in penetration of the BBB by inert radioactive tracers (sucrose or mannitol) have recently been reinterpreted actually to present alterations in cerebral blood flow [see review of Justesen, 1980]. Histological evaluations, based on protein-bound fluorescent dyes, or electron microscopic demonstration of enzyme reaction products (horseradish peroxidase) have demonstrated changes in BBB permeability, but quantitation of the results and subsequent extrapolation to physiological, pharmacological, or toxicological implications have been difficult. We have attempted to utilize the major advantageous characteristics of these two types of studies to delineate more clearly a microwave-induced alteration in BBB permeability. Thus we have developed an agonist/antagonist pharmacological assay technique that can duplicate the sensitivity of the radiotracer techniques [Oldendorf, 1970; Rapoport et al, 1978, 1979]. It shares some of the advantages of the discrete localization characteristics of histological techniques. Moreover, our assay has the distinct added advantages of monitoring an intact animal model without inducing tissue damage as well as demonstrating a pharmacologically relevant effect.

Although a number of studies have demonstrated a microwave-induced facilitation of other centrally acting pharmacologic agents [Thomas et al, 1979; Ashani et al, 1980; Benson et al, 1983], none of these studies took advantage of exogenous drug agonist/antagonist interactions. What we have attempted is the amplification of a small physiological effect by exploiting varying receptor affinities and/or availabilities for a centrally mediated agonist/antagonist interaction. Systemic challenge with the lipophilic agonist apomorphine permits rapid entry into the CNS without significant effects or changes in capillary endothelial cell permeability characteristics, since its uptake into the CNS is predominantly a function of its lipophilicity. Conversely, the systemic administration of the hydrophilic antagonist domperidone results in minimal penetration of the compound into the CNS, which results in maximal sensitivity to changes in capillary endothelial cell permeability characteristics. Thus we were able to monitor selectively the effects of altered BBB permeability on the CNS availability

of the antagonist. In addition, if the relative affinity of the antagonist is significantly greater than that of the agonist, we should be able to amplify greatly the behavioral response of the animal model to the agonist/antagonist interaction.

In the present investigation, the interaction between apomorphine and domperidone was selected for the following reasons. Apomorphine has clearly been shown to produce site-specific activation of dopaminergic receptors in the corpus striatum to evoke stereotypic climbing behavior [Protais et al, 1976]. Suppression of apomorphine-induced stereotypic climbing has in fact been popularly used as a screen for identification of drugs with potential neuroleptic activity [Costall et al, 1978; Wallach et al, 1980]. Domperidone has been demonstrated to possess a dopaminergic receptor blocking property, yet it does not readily penetrate the BBB, so its activity is largely restricted to the periphery [Laduron and Leysen, 1979]. Previous studies have shown that domperidone and haloperidol have similar IC_{50} values (5 nM) for displacement of ^{3}H-apomorphine in rat brain striatal tissue [Leysen, 1980]. However, domperidone is distributed in the CNS differently from classical neuroleptic agents [Laduron and Leysen, 1979]. Following peripheral administration, its duration of action is as long as 16 hr [Farah et al, 1983]. Thus using this unique combination of apomorphine and domperidone in our particular assay system fulfilled our requirements and has the potential for demonstrating microwave-induced alterations in BBB function.

Our findings in the present study show clearly that domperidone possessed central dopaminergic antagonistic properties normally not manifested because of its failure to penetrate the BBB. When domperidone is systemically administered, there is no change in apomorphine-induced stereotypic climbing. Microwave irradiation of systemic domperidone-pretreated animals produces significant antagonism of apomorphine by domperidone, comparable to the haloperidol-pretreated animals. This finding suggests an increase in the CNS availability of domperidone in microwave-irradiated animals. When domperidone is intracerebrally administered—bypassing the BBB—the apomorphine drug effect is markedly reduced, which verifies the inherent dopaminergic antagonistic property of domperidone. Microwave irradiation of the intracerebral domperidone-pretreated animals failed to increase the antagonism of the apomorphine drug effect. This suggests that the site of the microwave influence is not at the level of the dopaminergic receptor.

Our findings also indicate that microwave exposure can increase the antagonism of apomorphine drug effects by both haloperidol (at low concentrations) and domperidone. This observation suggests that haloperidol and domperidone share some common mechanism for gaining accessibility to the CNS since the apparent availability of each is enhanced by microwave irradiation.

One possible mechanism by which microwave irradiation could alter the CNS availability of exogenously adminstered drugs is through a change in the cerebral blood flow [Oscar and Hawkins, 1977; Preston et al, 1979; Oscar et al, 1981]. The CNS availability of exogenous compounds with low extraction coefficients, such as domperidone, is not dependent on tissue perfusion rates as demonstrated by in vivo studies [Wilkinson and Schand, 1975; Benson et al, 1983; Quock et al, 1986; Eger, 1974] and by mathematical models [Papenfuss and Gross, 1980]. These studies support the hypothesis that the increase in cerebral blood flow, secondary to the hyperthermic response to microwave irradiation, is not responsible for our observation of altered potency of domperidone. However, until the converse hypothesis is tested, the possibility of altered cerebral blood flow participating in our observations cannot be excluded.

Other investigators have also studied the influence of microwave irradiation on brain dopaminergic systems. Microwave irradation has been reported to augment apomorphine-induced hypothermia and stereotyped behavior in rats [Lai et al, 1983]. This is at first glance inconsistent with our findings, which showed no influence of microwave irradiation on apomorphine-induced stereotypic climbing activity. However, in the Lai et al study, rats were exposed to 1 mW/cm^2 of microwave irradiation for 45 min immediately prior to apomorphine challenge, whereas our mice were exposed to 20 mW/cm^2 of microwave irradiation for 10 min, ending 20 min before the apomorphine challenge. Since microwave-induced changes in permeability of the BBB are thought to be reversible in nature, it is possible that the potential for enhancement of the apomorphine drug effect in our mice had dissipated by 20 min after irradiation. However, other investigators have reported partial reversibility of the microwave effect on the BBB after 60 min [Oscar and Hawkins, 1977; Albert and Kerns, 1981].

In summary, our findings clearly demonstrate that exposure to microwave radiation can alter the CNS potency of systemically applied agents. This facilitation of apomorphine antagonism by domperidone appeared to be secondary to an alteration in CNS availability, which by experimental design was insensitive to microwave-induced alterations in cerebral blood flow. Microwave irradiation did not alter the central activity of domperidone by influencing its interaction with dopaminergic receptors, since direct intracerebral domperidone pretreatment was insensitive to potency changes following exposure to microwave radiation. Although histological evidence of altered capillary endothelial cell tight-junction dysfunction cannot be disclaimed at an SAR of 45.5 W/kg (20 mW/cm^2 near field), we have preliminary data demonstrating no alteration in tight-junction integrity at 23.7 W/kg (10 mW/cm^2 near field) in a similar agonist/antagonist interaction paradigm [Quock et al, 1986]. We believe that the most probable explanation for our observation of microwave-induced alteration in BBB permeability to domperidone is through a stimulation of micropinocytotic activity, as previously postulated by other investigators [Albert and Kerns, 1981]. However, additional confirmatory evidence must be achieved before this hypothesized mechanism can be successfully defended.

One final issue that must be addressed is the stimulus produced by the exposure to microwave radiation. Presently, it is proposed that our observations are secondary to a thermal response of the organism to the applied microwave field. Although the alteration in core body temperature, above control animals, is usually within the diurnal temperature fluctuation range of mice (± 1.0 °C) for exposure power of 20 mW/cm^2 for 10 min or less, it is obvious from the SAR data that a significant thermal stress had been applied in our animal model. Currently, we are investigating alternative thermal application techniques to evaluate the possibility that microwave irradiation, because of its relatively unique pattern of energy deposition in vivo, is much more effective at producing change in CNS micropinocytotic activity than other stimuli. This clearly appears to be the case in other organ systems but remains to be clarified in CNS capillary endothelial cells.

ACKNOWLEDGMENTS

This research was supported in part by NIH grant ES-03386 and the Clement J. Zablocki Veterans Administration Medical Center (Milwaukee). We are grateful to

Janssen Pharmaceutica (Beerse, Belgium) for the generous gift of domperidone. We also thank Dawn Braatz for her artwork.

REFERENCES

Albert EN (1977): Light and electron microscopic observations on the blood-brain barrier after microwave irradiation. In Hazzard DG (ed). "Symposium on Biological Effects and Measurements of Radio Frequency/Microwaves." Washington, DC: DHEW (HEW Publication FDA 77-8026), pp 294–304.

Albert EN (1979): Reversibility of microwave-induced blood-brain barrier permeability. Radio Sci 14:323–327.

Albert EN, Kerns JM (1981): Reversible microwave effects on the blood–brain barrier. Brain Res 230:153–164.

Arunlakshana O, Schild HO (1959): Some quantitative uses of drug antagonists. Br J Pharmacol Chemother 14:48–58.

Ashani K, Henry FH, Catravas GN (1980): Combined effects of anticholinesterase drugs and low level microwave radiation. Radiat Res 84:496–503.

Baranski S, Edelwejn Z (1968): Studies on the combined effects of microwaves and some drugs on bioelectric activity of the rabbit central nervous system. Acta Physiol Polon 19:37–50.

Benson EB, Lange DB, Fujimoto JM, Ishii TK (1983): Effects of acute microwave irradiation on phenobarbital sleep and disposition to brain in mice. J Toxicol Environ Health 11:261–274.

Berman E, Kinn JB, Ali J, Carter HB, Retinberg B, Stead AG (1985): Lethality in mice and rats exposed to 2450 MHz circularly polarized microwaves as a function of exposure duration and environmental factors. J Appl Toxicol 5:23–31.

Blackman CF, Black JA (1977): Measurement of microwave radiation absorbed by biological systems. 2. Analysis by Dewar-flask calorimetry. Radio Sci 12:9–14.

Christman CI, Ho HS, Yarrow S (1974): A microwave dosimetry system for measured sampled integral-dose rate. IEEE Trans Microwave Theory Tech MTT 22:1267–1272.

Costall B, Naylor RJ, Nohria V (1978): Climbing behavior induced by apomorphine in mice: A potential model for the detection of neuroleptic activity. Eur J Pharmacol 50:39–50.

Crone C (1963): The permeability of capillaries in various organs as determined by use of the "indicator diffusion" method. Acta Physiol Scand 58:292–305.

Durney CH, Iskander MF, Massoudi H, Allen SJ, Mitchell JC (eds) (1980): Dosimetric measurement techniques. In "Radiofrequency Radiation Dosimetry Handbook, 3rd ed." SAM TR-80-32. Springfield, IL: NTIS, pp 29–30.

Eger EI (1974): Chapter 7. Ventilation, circulation and uptake. In: "Anesthetic Uptake and Action." Baltimore: Williams and Wilkins, pp 122–145.

Farah JM Jr, Demarest KT, Moore KE (1983): A comparison of domperidone and haloperidol effects of different dopaminergic neurons in rat brain. Life Sci 33:1561–1566.

Frey AH, Feld SR, Frey B (1975): Neural function and behavior: Defining the relationship. Ann NY Acad Sci 247:433–438.

Haley TJ, McCormick WG (1957): Pharmacological effects produced by intracerebral injection of drugs in the conscious mouse. Br J Pharmacol 12:12–15.

Ho HS, Ginns EI, Christman CL (1973): Environmentally controlled waveguide irradiation facility. IEEE Trans Microwave Theory Tech MTT 21:837–840.

Justesen DR (1980): Microwave irradiation and the blood-brain barrier. Proc IEEE 68:60–67.

Laduron PM, Leysen JE (1979): Domperidone, a specific in vitro dopamine antagonist, devoid of in vivo central dopaminergic activity. Biochem Pharmacol 28:2161–2165.

Lai H, Horita A, Chou CK, Guy AW (1983): Psychoactive-drug response is affected by acute low-level microwave irradiation. Bioelectromagnetics 4:205–214.

Lai H, Horita A, Chou CK, Guy AW (1984a): Effects of acute low-level microwaves on pentobarbital-induced hypothermia depend on exposure orientation. Bioelectromagnetics 5:203–211.

Lai H, Horita A, Chou CK, Guy AW (1984b): Ethanol-induced hypothermia and ethanol consumption in the rat are affected by low-level microwave irradiation. Bioelectromagnetics 5:213–220.

Lai H, Horita A, Chou CK, Guy AW (1986): Effects of low-level microwave irradiation on amphetamine hyperthermia are blockage by naloxone and classically conditionable. Psychopharmacology 88:354–361.

Leysen JE (1980): ^{3}H-apomorphine receptors in various rat brain regions: A study of specific and non-specific binding. Influence of chronic neuroleptic treatment. In Cattabeni F, Spano PF, Racagni G, Costa E (eds): "Long-Term Effects of Neuroleptics." New York: Raven Press (Adv Biochem Psychopharmacol Vol 24) pp 123–132.

Merritt JH, Chamness AF, Allen SJ (1978): Studies on blood–brain barrier permeability after microwave radiation. Radiat Environ Biophys 15:367-377.

Oldendorf WH (1970): Measurement of brain uptake of radiolabeled substances using a tritiated water internal standard. Brain Res 24:372–376.

Oscar KJ, Gruenau SP, Folker MT, Rapoport SI (1981): Local cerebral blood flow after microwave exposure. Brain Res 204:220–225.

Oscar KJ, Hawkins TD (1977): Microwave alterations of the blood–brain-barrier system of rats. Brain Res 126:281–293.

Papenfuss HD, Gross JF (1980): Transluminal filtration. In Gross JF, Popel A (eds): "Mathematics of Microcirculation Phenomena." New York: Raven Press, pp 41–62.

Preston E, Préfontaine G (1980): Cerebrovascular permeability to sucrose in the rat exposed to 2450 MHz microwaves. J Appl Physiol [Resp Environ Physiol] 49:218–223.

Preston E, Vavasour EJ, Assenheim HM (1979): Permeability of the blood-brain barrier to mannitol in the rat following 2450 MHz microwave irradiation. Brain Res 174:109–117.

Protais P, Costentin J, Schwartz JC (1976): Climbing behavior induced by apomorphine in mice: A simple test for the study of dopamine receptors in striatum. Psychopharmacology 50:1–6.

Quock RM, Fujimoto JM, Ishii TK, Lange DG (1986): Microwave facilitation of methylatropine antagonism of central cholinomimetic drug effects. Radiat Res 105:328–340.

Quock RM, Lucas TS (1981): Enhancement of apomorphine-induced climbing in mice by reversible and irreversible narcotic antagonist drugs. Life Sci 28:1421–1424.

Quock RM, Lucas TS, Hartl TJ (1983): Potentiation of apomorphine-induced stereotypes by naloxone and L-prolyl-L-leucyl-glycinamide. Pharmacol Biochem Behav 19:49–52.

Rapoport SI, Ohno K, Fredericks WR, Pettigew KD (1978): Regional cerebrovascular permeability to [^{14}C]-sucrose after osmotic opening of the blood-brain barrier. Brain Res 150:653–657.

Rapoport SI, Ohno K, Fredericks WR, Pettigew KD (1979): A quantitative method for measuring altered cerebrovascular permeability. Radio Sci 14:345–348.

Siegel S (1956): "Nonparametric Statistics for the Behavioral Sciences." New York: McGraw-Hill.

Sutton CH, Carroll FB (1979): Effects of microwave-induced hyperthermia on the blood–brain barrier of the rat. Radio Sci 14:329–334.

Sutton CH, Nunnally RL (1973): Exogenous peroxidase activity in the selectively hyperthermic rat brain. Fed Proc 32:849.

Thomas JR, Burch LS, Yeandle SS (1979): Microwave radiation and chlordiazepoxide: Synergistic effects on fixed-internal behavior. Science 203:1357–1358.

Thomas JR, Maitland G (1979): Microwave radiation and dextroamphetamine: Evidence of combined effects on behavior of rats. Radio Sci 14(6S):253–258.

Thomas JR, Schrot J, Banvard RA (1980): Behavioral effects of chlorpromazine and diazepam combined with low-level microwaves. Neurobehav Toxicol 2:131–135.

Wallach MB, Hedley LR, Peterson KE, Schulz CH (1980): Antagonism of apomorphine induced climbing: Is it a valid model for neuroleptic activity? Proc West Pharmacol Soc 23:93–98.

Webb JL (1963): "Enzyme and Metabolic Inhibitors." New York: Academic Press.

Wilkinson GR, Shand DG (1975): Commentary: A physiological approach to hepatic drug clearance. Clin Pharmacol Ther 18:377–390.

Bioelectromagnetics 8:57–72 (1987)

Effects of 60-Hz Electric Fields on Cellular Elongation and Radial Expansion Growth in Cucurbit Roots

Andrew A. Brayman, Morton W. Miller, and Christopher Cox

Department of Radiation Biology and Biophysics (A.A.B., M.W.M.), and Division of Biostatistics (C.C.), School of Medicine and Dentistry, The University of Rochester, Rochester, New York

Serial longitudinal and transverse sections were prepared from roots of *Cucumis sativus* and *Cucurbita maxima* that had been exposed/sham-exposed to 60-Hz electric fields for 0–2 days. Field exposures were selected to produce a 10–20% or a 70–80% growth inhibition in whole roots of both species. Cortical cell length and diameter were measured using a microscope and eyepiece micrometer; measurements were conducted "blind." In both species, inhibition of cellular elongation was associated with exposure to electric fields (EF). Cellular radial expansion was apparently unaffected by exposure to electric fields. The diameters of radially unexpanded or fully expanded *C. sativus* cortical cells were about 25–30% smaller than those of comparable cells in *C. maxima* roots. Previous studies of the relationship between rates of root growth and applied EF strength showed that the response thresholds of *C. sativus* and *C. maxima* differed by a similar relative amount. These results are consistent with the postulate that EF-induced effects in roots are elicited by induced transmembrane potentials.

Key words: root cell growth, *Cucumis sativus* roots, *Cucurbita maxima* roots

INTRODUCTION

The growth of plant roots exposed to 60-Hz electric fields (EF) in an aqueous medium is inhibited at field strengths greater than a defined threshold value, which varies among species [Brayman and Miller, 1986; Inoue et al, 1985b; Robertson and Miller, 1981]. Cytohistological analysis of 60-Hz EF-exposed *Pisum* roots indicates that the applied EF has a minimal effect on cell proliferation and a large effect on cellular elongation [Brulfert et al, 1985]. Indirect evidence suggests that a similar phenomenon occurs in 60-Hz EF-exposed cucurbit roots [Brayman et al, 1986]. EF-induced effects on elongation growth were observed within the region of elongation of *Cucumis* and *Cucurbita* roots, the severity of which increased with increasing distance from the root tip. At EF strengths sufficient to reduce rates of root growth by 70–80% there was no effect on the growth of the terminal 1 mm of the root in either species [Brayman et al, 1986].

The experiments described herein were designed to test directly the postulate that 60-Hz EF exposure inhibits cellular elongation growth in cucurbitaceous roots as

Received for review January 28, 1986; revision received June 26, 1986.

Address reprint requests to Dr. A.A. Brayman, Dept. of Radiation Biology and Biophysics, School of Medicine and Dentistry, The University of Rochester, Rochester, NY 14642.

it does in *Pisum* roots. An additional goal was to test further the hypothesis that such effects are related to 60-Hz-induced transmembrane potentials [Miller et al, 1980, 1983, 1985; Inoue et al, 1985b] by using the cell size data to estimate the induced potentials arising in the root cells under various EF exposure conditions.

MATERIALS AND METHODS

Exposure of Roots and Preparation of Sections

Seeds of *Cucumis sativus* (L.) c.v. "Regal" (cucumber) or *Cucurbita maxima* (Duchesne) c.v. "Big Max" (pumpkin) were prepared for use as described previously [Brayman and Miller, 1986]. Approximately 160 roots were selected on the basis of uniform root length (≈ 5 cm) and straightness. Twelve roots were randomly selected from this population; the terminal 5 cm of these roots was excised and immediately fixed in formalin:acetic acid:ethanol fixative (9 vol. 50% ethanol:0.5 vol. glacial acetic acid:0.5 vol. commercial formalin solution). These roots served as day 0 controls. The remaining roots were used to constitute the "exposure" and "sham-exposure" portions of two EF-generation devices described in detail elsewhere [Robertson and Miller, 1981; Robertson et al, 1981]. Briefly, roots were exposed/sham-exposed in Voth and Hamner [1943] No. 5 inorganic growth medium (60-Hz conductivity ≈ 0.07 S $\cdot$ m^{-1}); the applied EF were perpendicular to the long axes of the roots. The roots of each species were exposed/sham-exposed to low-strength 60-Hz EF (*C. sativus*: 350 V $\cdot$ m^{-1}; *C. maxima*: 225 V $\cdot$ m^{-1}) or high-strength 60-Hz EF (*C. sativus*: 450 V $\cdot$ m^{-1}; *C. maxima*: 350 V $\cdot$ m^{-1}). The terms low- and high-strength electric fields were assigned on the basis of the known response of whole root growth to these fields: The low field exposure reduced the second-day growth rate of exposed roots to about 80–90% of sham-exposed rates; high-field exposure reduced the relative growth rate of exposed roots to $\approx$25–30% of sham-exposed root growth rates after 2 days of exposure [Brayman and Miller, 1986].

After 24 hr of exposure/sham-exposure, 12 field-exposed roots were randomly withdrawn from both the high- and low-field incubators. The terminal 5 cm of these roots was excised and fixed as described. Six sham-exposed roots were randomly withdrawn from the sham-exposure side of each incubator (low-field and high-field), pooled to provide n = 12 sham-exposed roots, and similarly treated. After 48 hr of exposure, the procedure was repeated. Thus, the terms sham-exposed and 0 V $\cdot$ m^{-1}-exposed are synonymous, with sham-exposure representing a random sampling of roots not exposed to 60-Hz EF but exposed to growth medium from either the low- or high-field exposure apparatus.

The fixed roots were sent to a histology laboratory (Western New York Pathology Services, P.C., Buffalo, NY) where they were dehydrated, embedded in paraffin, sectioned, and stained with safranin and fast green. From the 12 fixed roots within each series (field strength $\times$ exposure duration $\times$ species), eight roots were selected by personnel at the histology laboratory for sectioning. Four of these roots were used to prepare serial longitudinal sections of the distal $\approx$1.2–1.5 cm of the root, and another four were used to prepare serial cross sections of the distal $\approx$1.2 cm of the root. Section thickness was 10 μm in both series. Every tissue section was mounted and stained.

Analysis of Sections

The prepared slides were encoded by the histology laboratory personnel with a series number corresponding to the EF-exposure history of that particular root. The

root sections were thus scored "blind," with the investigator unaware of the exposure history of the material under study.

Root cell dimensions were measured using a Zeiss photomicroscope fitted with an eyepiece micrometer. The eyepiece micrometer had 100 divisions and was calibrated with a stage micrometer slide having 10-μm divisions.

Cortical cells were selected for study because they constitute a large fraction of the root volume, undergo elongation and radial expansion growth, and collectively form a homogeneous tissue. To quantify the position of a particular location in the root, the anatomical reference point used by Mallory et al [1970] was adopted for use in this study. This reference point was the region of the root where a complete procambial cylinder was first evident and was designated VC_d (vascular cylinder distinguishable). In cross section, VC_d was readily identified, and fixed distances from VC_d were determined by counting the number of 10-μm sections between VC_d and the desired location. In longitudinal section, determination of the distance of a particular point from VC_d was more difficult. A mask of translucent tape was placed on the coverslip directly over the three sections most closely approximating the median longitudinal plane through each root. The slide was placed under a stereomicroscope and the outline of the sections incised in the tape. The tape directly over the specimens was then removed. Reference nicks were made in the adhesive tape mask adjacent to where the vascular cylinder was first visible in the sections. With the use of a calibrated eyepiece micrometer, the tape was incised with reference marks at 0.5-mm intervals from 0 to 3 mm from VC_d, at 1-mm intervals from 3 to 6 mm from VC_d, and at 2-mm intervals from 6 to 10 mm from VC_d. A reference scalar was thus generated for each longitudinal section.

Cellular radial dimension was measured using slides prepared from serial cross sections of the roots. After identification of the tissue section representing VC_d, the tissue sections corresponding to the desired distances from VC_d were examined. By manipulation of the microscope stage controls, radial transects of each tissue section were achieved; the cell wall-to-cell wall radial dimension of each cortical cell lying along these transects was measured until 40 independent cell diameter observations had been recorded at each of the specified locations along the root. Three roots were examined per treatment group. At each sampling location within individual roots, the 40 cell diameter observations were averaged, providing an individual root mean estimate of cell diameter at each distance from VC_d. When cell diameters were compared between species or treatments, the average of the individual root means ($n = 3$) was calculated for each species, treatment group, and sampling location.

Cortical cell length was measured using slides prepared from serial longitudinal sections of the roots. With the adhesive tape scalars described earlier to locate the desired regions of the root sections (ie, distances from VC_d), transects were conducted perpendicular to the root axis and parallel to the scalar graduations. The distance between the transverse walls of each cortical cell lying along a transect was measured. However, many of the cortical cells lacked one of the transverse cell walls, and the root cortex in cucurbits is only about 10 cells thick [Hayward, 1938]. It was therefore difficult to measure an adequate number of cells at a particular distance from VC_d when only one longitudinal section was examined per root. Accordingly, the three consecutive serial sections approximating the median longitudinal plane of each root were examined. When possible, 15 cortical cell lengths were measured at the specified distance from VC_d in each of these sections. Data for each distance from VC_d were

pooled across sections and within individual roots; there were thus 45 cell length measurements per distance from VC_d for each root examined. Three roots were examined from each treatment group. Cell length data were treated as described for the cell diameter data. The 45 cell length observations obtained at each sampling location within a root were averaged to provide an individual root mean cell length at those locations. Beween-species and between-treatment analyses of cell length were accomplished using the species or treatment group average of the individual root means (n = 3).

Statistical Analysis

As described above, the data available for analysis consisted of the means of 30–45 observations at each of several locations (10–12) along individual roots. The simplest statistical analysis that can be applied to these data is one based on the individual root mean cellular dimension at each sampling location rather than the individual cellular measurements. Although this approach sacrifices the potential for assessing variability within individual root sampling locations, this concern appears relatively unimportant when compared to the variability between roots, since exposure treatments are applied to an entire root. The analysis of variance (ANOVA) is the natural approach to these data. By including all the data from an individual root in one ANOVA, enough data are obtained for an adequate assessment of variability, and simultaneously the problem of multiplicity that attends repetitively applied t tests is avoided [for a similar analysis, see Cox et al, 1980].

For each combination of cell length/diameter and species of root, a three-way ANOVA was performed for a total of four analyses. In each case, data from the second day of field exposure or sham exposure were used. The analytical factors were treatment (field strength), distance (from VC_d), and root, which was nested within treatment. Nesting in this case means that a single treatment was applied along the entire length of each root. The effect of such nesting is to change the denominator mean square used in certain of the ANOVA F tests [Cox et al, 1980].

In addition to this primary analysis, a comparison of the two species (unexposed, day 0 roots) was performed with respect to both cell length and diameter. A three-way ANOVA similar to those just described was performed; the factors in this analysis were species, distance (from VC_d), and root, which was nested within species.

RESULTS

The growth rates of roots exposed to 60-Hz EF for histological examination were not measured during the exposure period to prevent any potential damage to the root tissues. An estimate of how much the roots could be expected to grow under the exposure conditions was provided by data obtained during the dose-response measurements of whole root growth [Brayman and Miller, 1986]. Table 1 presents the rates of whole root growth in sham- and field-exposed *C. sativus* (350 and 450 $V \cdot m^{-1}$) and *C. maxima* (225 and 350 $V \cdot m^{-1}$). In both species, field-exposed roots grew between ≈ 1 and 3 cm, whereas sham-exposed roots grew ≈ 4–6 cm over the same period. On the basis of these data, the assumption was made that, in roots that had grown for 2 days under these exposure conditions, the terminal 1 cm of the root would be largely or entirely composed of cells that had undergone their development in the specified field environment.

TABLE 1. Rates of Whole Root Growth (mm · day^{-1}) Under Exposure Conditions Used to Prepare Roots for Histological Analysis†

Species	Field strength (V · m^{-1})	Treatment	Growth rate (mm · day^{-1}) Day 1	Day 2
Cucurbita maxima	225	Exposed	10.1 ± 0.6	20.4 ± 0.9
		Sham	13.2 ± 0.9*	27.0 ± 0.9*
	350	Exposed	6.1 ± 0.3	8.1 ± 0.4
		Sham	25.1 ± 0.8*	36.7 ± 0.8*
Cucumis sativus	350	Exposed	11.1 ± 0.7	20.5 ± 0.7
		Sham	25.3 ± 0.4*	24.1 ± 0.6*
	450	Exposed	3.2 ± 0.2	6.6 ± 0.4
		Sham	29.4 ± 0.6*	24.9 ± 0.5*

†Historical rates are presented; growth of roots used for histological analysis was not measured to prevent potential perturbation or damage from repeated handling of roots. The mean ± SEM of 60 observations/treatment group/species/day is presented.
*H_A, $\mu_{exposed} < \mu_{sham}$; $P < 0.01$ (t test).

TABLE 2. Comparison of Treatment Group Mean Cellular Dimensions in Day 0 Unexposed Roots of *Cucurbita maxima* and *Cucumis sativus* at Corresponding Locations in the Roots†

Distance from VC_d (mm)	Length (μm; $\bar{X}$ ± SEM) *C. maxima*	*C. sativus*	Diameter (μm; $\bar{X}$ ± SEM) *C. maxima*	*C. sativus*
0.0	11.8 ± 0.1	9.0 ± 0.1	11.9 ± 0.6	9.5 ± 0.1
0.5	12.1 ± 0.5	9.9 ± 1.9	16.6 ± 0.7	15.7 ± 0.8
1.0	13.8 ± 0.6	17.4 ± 1.5	20.9 ± 0.3	21.4 ± 1.2
1.5	18.4 ± 0.2	33.0 ± 3.2	24.8 ± 0.8	25.0 ± 1.4
2.0	28.6 ± 0.6	52.7 ± 4.7	27.4 ± 0.7	25.6 ± 1.5
2.5	42.9 ± 1.0	76.8 ± 4.6	29.8 ± 0.3	27.3 ± 2.9
3.0	62.2 ± 3.9	95.3 ± 4.7	31.9 ± 1.1	27.1 ± 0.8
4.0	92.6 ± 7.2	142.0 ± 4.5	32.8 ± 1.0	27.2 ± 0.5
5.0	135.7 ± 6.8	169.5 ± 5.2	34.2 ± 0.7	26.8 ± 1.0
6.0	161.6 ± 13.5	175.8 ± 0.9	35.8 ± 2.4	27.1 ± 0.6
8.0	166.7 ± 11.8	184.0 ± 4.4	—	—
10.0	175.8 ± 6.7	190.0 ± 2.7	—	—

†VC_d was defined as that region of the young root tip in which a complete procambial cyclinder was first distinguishable. Each value represents the mean ± SE of n = 3 individual root means at each sampling location.

Cortical cell dimensions at various distances from VC_d for day 0 roots of *C. sativus* and *C. maxima* are compared in Table 2. In both species, cortical cells are nearly isodiametric at VC_d. At VC_d, cortical cell length and diameter in *C. sativus* roots were about 9 μm; in *C. maxima* roots, cell length and diameter were about 12 μm.

Between 1.5 and 10.0 mm from VC_d, the mean length of *C. maxima* root cells was consistently less than that of *C. sativus* root cells at each sampling location. When nearly or fully expanded (10.0 mm from VC_d), *C. sativus* and *C. maxima* cells were about 190 and 175 μm long, respectively. The cell diameter data show an opposite trend. Between 0.5 and 2.5 mm from VC_d, cortical cell diameters were approximately equivalent between the two species; however, from 3.0 to 6.0 mm VC_d, the mean diameter of *Cucurbita* cortical cells consistently exceeded that of

Cucumis cells by 5–9 μm. At 6.0 mm from VC_d, where cellular radial expansion was essentially complete, the average diameters of *Cucumis sativus* and *Cucurbita maxima* root cortical cells were approximately 27 and 36 μm, respectively (Table 2).

The data in Table 2 were subjected to ANOVA, which compared cellular dimensions between the two species of roots. The results of the ANOVA are presented in Table 3, in which significant main effects and interactions indicate a clear difference in the pattern of cellular growth between the species. This difference is apparent from inspection of Figure 1A and B, in which the species mean (n = 3) cellular length (Fig. 1A) or diameter (Fig. 1B) was relativized to the cell length at 10 mm from VC_d or cell diameter at 6.0 mm from VC_d, respectively. Figure 1A indicates that the rapid phase of cellular elongation, with respect to increasing distance from VC_d, commences at about 0.5 mm from VC_d in *C. sativus* roots and at about 1.0 mm from VC_d in roots of *C. maxima*. *C. sativus* cells appear to attain about 90% of their final length at 5 mm from VC_d; a comparable degree of elongation is attained at about 6 mm from VC_d in *C. maxima*. Figure 1B indicates that in roots of both species the rapid phase of cell diameter increase, with increasing distance from VC_d, commences directly at VC_d. However, as was the case with cellular elongation growth, the cells of *Cucumis* appear to approach their final diameter nearer to VC_d than those of *Cucurbita*. In *Cucumis sativus* roots, cells attained about 90% of their final diameter at about 1.5 mm from VC_d; a comparable degree of radial expansion was attained at about 3.0 mm from VC_d in *Cucurbita maxima* roots.

Previous studies of 60-Hz EF- and sham-exposed *C. sativus* and *C. maxima* roots have shown that, after 48 hr of exposure/sham-exposure, root growth stabilizes at a relatively constant rate, which persists for an additional 72 hr of exposure [Inoue et al, 1985]. Therefore, comparison of day 2 cortical cell dimensions offers insight into the internal condition of the roots as they approach equilibrium with the field environment.

The day 2 cortical cell lengths of *Cucumis sativus* and *Cucurbita maxima* roots exposed to sham, low-, or high-strength 60-Hz electric fields for 2 days are presented in Table 4. These data were calculated as treatment group averages from the individual root mean cell length at each sampling location (n = 3). The individual root mean cell lengths in sham-, low-field, or high-field-exposed *C. sativus* roots are illustrated in Figure 2A, B, and C, respectively. Similar data are presented for *C. maxima* roots in Figure 3A, B, and C.

In *Cucumis sativus* roots, a monotonic decrease in cell length was associated with increasing field strength at each sampling location from 1.5 to 10.0 mm from VC_d inclusive (Table 4). From 2.5 to 10.0 mm from VC_d, the treatment group mean (n = 3) cell length in 350 V $\cdot$ m^{-1}-exposed roots was 12–43 μm less than in sham-exposed roots.

In high (450 V $\cdot$ m^{-1})-field-exposed *Cucumis sativus* roots, cortical cell length was consistently less than in sham-exposed roots at every sampling location from 1.0 to 10.0 mm from VC_d inclusive (Table 4). Over the interval from 1.5 to 10.0 mm from VC_d, the treatment group mean (n = 3) cell length in the high-field-exposed roots was between $\approx$30–90 μm less than in the sham-exposed roots.

Figure 2A–C presents the individual root mean cell lengths in *Cucumis* roots exposed to the sham field (Fig. 2A), 350 V $\cdot$ m^{-1} field (Fig. 2B), and 450 V $\cdot$ m^{-1} field (Fig. 2C). This figure illustrates the high degree of consistency between individual roots within a treatment group. Figure 2A–C visually demonstrates the marked

TABLE 3. Analysis of Variance Table Comparing Cell Length or Diameter of *Cucumis* and *Cucurbita* Roots Prior to the Onset of 60-Hz Electric Field Exposure/Sham Exposure (Day 0)

Source of variation	Cell length					Cell diameter				
	Sum of squares	d.f.	Mean square	F	P	Sum of squares	d.f.	Mean square	F	P
Species	6,676	1	6,676.0	19.4[a]	0.01	167.3	1	163.7	9.46[a]	0.04
Distance	314,098	11	28,554.0	520.2	<0.001[b]	2,590.8	9	287.9	113.50	<0.001[b]
Species × Distance	4,239	11	385.4	7.0	0.02[b]	138.0	9	15.3	6.04	0.02[b]
Roots (species)	1,395	4	348.6	—	—	70.7	4	17.7	—	—
Error	2,415	44	54.9	—	—	91.3	36	2.5	—	—
Corrected total	328,924	71	—	—	—	3,058.2	59	—	—	—

[a]The denominator mean square was the root (species) M.S.
[b]P value adjusted using the correction of Greenhouse-Geisser.

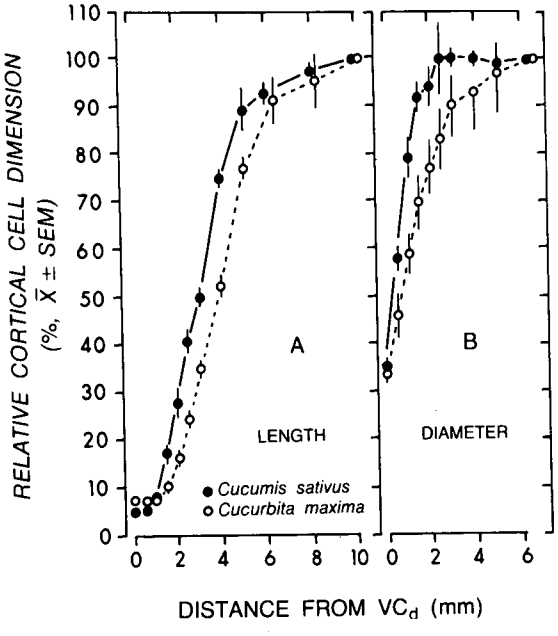

Fig. 1. Relative cortical cell length **(A)** and diameter **(B)** as a function of distance from VC_d in day 0 unexposed roots of *Cucumis sativus* (solid lines) and *Cucurbita maxima* (broken lines). Cell length at each sampling location was relativized to the average cell length attained by individual roots at 10.0 mm from VC_d. Cell diameter data were similarly relativized to the average cell diameter attained by individual roots at 6.0 mm from VC_d. Each point represents the mean of n = 3 individual root means; error bars represent the SEMs. VC_d represents the region of the young root tip in which a complete procambial cylinder was first distinguishable.

TABLE 4. Treatment Group Mean Cortical Cell Lengths at Various Distances From VC_d in Cucurbit Roots Exposed to Sham or Low- or High-Strength 60-Hz Electric Fields for 2 Days*

Distance from VC_d (mm)	Cortical cell length (μm; $\bar{X}$ ± SEM)					
	Cucumis sativus			*Cucurbita maxima*		
	Sham (0 V · m^{-1})	Low (350 V · m^{-1})	High (450 V · m^{-1})	Sham (0 V · m^{-1})	Low (225 V · m^{-1})	High (350 V · m^{-1})
0.0	9.6 ± 0.0	9.8 ± 0.6	9.7 ± 0.4	11.4 ± 0.4	11.1 ± 0.2	13.6 ± 1.6
0.5	10.6 ± 0.5	14.0 ± 1.6	11.6 ± 0.9	11.9 ± 0.6	11.3 ± 0.3	14.1 ± 1.1
1.0	29.8 ± 2.0	37.2 ± 3.4	28.4 ± 2.6	15.4 ± 1.1	15.3 ± 0.8	24.4 ± 1.0
1.5	69.0 ± 5.2	67.5 ± 6.8	39.9 ± 3.7	20.7 ± 2.1	25.4 ± 1.8	35.8 ± 3.7
2.0	93.1 ± 0.9	83.3 ± 6.7	48.6 ± 9.9	30.5 ± 2.3	37.3 ± 2.6	54.4 ± 3.9
2.5	107.1 ± 2.8	95.2 ± 5.2	52.1 ± 8.3	39.8 ± 2.1	51.3 ± 4.9	68.2 ± 6.0
3.0	144.9 ± 7.9	101.6 ± 5.2	53.7 ± 4.2	53.5 ± 2.4	63.1 ± 5.4	76.6 ± 4.3
4.0	151.9 ± 5.2	121.4 ± 2.6	63.8 ± 6.7	79.3 ± 4.1	91.5 ± 6.7	86.5 ± 6.6
5.0	158.3 ± 9.2	131.9 ± 5.7	67.0 ± 10.9	106.6 ± 4.4	121.3 ± 2.6	100.1 ± 4.3
6.0	164.0 ± 3.0	122.7 ± 6.7	71.1 ± 7.7	142.1 ± 6.1	139.8 ± 2.8	103.4 ± 14.2
8.0	165.0 ± 3.4	127.9 ± 6.8	81.7 ± 0.6	162.8 ± 4.5	167.0 ± 3.5	130.4 ± 14.3
10.0	159.3 ± 3.6	124.8 ± 3.2	89.4 ± 10.2	173.7 ± 6.2	177.5 ± 5.0	135.1 ± 20.9

*VC_d was defined as that region of the young root tip in which a complete procambial cylinder was first distinguishable. Each value represents the mean ± SE of n = individual root means at each sampling location.

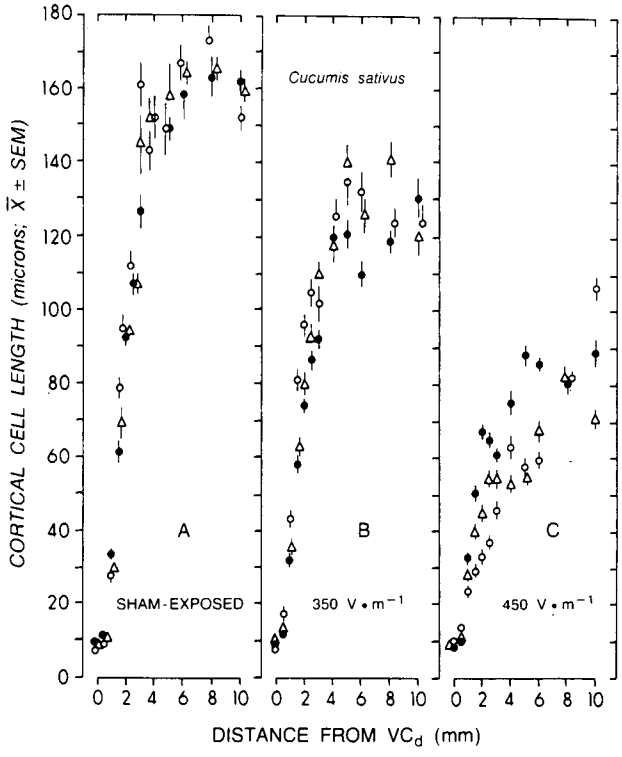

Fig. 2. Individual root mean cortical cell length as a function of distance from VC_d in *Cucumis sativus* roots exposed to 0 **(A)**, 350 **(B)**, or 450 **(C)** V · m^{-1} 60-Hz electric fields for 2 days. Each point represents the mean of 45 cell length observations; error bars represent the SEMs. Data from three roots (various symbols) are presented for each treatment group. VC_d represents the region of the young root tip in which a complete procambial cylinder was first distinguishable.

effect of field exposure on *Cucumis* root cellular elongation, which is seen to increase in severity with increasing field strength.

Exposure of *Cucurbita maxima* roots to low (225 V · m^{-1})-strength EF fields was without apparent effect on cell elongation growth (Table 4, Fig. 3A,B). High (350 V · m^{-1})-strength EF exposure of *C. maxima* appears to affect cellular elongation growth (Table 4, Fig. 3A,C). From 0.0 to 4.0 mm from VC_d, the treatment group mean cell length in high (350 V · m^{-1}) field-exposed *C. maxima* roots was consistently greater than in sham-exposed roots (Table 4). Over the interval of 5.0–10.0 mm from VC_d, the treatment group mean cell length was consistently between 6 and 39 μm less in 350 V · m^{-1}-exposed roots than in sham-exposed roots. Comparison of Figure 3A and C suggests that 350 V · m^{-1} field exposure markedly inhibited cellular elongation growth in two of the exposed roots, whereas the third exposed root apparently did not respond to the applied field.

The results of the ANOVA performed on the day 2 cell length data from both species are summarized in Table 5. A statistically significant interaction between treatment and distance from VC_d provides evidence that the pattern of cell elongation growth is different for the different treatments. The treatment main effect is more difficult to interpret; it represents an average across the various distances from VC_d. In both species, there is a clear interaction between treatment and distance from VC_d.

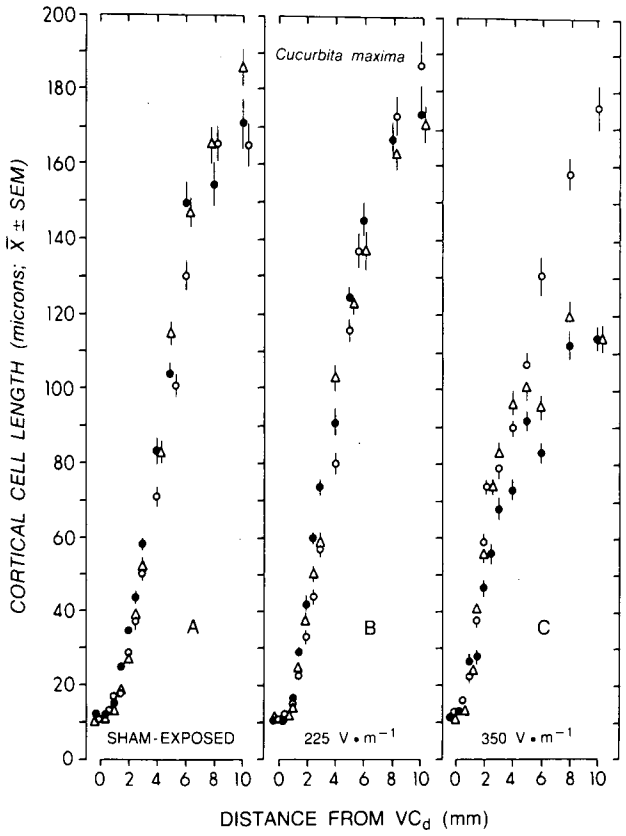

Fig. 3. Individual root mean cortical cell length as a function of distance from VC_d in *Cucurbita maxima* roots exposed to 0 **(A)**, 225 **(B)**, or 350 **(C)** V · m^{-1} 60-Hz electric fields for 2 days as in Figure 2. VC_d represents the region of the young root tip in which a complete procambial cylinder was first distinguishable.

For *C. sativus* roots, the P value for this interaction was less than 0.001; for *C. maxima* roots, the P value was 0.006 (Table 5). As a check on these parametric analyses, a nonparametric growth curve analysis was also performed [Zerbe and Walker, 1977]. The results of this analysis were essentially identical to those obtained with the ANOVA. The P values resulting from this analysis were 0.004 for *C. sativus* and 0.006 for *C. maxima* cell length data.

The treatment group mean (n = 3) cell diameter data obtained from *Cucumis sativus* and *Cucurbita maxima* roots exposed for 2 days to sham and low- and high-strength EF are presented in Table 6. The individual root mean cell diameters at each sampling location are presented in Figure 4A, B, and C (*C. sativus*; 0, 350, and 450 V · m^{-1}, respectively) and in Figures 5A, B, and C (*C. maxima*; 0, 225, and 350 V · m^{-1}). Table 6 and Figure 4 illustrate the apparent lack of effect of field exposure on cell radial expansion in *C. sativus* roots. Similarly, Table 6 indicates that field exposure of *C. maxima* roots was without conspicuous effect on radial expansion growth; this is illustrated by comparison of the individual root mean cell diameter data for *Cucurbita maxima* roots (Fig. 5A, B, C).

The results of the ANOVA performed on the day 2 cell diameter data from both species are presented in Table 7. In contrast to the ANOVA results for cell length,

TABLE 5. Analysis of Variance Table Comparing Cell Length of *Cucumis* and *Cucurbita* Roots Exposed to 60-Hz Electric Fields for 2 Days

	Cucumis sativus					*Cucurbita maxima*				
Source of variation	Sum of squares	d.f.	Mean square	F	P	Sum of squares	d.f.	Mean square	F	P
Treatment	53,675	2	26,837	78.57[a]	<0.001	750	2	375	0.85[a]	<0.47
Distance	187,860	11	17,078	243.88	<0.001[b]	296,294	11	26,935	343.70	<0.001[b]
Tmt × Distance	24,904	22	1,132	16.17	<0.001[b]	12,218	22	555	7.09	0.006[b]
Roots (Tmt)	2,049	6	342	—	—	2,654	6	442	—	—
Error	4,622	66	70	—	—	5,172	66	78	—	—
Corrected total	273,110	107	—	—	—	317,090	107	—	—	—

[a]The appropriate error mean square is the root (Tmt) M.S.
[b]P value adjusted using the correction of Greenhouse-Geisser.

TABLE 6. Treatment Group Mean Cortical Cell Radial Dimensions at Various Distances From VC_d in Cucurbit Roots Exposed to Sham or Low- or High-Strength 60-Hz Electric Fields for 2 Days*

Distance from VCD_d (mm)	Cortical cell radial dimension (μm; $\bar{X} \pm$ SEM)					
	Cucumis sativus			*Cucurbita maxima*		
	Sham (0 $V \cdot m^{-1}$)	Low (350 $V \cdot m^{-1}$)	High (450 $V \cdot m^{-1}$)	Sham (0 $V \cdot m^{-1}$)	Low (225 $V \cdot m^{-1}$)	High (350 $V \cdot m^{-1}$)
0.0	9.4 ± 0.2	9.3 ± 0.4	10.3 ± 0.8	12.9 ± 0.4	13.9 ± 0.4	13.7 ± 0.5
0.5	18.5 ± 2.0	18.1 ± 0.5	20.6 ± 2.0	17.9 ± 0.8	19.5 ± 0.6	19.8 ± 1.0
1.0	27.7 ± 1.5	23.8 ± 0.4	26.4 ± 3.2	23.3 ± 1.2	25.4 ± 2.3	26.8 ± 2.0
1.5	26.9 ± 0.8	26.6 ± 0.8	28.4 ± 3.0	27.4 ± 1.2	30.8 ± 1.4	32.5 ± 3.2
2.0	26.5 ± 0.4	27.5 ± 0.4	31.2 ± 1.4	31.9 ± 1.4	32.2 ± 2.1	35.1 ± 2.9
2.5	27.2 ± 0.9	28.9 ± 0.2	32.1 ± 2.6	33.3 ± 1.0	32.7 ± 2.3	39.7 ± 3.2
3.0	28.9 ± 1.0	28.6 ± 1.1	31.0 ± 2.4	35.8 ± 0.9	32.8 ± 2.4	43.7 ± 3.7
4.0	29.0 ± 0.4	31.0 ± 0.6	30.5 ± 2.7	36.2 ± 1.4	34.5 ± 3.2	43.0 ± 2.6
5.0	28.1 ± 0.0	30.1 ± 1.1	32.6 ± 2.2	37.2 ± 1.7	36.4 ± 2.6	44.5 ± 1.7
6.0	29.9 ± 1.4	29.3 ± 0.8	33.3 ± 2.9	37.6 ± 0.7	36.0 ± 2.8	45.6 ± 0.7

*VC_d was defined as that region of the young root tip in which a complete procambial cylinder was first distinguishable. Each value represents the mean ± SE of n = 3 individual root means at each sampling location.

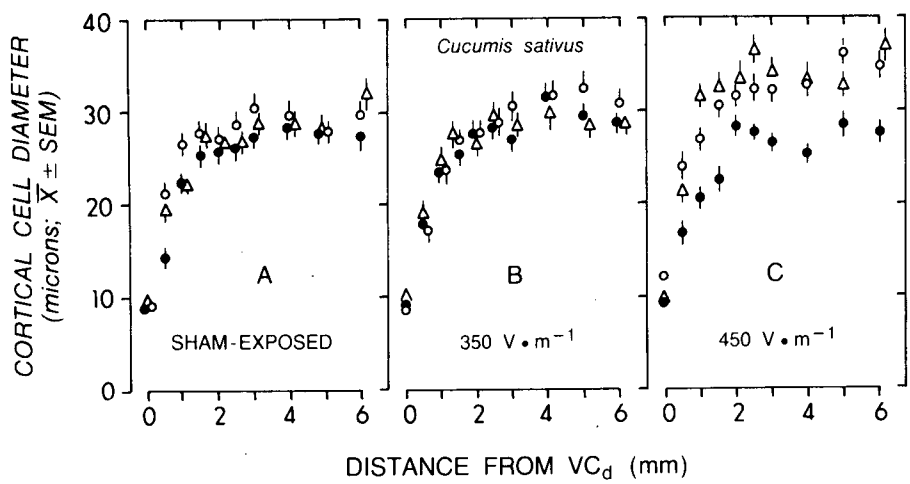

Fig. 4. Individual root mean cortical cell diameter as a function of distance from VC_d in *Cucumis sativus* roots exposed to 0 **(A)**, 350 **(B)**, or 450 **(C)** $V.m^{-1}$ 60-Hz electric fields for 2 days. Each point represents the mean of 40 cell diameter observations; error bars represent the SEMs. Data from three roots (various symbols) are presented for each treatment group. VC_d represents the region of the young root tip in which a complete procambial cylinder was first distinguishable.

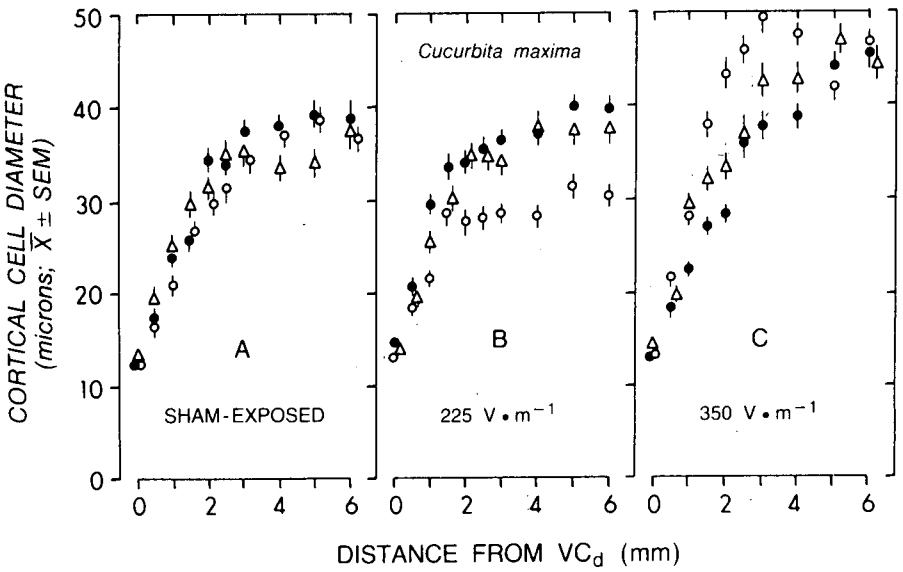

Fig. 5. Individual root mean cortical cell diameter as a function of distance from VC_d in *Cucurbita maxima* roots exposed to 0 **(A)**, 225 **(B)**, or 350 **(C)** V · m^{-1} 60-Hz electric fields for 2 days as in Figure 4. VC_d represents the region of the young root tip in which a complete procambial cylinder was first distinguishable.

there was no significant distance x treatment interaction in the case of cell diameter. For *C. sativus* roots, the P value for this interaction was 0.41; that for *C. maxima* roots was 0.09. Again, as a check on the parametric ANOVA tests, growth curve analysis was applied to the cell diameter data. Once more, the agreement between these two quite different methods of analysis was striking; the growth curve analysis produced P values of 0.29 and 0.039 for *C. sativus* and *C. maxima*, respectively. The treatment difference P value of 0.039 for day 2 *C. maxima* cell diameter suggests a treatment effect on cellular radial expansion growth in this species. However, although $P = 0.039$ is less than the traditional $P = 0.05$, it is not very impressive when compared to the results obtained for the cell length measurements. The conclusion is that the relationship between distance from VC_d and cell length differs between treatment groups in both species, whereas the relationship between cell diameter and distance does not.

DISCUSSION

EF exposures of *Cucumis sativus* roots and *Cucurbita maxima* roots were seen to inhibit cellular elongation significantly. In *C. sativus* roots exposed to 350 and 450 V · m^{-1} EF, the magnitude of the effect on elongation increased with increasing field strength. No apparent effect on cell diameter was observed in *C. sativus* roots exposed to the EF. As in *C. sativus* roots, exposure of *C. maxima* roots to EF had no effect on the final diameter attained by cortical cells.

The results of the present study are consistent with the hypothesis that 60-Hz electric field bioeffects in roots are stimulated by field-induced transmembrane potential perturbations. Previous studies have shown that the roots of *C. maxima* are

TABLE 7. Analysis of Variance Table for Cell Diameter of *Cucumis* and *Cucurbita* Roots Exposed to 60-Hz Electric Fields for 2 Days

	Cucumis sativus					*Cucurbita maxima*				
Source of variation	Sum of squares	d.f.	Mean square	F	P	Sum of squares	d.f.	Mean square	F	P
Treatment	136.3	2	68.1	1.27[a]	0.34	512.8	2	256.4	3.42[a]	0.10
Distance	3,657.0	9	406.3	174.40	<0.001[b]	6,660.6	9	740.1	122.09	<0.001[b]
Tmt × Distance	45.0	18	2.5	1.07	0.41[b]	255.7	18	14.2	2.34	0.09[b]
Roots (Tmt)	322.3	6	53.7	—	—	450.1	6	75.0	—	—
Error	125.8	54	2.3	—	—	327.3	54	6.1	—	—
Corrected total	4,286.4	89	—	—	—	8,206.6	89	—	—	—

[a]The appropriate error mean square is the root (Tmt) M.S.
[b]P value adjusted using the correction of Greenhouse-Geisser.

35–40% more sensitive to applied 60-Hz EF than are *C. sativus* roots as assessed by the response thresholds for the growth effect [Brayman and Miller, 1986]. In the present study, it was shown that the diameters of both unexpanded and fully expanded cortical cells are about 25–30% larger in *C. maxima* than in *C. sativus*. When roots of *C. sativus* and *C. maxima* are exposed to the same 60-Hz EF strength, and the field direction is perpendicular to the root axes, proportionately larger induced membrane potentials will arise in the larger-celled species.

Low-strength EF exposures of 350 and 225 $V \cdot m^{-1}$ were selected to produce comparable growth rate reductions of $\approx$ 10–20% in *C. sativus* and *C. maxima* roots, respectively. High-strength EF exposures of 450 and 350 $V \cdot m^{-1}$ were selected to produce growth rate reductions of 70–80% in *C. sativus* and *C. maxima* roots, respectively. It is of interest to compare the magnitudes of the 60-Hz membrane potentials induced in the cortical cells of these species under exposure conditions that produce comparable reductions in the rates of exposed root growth. The 60-Hz transmembrane potentials arising in exposed root cells can be estimated as the product of the applied field strength and the cellular radius [Rushton, 1927]. From the data in Table 2, the 60-Hz membrane potentials that would arise in unexpanded (0 mm from VC_d) and fully expanded (6 mm from VC_d) cortical cells immediately after the onset of exposure to a specific field strength can be estimated. Exposure of the roots to low-strength EF will induce 60-Hz membrane potentials ranging from about 1.7 to 4.7 mV in *C. sativus*; the membrane potentials induced in comparable cells of low-field-exposed *C. maxima* range from about 1.3 to 4.0 mV. Under high-strength field exposure conditions, the membrane potentials induced in *C. sativus* and *C. maxima* cortical cells range from about 2.1 to 6.1 and 2.1 to 6.3 mV, respectively. Between these two species, therefore, there is good agreement between the relative magnitude of field-induced root growth rate inhibition and the estimated range of 60-Hz membrane potentials induced in the cortical cells within the growing region of the root tip. This suggests that the growth rate effect severity is proportional to the induced membrane potential magnitude, and thus the involvement of induced potentials in eliciting the observed effects in field-exposed roots.

ACKNOWLEDGMENTS

Major support for this project was provided by the Empire State Electric Energy Research Corporation (whose members include: Central Hudson Gas & Electric Corporation, Consolidated Edison Company of New York, Inc., New York Power Authority, New York State Electric & Gas Corporation, Niagara Mohawk Power Corporation, Orange and Rockland Utilities, Inc., and Rochester Gas and Electric Corporation). The authors thank Mark Espeland and Bill Murphy for performing the randomization tests and Anna Choi for statistical programming. We acknowledge the excellent botanical microtechnique of Caroline Vaughan and Christine Becker of CMX Laboratories, Buffalo, New York.

REFERENCES

Brayman AA, Brulfert A, Miller MW (1986): Induction of ELF transmembrane potentials in relation to power-frequency electric field bioeffects in a plant root model system. II. The effect of 60-Hz electric fields on the growth of different regions of the cucurbit root elongation zone. Radiat Environ Biophys 25:151–157.

Brayman AA, Miller MW (1986): Induction of ELF transmembrane potentials in relation to power-frequency electric field bioeffects in a plant root model system. I. Relationship between applied field strength and cucurbitaceous root growth rates. Radiat Environ Biophys 25:141–149.

Brulfert A, Miller MW, Robertson D, Dooley DA, Economou P (1985): A cytohistological analysis of roots whose growth is affected by a 60 Hz electric field. Bioelectromagnetics 6:283–291.

Cox C, Davis HT, Miller MW, Robertson D (1980): Statistical analysis of root growth rate determinations. Environ Exp Bot 20:389–396.

Hayward HE (1938): "The Structure of Economic Plants." New York: Macmillan, pp 280–300.

Inoue M, Miller MW, Carstensen EL, Brayman AA (1985a): The relationship between sensitivity to 60 Hz electric fields and induced transmembrane potentials in plant root cells. Radiat Environ Biophys 24:303–314.

Inoue M, Miller MW, Cox C, Carstensen EL (1985b): Growth rate and mitotic index effects in *Vicia faba* roots exposed to 60 Hz electric fields. Bioelectromagnetics 6:293–303.

Mallory TE, Chiang S-H, Cutter EG, Gifford EM Jr (1970): Sequence and pattern of lateral root formation in five selected species. Am J Bot 57:800–809.

Miller MW, Carstensen EL, Robertson D, Child SZ (1980): 60 Hz electric field parameters associated with the perturbation of an eukaryotic cell system. Radiat Environ Biophys 18:289–300.

Miller MW, Dooley DA, Cox C, Carstensen EL (1983): On the mechanism of 60 Hz electric field induced effects in *Pisum sativum* (L.) roots: Vertical field exposures. Radiat Environ Biophys 22:293–302.

Miller MW, Inoue M, Carstensen EL, Brayman AA (1985): Biophysical aspects of electric field bioeffects at the cellular level. In: "Proc. 23rd Annual Hanford Life Sciences Symposium (Oct. 2–4, 1984, Richland, WA)." Oak Ridge, TN: Technical Information Center (in press).

Robertson D, Miller MW (1981): 60 Hz electric field induced inhibition and recovery of growth processes in roots of *Pisum sativum*. Bioelectromagnetics 2:329–340.

Robertson D, Miller MW, Carstensen EL (1981): Relationship of 60 Hz electric field parameters to the inhibition of growth of *Pisum sativum* roots. Radiat Environ Biophys 19:227–233.

Rushton WAH (1927): The effect upon the threshold for nervous excitation of the length of the nerve exposed, and the angle between current and nerve. J Physiol 63:357–377.

Voth PD, Hamner N (1943): Effects of nutrient solution concentration on the growth of *Marchantia polymorpha*. Bot Gaz 104:591–601.

Zerbe G, Walker SH (1977): A randomization test for comparison of groups of growth curves with different polynomial design matrices. Biometrics 33:653–657.

Bioelectromagnetics 8:73–89 (1987)

Metabolic and Vasomotor Responses of Rhesus Monkeys Exposed to 225-MHz Radiofrequency Energy

W. Gregory Lotz and Jack L. Saxton

Naval Aerospace Medical Research Laboratory, Pensacola, Florida

A previous study showed a substantial increase in the colonic temperature of rhesus monkeys (*Macaca mulatta*) exposed to radiofrequency (RF) fields at a frequency near whole-body resonance and specific absorption rates (SAR) of 2–3 W/kg. The present experiments were conducted to determine the metabolic anad vasomotor responses during exposures to similar RF fields. We exposed five adult male rhesus monkeys to 225 MHz radiation (E orientation) in an anechoic chamber. Oxygen consumption and carbon dioxide production were measured before, during, and after RF exposure. Colonic, tail and leg skin temperatures were continuously monitored with RF-nonperturbing probes. The monkeys were irradiated at two carefully-controlled ambient temperatures, either cool (20 °C) or thermoneutral (26 °C). Power densities ranged from 0 (sham) to 10.0 mW/cm^2 with an average whole-body SAR of 0.285 $(W/kg)/(mW/cm^2)$. We used two experimental protocols, each of which began with a 120-min pre-exposure equilibration period. One protocol involved repetitive 10-min RF exposures at successively higher power densities with a recovery period between exposures. In the second protocol, a 120-min RF exposure permitted the measurement of steady-state thermoregulatory responses. Metabolic and vasomotor adjustments in the rhesus monkey exposed to 225 MHz occurred during brief or sustained exposures at SARs at or above 1.4 W/kg. The SAR required to produce a given response varied with ambient temperature. Metabolic and vasomotor responses were coordinated effectively to produce a stable deep body temperature. The results show that the thermoregulatory response of the rhesus monkey to an RF exposure at a resonant frequency limits storage of heat in the body. However, substantial increases in colonic temperature were not prevented by such responses, even in a cool environment.

Key words: thermoregulation, microwaves, rhesus monkeys, radiofrequency, metabolic heat production, vasodilation.

INTRODUCTION

The absorption of radiofrequency (RF) energy by biological organisms is dependent upon the frequency and orientation of the incident energy. For whole-body exposure, energy absorption is greatest for electric fields polarized parallel to the longest dimension of the body at the resonant frequency, i.e., when this long dimension is about 0.4 times the free-space wavelength [Gandhi, 1975]. As a result of this dependency, the possibility exists that whole-body irradiation of an organism with

Received for review June 14, 1985; revision received May 1, 1986.

Address reprint requests to Dr. W. Gregory Lotz, NAMRL Code 41, Naval Air Station, Pensacola, FL 32508-5700.

energy at the resonant frequency represents a "worst-case" exposure with respect to biological effects. In earlier studies with rhesus monkeys, we observed that exposure to RF energy near theoretical whole-body resonance [Durney et al, 1978] produced marked increases in colonic temperature at relatively low average specific absorption rates (SAR) [Lotz, 1982; 1985].

These observations, which were made in experiments designed to study endocrine responses, raised questions about thermoregulatory function and the ambient conditions under which the exposures were conducted. In those experiments, control of the ambient environment was limited to circulation of room air through the microwave chamber, and increases in ambient temperature during RF exposure were noted. No measurements of metabolic heat production or heat dissipation efforts by the animal had been taken to indicate if thermoregulatory responses had occurred. To address these questions, several changes were made in our experimental approach, and experiments were performed to study the vasomotor and metabolic responses of rhesus monkeys whole-body exposed to 225-MHz radiation. The changes in experimental approach provided both improved control of the thermal characteristics of the environment and additional indices of thermoregulatory function. Thermoregulatory responses were qualitatively appropriate to compensate partially for the increased thermal load of RF exposure. Internal body heating occurred to a greater degree than has been associated with exposure at the same SAR to higher frequencies.

MATERIALS AND METHODS

Subjects

We used five adult male rhesus monkeys (*Macaca mulatta*), 6.5–8.5 kg, in these experiments. The animals were born and raised in the monkey colony of the Naval Aerospace Medical Research Laboratory. During this study, they were housed indoors in standard metal primate laboratory cages, given water ad libitum in their home cage, and fed a commercial monkey diet twice daily (Wayne Monkey Chow, Allied Mills, Inc, Chicago, IL). The light cycle in the home cage rooms was 16-hr light: 8-hr dark with the lights on from 0600 to 2200. Ambient temperature in these rooms ranged from 21–25 °C. Prior to these experiments, the monkeys had been used in other microwave/RF radiation studies of a similar nature. They were accustomed to restraint and the experimental apparatus used, including the hood. This adaptation process involved three to five additional trial experiments with the added apparatus (hood, microchamber, and probes) before the data were collected for subsequent use. During these adaptation sessions, the animals were observed for evidence of unusual activity or elevated body temperatures that might indicate an unstable experimental model.

Apparatus

The monkeys were restrained during each experiment in a chair built of rigid and foamed (Styrofoam) polystyrene. Experiments were conducted in an RF anechoic chamber (3.3 × 3.3 × 6.7 m) diagrammed in Figure 1. This was the same chamber used previously for 225-MHz experiments [Lotz, 1982; 1985].

Continuous wave (CW) RF power at 225 MHz was provided by a military type GRT-3 radio set, and was amplified by a cavity-type amplifier. Monkeys were irradiated frontally 240 cm from a locally constructed copper-lined horn antenna

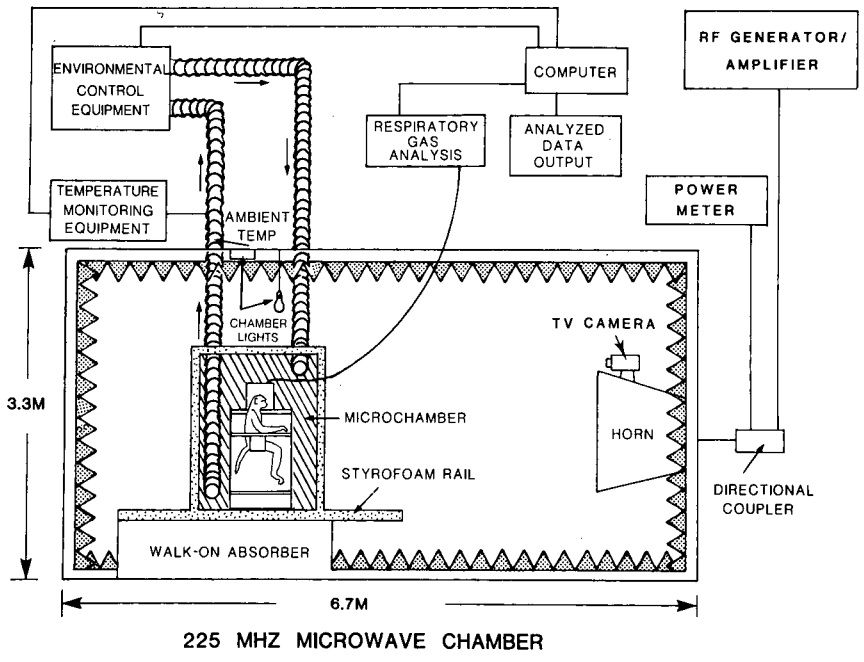

Fig. 1. Diagram of the 225-MHz exposure chamber showing the monkey and major pieces of experimental apparatus.

described previously [Olsen and Griner, 1982]. This exposure location was 0.78 of the normal ($2D^2/\lambda$) far-field distance. Chamber lights and a video camera above the horn antenna were placed as shown in Figure 1. The electric field was oriented parallel to the long axis of the body for all exposures. Power densities were measured in the absence of the animal and Styrofoam apparatus (chair and enclosure) with a Narda Model 8608 monitor system at 25-cm intervals vertically and 10-cm intervals horizontally in a plane that would bisect the animal along the coronal plane. Power density values specified here represent the mean calculated over the region occupied by the animal. Average SAR was 0.285 (W/kg)/(mW/cm^2), as determined by Olsen and Griner [1982] in a tissue-equivalent model of a rhesus monkey.

An essential addition to the apparatus for this study was the Styrofoam microchamber that enclosed the chaired monkey (see Fig. 1). The ambient temperature and humidity in the microchamber were carefully controlled. Temperature was maintained within ± 0.5 °C of the target value, and relative humidity was 50 $\pm$ 5% (range) at 26 °C or 65 $\pm$ 5% at 20 °C. Conditioned air was blown into the microchamber at the top front and drawn out at the bottom near the back. Air velocity over the animal (from front to back) was measured with a Kurz Model 441S Air Velocity Meter (Kurz Instruments, Inc., Carmel Valley, CA) and ranged from 10–30 m/min, with the highest flow rate near the tail. The temperature distribution within the microchamber was determined by inserting temperature probes through the walls of the Styrofoam enclosure and chair with the animal in place. This was done with and without RF exposure. The temperature within the microchamber varied ± 0.5 °C (range) from the target value, with the lowest readings near the tail and the highest around the torso of the animal.

A Plexiglas hood (20 cm in diameter) was placed over the monkey's head to capture the exhaled air. This air was exhausted from the chamber at a flow rate from 6–10 l/min and analyzed for oxygen (O_2) and carbon dioxide (CO_2) concentrations with Beckman Model 755 (paramagnetic) and 864 (infrared) analyzers, respectively. The system was an "open" one in that ambient air drawn from around the monkey's head and neck was not recirculated to the monkey after analysis. Tests using smoke and certified calibration gases were conducted in the absence of the animal to establish that this system, when operating at flow rates of 6–10 l/min, completely captured the exhaled air of the monkey. The air flow for an experiment was normally about 8 l/min, with fluctuations of less than ± 150 ml/min (range) from the mean during the experiment.

Colonic, tail-skin, and inner-thigh skin temperatures were continously monitored with Vitek Electrothermia Model 101 monitors that were calibrated against a certified mercury thermometer. The colonic probe was inserted 10 cm past the anal sphincter. The tail-skin probe was placed on the dorsal surface midway between the base and tip of the tail. The leg skin probe was placed on the medial side of the upper leg near the apex of the femoral triangle. The two skin probes were attached by inserting the Vitek probe tip through the side of a 1-cm diameter doughnut-shaped piece of Plexiglas and taping the doughnut in place. The probe tip itself was not covered by tape. Data from the O_2 and CO_2 analyzers, the Vitek probes, and an ambient temperature probe placed in the exhaust air duct from the microchamber were sampled four times a minute by a computer. The average value of each variable was printed and plotted for each minute of the experiment. Metabolic heat production (M) was calculated from the O_2 data with corrections for flow rate and standard temperature and pressure.

Procedure

We used two different experimental protocols. One was designed to determine the threshold exposure for the onset of vasomotor or metabolic thermoregulatory responses, and will be referred to as a step-acute exposure. Following a 120-min pre-exposure equilibration period, repetitive 10-min exposures were conducted at successively higher power densities until a marked vasomotor response was indicated by a rapid change in tail skin temperature (T_t). After each 10-min exposure, the animal was allowed a re-equilibration period that lasted until T_t returned to within 0.3 °C (or less) of its pre-exposure value. Depending upon the power density used, this re-equilibration took from 10–60 min. Power densities of 1.2, 2.5, 5.0, 7.5, 10.0, and 12.5 mW/cm^2 were used, but some experiments did not use all of the power densities. To distinguish between direct (passive) tail heating by RF energy and increases in T_t that index vasodilation, the criteria were established that T_t had to show marked increases in slope, or continue increasing after RF exposure stopped. The determination of a threshold response for M was more difficult to establish. A similar transition could not be as readily defined as for vasodilation. The observed pulsatile nature of variations in M also added to the complexity. Both statistical analyses and visual examination of the variability were considered and are discussed below. Step-acute experiments were conducted twice for each monkey at both 20 and 26 °C ambient temperatures, i.e., each monkey was studied during four experiments with this protocol. If the duplicate experiments with a given monkey did not show good

replication of the results, at least one additional experiment was conducted with that set of conditions.

The second exposure protocol was designed to evaluate thermoregulatory adjustments during microwave exposure in the steady-state. Following the 120-min pre-exposure period, a 120-min RF exposure was conducted, and data were collected for 10–60 min following exposure. In this protocol, each monkey was exposed a single time to each power density at 20 and 26 °C ambient temperatures (T_a). The power densities used were 0 (sham), 2.5, 5.0, 7.5, and 10.0 mW/cm^2 at T_a = 20 °C; and 0(sham), 1.2, 2.5, 5.0, and 7.5 mW/cm^2 at T_a = 26 °C. Average SARs were 0.4, 0.7, 1.4, 2.1, and 2.9 W/kg for the series of power densities used.

Data Analysis

To reduce noise from inherent variability, data for M and leg skin temperature (T_{le}) were "smoothed" before plotting by calculating successive 5-min means. In this technique, the mean of the first five readings (one each minute) was calculated initally, and subsequent means were calculated by adding the next reading and dropping the first (1–5, then 2–6, etc.). This produced a record of minute-to-minute changes from t = 5 min, in which each value plotted was based on five readings rather than just one.

In the analysis of the steady-state experiments, data were averaged over the last 30 min of each period (pre-exposure and exposure) for comparison. Steady-state conditions were considered to be fulfilled because colonic temperature (T_{co}) was stable within ± 0.1 °C during these periods. Skin temperatures were also generally stable during this period, although variability was somewhat greater than for T_{co}.

Metabolic heat production data were analyzed statistically using one-way analysis of variance (ANOVA) for repeated measures, followed by Tukey's highly significant difference (HSD) test for multiple comparisons [Kirk, 1968]. The 0.05 level of significance was the criterion for a difference to be considered significant. For step-acute experiments, the mean M for the 10-min exposure at a given power density for each animal (two sessions) was used as the test value. For baseline comparison to an unexposed period, the mean M for the 10-min period immediately preceding the associated exposure step was used. The data were converted to the percentage of pre-exposure values [100 × (exposure M/pre-exposure M)] for each exposure level, and the ANOVA and Tukey's tests were then applied to these ratio data. For the steady-state exposures, the same tests were applied to the data of all exposure levels, including sham exposure, to test for differences between the values recorded during the last 30 min of the exposure period.

RESULTS

The raw data from a representative experiment under the step-acute protocol at T_a = 20 °C for subject 15 are shown in Figure 2. At this T_a, the metabolic response occurred before vasodilation was indicated, but additional exposure steps were conducted until tail vasodilation was also observed. In Figure 2, M did not seem to be altered at 1.2 mW/cm^2, declined somewhat at 2.5 mW/cm^2, and was even more suppressed at power densities of 5.0 mW/cm^2 and above. The pre-exposure M at T_a = 26 °C was approximately 28% below M at 20 °C, and was not changed by 10-min RF exposures. The progressive recruitment of thermoregulatory effectors in response

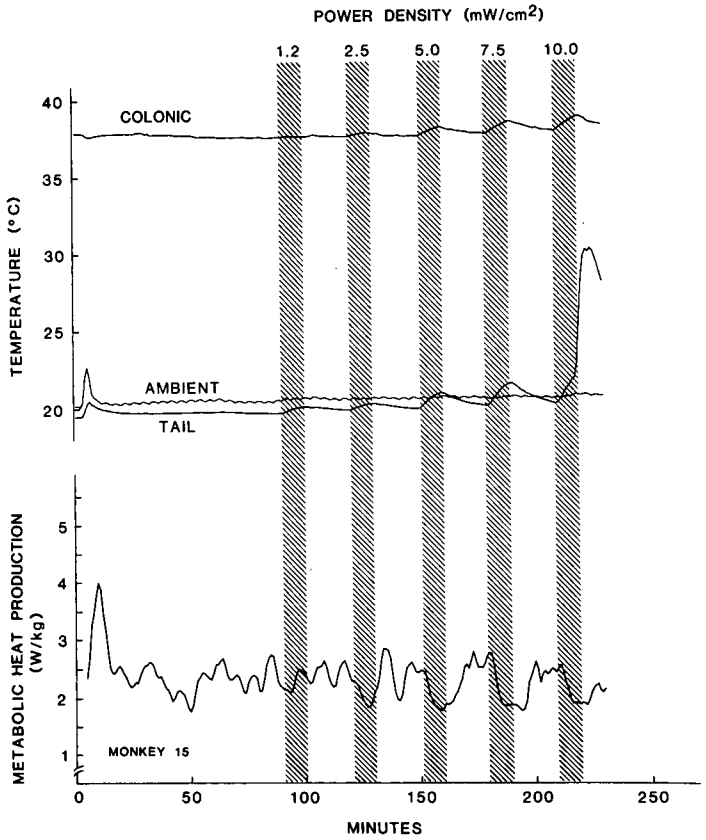

Fig. 2. Plots of data from a representative step-acute experiment with monkey 15 at T_a of 20 °C showing colonic, tail skin and ambient temperatures, and metabolic heat production (M). The hatched zones indicate the periods of RF exposure (10 min) at the power density indicated at the top of the zone. The data for M in this figure and in Figures 5 and 6 have been smoothed by calculating 5-min running averages, as defined in the text.

to RF-induced heating is dramatically illustrated in Figure 2. While M was clearly reduced at or above 5 mW/cm^2, the vasomotor response did not occur until exposure at 10 mW/cm^2. This response pattern of progressive recruitment of metabolic and vasomotor effectors was seen in every animal, even though the minimal power density for onset of the individual responses varied among subjects. The lowest power densities that caused vasodilation of the tail during 225-MHz exposure in the step-acute protocol are shown in Figure 3. As expected, a clear shift in this threshold occurred with the change in T_a, with higher power densities required to produce vasodilation at the lower T_a.

The mean values of M ratios are shown in Figure 4. At T_a = 20 °C, M was less than 100% for the pre-exposure value at each intensity, with a progressively greater reduction of M at 5 mW/cm^2 or higher intensities. The ANOVA indicated that the effect of exposure was significant ($F = 6.44$, $df = 4,16$; $p = .003$). Tukey's HSD test revealed that the differences among means were significant for 7.5 and 10 mW/cm^2 exposures. For T_a = 26 °C, the ANOVA confirmed that M ratio (percentage of pre-exposure) also was significantly affected by exposure ($F = 9.71$, $df = 2,8$: $p = .007$). Tukey's HSD test demonstrated that this effect occurred at 5 mW/cm^2.

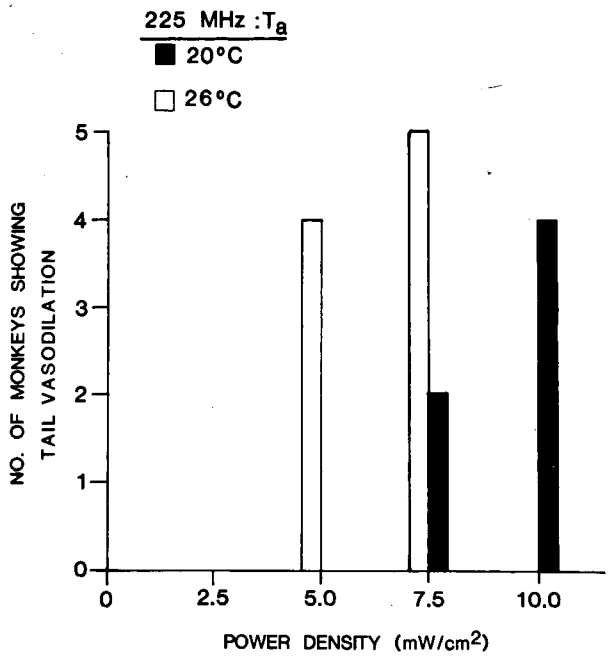

Fig. 3. Thresholds for vasodilation of the tail of RF-exposed rhesus monkeys at two different ambient temperatures, 20 and 26 °C.

Based on these data, the lowest power density that reliably altered M during 10-min exposures was in the range of 5–7.5 mW/cm^2.

The response patterns of representative steady-state experiments (120-min exposure) are shown in Figures 5 and 6 for T_a = 26 °C and 20 °C, respectively. The M (mean ± SE) for the last 30 min of the pre-exposure periods of all steady-state experiments (five monkeys, five runs each) was 2.26 ± 0.09 W/kg at T_a = 26 °C, and 3.13 ± 0.07 W/kg at T_a = 20 °C. The mean respiratory quotient (RQ) for these periods was 0.81. The lower pre-exposure level of M at T_a = 26 °C compared to T_a = 20 °C is apparent in the figures, as is the fact that M did not change much during RF exposure at a T_a of 26 °C. The progressive recruitment of metabolic and vasomotor responses during RF exposure at a T_a of 20 °C is again evident in Figure 6. The delay between the initiation of these two responses was dependent on power density, i.e., vasodilation occurred sooner after the reduction in M at higher power densities. In general, at a T_a of 20 °C, T_{co} stabilized after vasodilation occurred; at T_a = 26 °C, T_{co} continued to increase after vasodilation occurred, although a steady-state was achieved after approximately 90 min of exposure.

The mean T_{co} of all animals during the last 30 min of RF exposure in the steady-state experiments is shown in Figure 7. Even at 2.5 mW/cm^2, which is below the thresholds observed for thermoregulatory effector action, T_{co} was increased over sham levels an average of 0.4 °C at a T_a of 26 °C and 1.0 °C at a T_a of 20 °C. The mean T_{co} was similar at both ambient temperatures, except under sham or 7.5 mW/cm^2 exposure conditions.

The mean M during steady-state exposures (120 min) at each power density is shown in Figure 8. As noted for an individual experiment (Fig. 5), M did not change

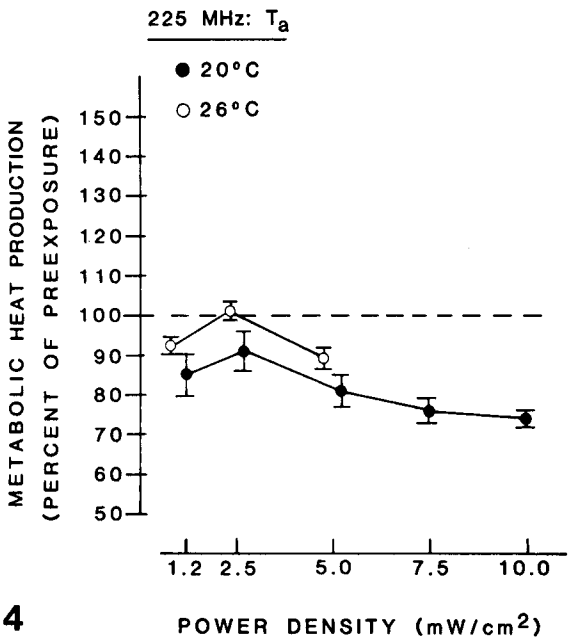
225 MHz: T_a
● 20°C
○ 26°C
METABOLIC HEAT PRODUCTION (PERCENT OF PREEXPOSURE)
150
140
130
120
110
100
90
80
70
60
50
1.2 2.5 5.0 7.5 10.0
POWER DENSITY (mW/cm²)

4

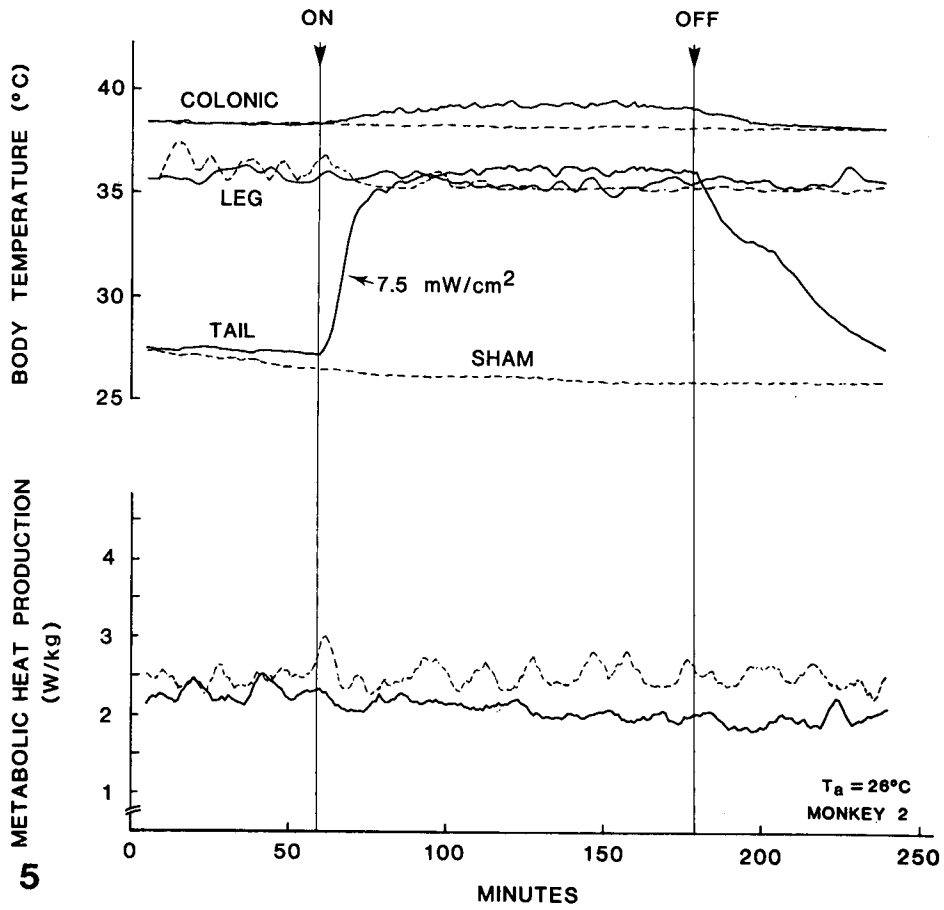
ON
OFF
BODY TEMPERATURE (°C)
40
35
30
25
COLONIC
LEG
TAIL
SHAM
7.5 mW/cm²
METABOLIC HEAT PRODUCTION (W/kg)
4
3
2
1
T_a = 26°C
MONKEY 2
0 50 100 150 200 250
MINUTES

5

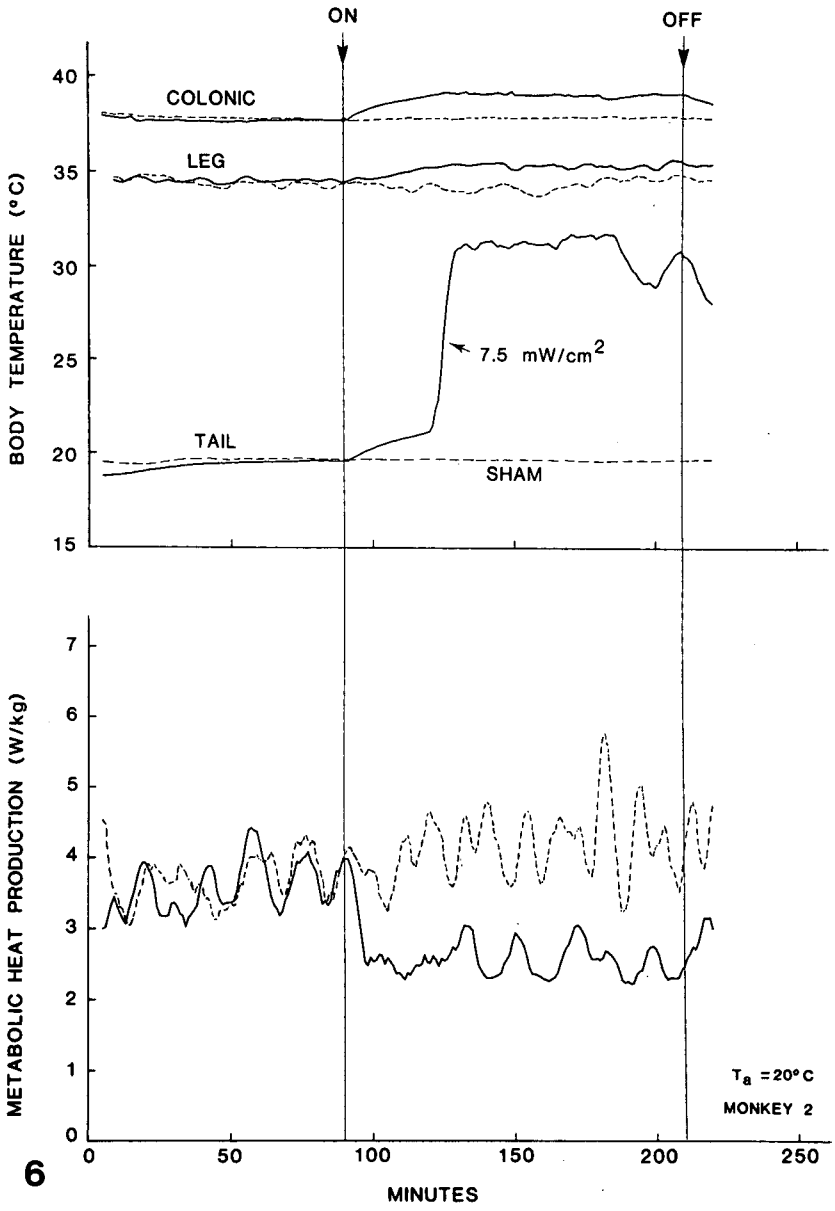

Fig. 6. Plots of data from a representative steady-state experiment with monkey 2 at a T_a of 20 °C, showing the same variables with the same details and representations as in Figure 5.

Fig. 4. Mean (± SE) metabolic heat production (M) ratio (percentage of pre-exposure) during 10-min RF exposures of rhesus monkeys to 225 MHz at either 20 or 26 °C ambient temperature. The value for pre-exposure M was the mean M for the 10 min immediately preceding the associated exposure step.

Fig. 5. Plots of data from a representative steady-state experiment with monkey 2 at a T_a of 26 °C, showing colonic, leg skin, and tail skin temperatures, and M. The heavy, solid lines show the results of exposure to 7.5 mW/cm^2; the lighter-dashed lines show the corresponding sham-exposure data. The data for T_{le}, as well as M, in this figure and in Figure 6 have been smoothed by calculating 5-min running averages. The vertical lines and arrows indicate the beginning and end of exposure.

appreciably for exposures at T_a = 26 °C except at 7.5 mW/cm^2. Statistical comparisons indicated that there was no difference in M among any of the exposure conditions at T_a = 26 °C. At a T_a of 20 °C, the level of M in sham-exposed animals was actually higher than the pre-exposure level, and M was consistently reduced at all power densities. Differences in M between sham and RF conditions were significant ($F = 4.45$, $df = 20$, $p = .013$). Tukey's HSD test showed that M was significantly different from the sham level at 7.5 and 10.0 mW/cm^2. At 5 mW/cm^2, one animal had a much higher M than during sham exposure, causing the slightly higher mean M at 5 than at 2.5 mW/cm^2. The reduction in M during RF exposure at 20 °C seemed to have a limit of about 0.7–1.0 W/kg.

DISCUSSION

When colonic temperature increases caused by resonant frequency RF exposure of the monkey were first reported [Lotz, 1982], many questions were raised regarding thermoregulatory function and control of ambient temperature in those experiments. The data from this study indicate that the thermoregulatory responses of the rhesus monkey exposed to 225 MHz energy are appropriate to reduce accumulation of heat within the body. The effector actions were qualitatively similar to the responses known to occur in the presence of other thermal stimuli, e.g., changes in T_a [Johnson and Elizondo, 1979]. These effector actions, however, did not prevent the development of measurable increases in T_{co}, even at the lowest intensities studied. Depending on the ambient temperature, we consistently observed either a reduction in M or a vasodilation of the tail during a 10-min exposure to 5 mW/cm^2 (1.4 W/kg) and above. The mean level of M was significantly lower during 10-min exposures at 7.5 mW/cm^2 and higher power densities than during exposures to 5.0 mW/cm^2 and lower power densities. The mean increase in T_{co} for a 10-min exposure at 1.2 or 2.5 mW/cm^2 (0.4 or 0.7 W/kg) was 0.1 or 0.2 °C, respectively, at both T_a. At 5.0 mW/cm^2, the mean increase in T_{co} for a 10-min exposure was 0.3 or 0.4 °C at a T_a of 20 or 26 °C, respectively. The increases in T_{co} in the steady-state condition, shown in Figure 7, are larger than the ΔT_{co} during 10-min exposures, as expected (see Figs. 5 and 6). Generally, a steady-state was achieved in about 90 min during RF exposure, whether at a T_a of 20 or 26 °C (see Figs. 5 and 6).

At a T_a of 20 °C, the successive recruitment of thermoregulatory effectors — first the reduction in M, and later peripheral vasodilation — was seen in each subject at all but the lowest power density (see Figs. 2, 5, and 6). In general, body temperatures did not equilibrate at a T_a of 20 °C until after vasodilation occurred. At a T_a of 26 °C, only vasodilation was observed during 120-min exposures, but a steady-state colonic temperature was not achieved until long after the vasomotor response occurred. At a T_a of 26 °C, sweating may have been initiated sometime after the vasomotor response, but sweating was not measured in this study. A sudomotor response would have provided the secondary recruitment of effectors at a T_a of 26 °C to achieve steady-state equilibrium that corresponds to the two-stage process demonstrated at a T_a of 20 °C. Johnson and Elizondo [1979] reported significant linear correlations between evaporative heat loss due to sweating (E_{sw}) and rectal temperature (T_{re}) or mean skin temperature ($\overline{T}_{sk}$) for T_{re} above 38.5 °C and for $\overline{T}_{sk}$ above 36 °C. In our study, steady-state mean T_{re} exceeded 38.5 °C for exposures at 2.5 mW/cm^2 and higher at either T_a. At a T_a of 26 °C, mean T_{co}

exceeded 39 °C during exposure at 7.5 mW/cm^2. Thus, if the relationships found by Johnson and Elizondo are valid in these RF exposure studies, significant sweating should have occurred in the more intense exposures at a T_a of 26 °C. Such predictions are only approximate due to differences between studies in air velocity and other significant ambient factors. The increases in M that we observed during the latter portion of 120-min exposures at 26 °C are consistent with the possibility that the monkeys were sweating to achieve thermal balance. However, such increases could also have been simply due to a thermodynamic effect of body heating or to emotional factors.

The work of Johnson and Elizondo [1979] also provides reference data for comparing thermoregulatory data to this study. The steady-state mean M at a T_a of 26 °C during sham exposure in the present study was 2.26 W/kg, representing the condition nearest to that of a resting metabolic rate (RMR). Bourne [1975] reported a RMR of 2.4 W/kg for the rhesus monkey. Using the equation provided by Johnson and Elizondo [1979] to convert our data to surface area in terms of W/m^2, the mean steady-state M during sham-exposure at T_a of 26 °C was 39.6 W/m^2. Johnson and Elizondo reported that the mean M for considerably smaller monkeys (3–5 kg) at T_a of 25 °C was 55.2 W/m^2. They also reported that M at a T_a of 20 °C was 25 and 37% above M at a T_a of 25 °C and 28 °C, respectively. In our study, M at a T_a of 20 °C was 38% above M at a T_a of 26 °C.

The pulsatile nature of M in our study is more pronounced than we expected, particularly at a T_a of 20 °C. Although activity was variable among subjects, it was generally low, and we found no indication that the pulses in M were related to activity or to shivering by the animal. The only data we found in the literature for comparison were those of Johnson and Elizondo [1979, see Fig. 2], which show moderate repetitive fluctuations over 5–10 min intervals. Their time intervals correspond to the interval of M pulses noted in our data, but the magnitude of the variability in their study was much lower than in our study. However, Johnson and Elizondo displayed data for a T_a of 33.6 °C. The magnitude of pulses in M apparent in our data was much less at a T_a of 26 °C than at a T_a of 20 °C (Fig. 6). Furthermore, the pulses in M at a T_a of 20 °C were also suppressed by RF exposure at levels that caused body heating. Thus, these pulses may be an inherent property of rhesus monkey metabolism that is temperature dependent. Another reason why Johnson and Elizondo may not have found such a strong pulsatile nature in M of the rhesus monkey is that air flow through the hood and gas meters of their study was roughly half of the flow rate we used. A slower flow rate would damp any measurable fluctuations in M. In an additional effort to smooth out the variations in M, we replotted our data after calculating the running averages (Figs. 5 and 6). Although the running averages smoothed the data, the pulsatile nature was not eliminated because of the regular periodicity in M.

Inner thigh skin temperature (T_{le}) was monitored to provide an estimate of mean skin temperature ($\bar{T}_{sk}$) because Johnson and Elizondo [1974] found a strong correlation between mean skin temperature ($\bar{T}_{sk}$) and T_{le}. Technical problems with our measurements of T_{le} resulted in unacceptably high variability. We attributed these problems to animal movement and to the use of nonperturbing temperature probes. The latter were absolutely essential to measure temperature accurately at this frequency, but did not function particularly well as skin temperature probes. The variability in T_{le} can be seen in Figures 5 and 6. The group mean steady-state T_{le}

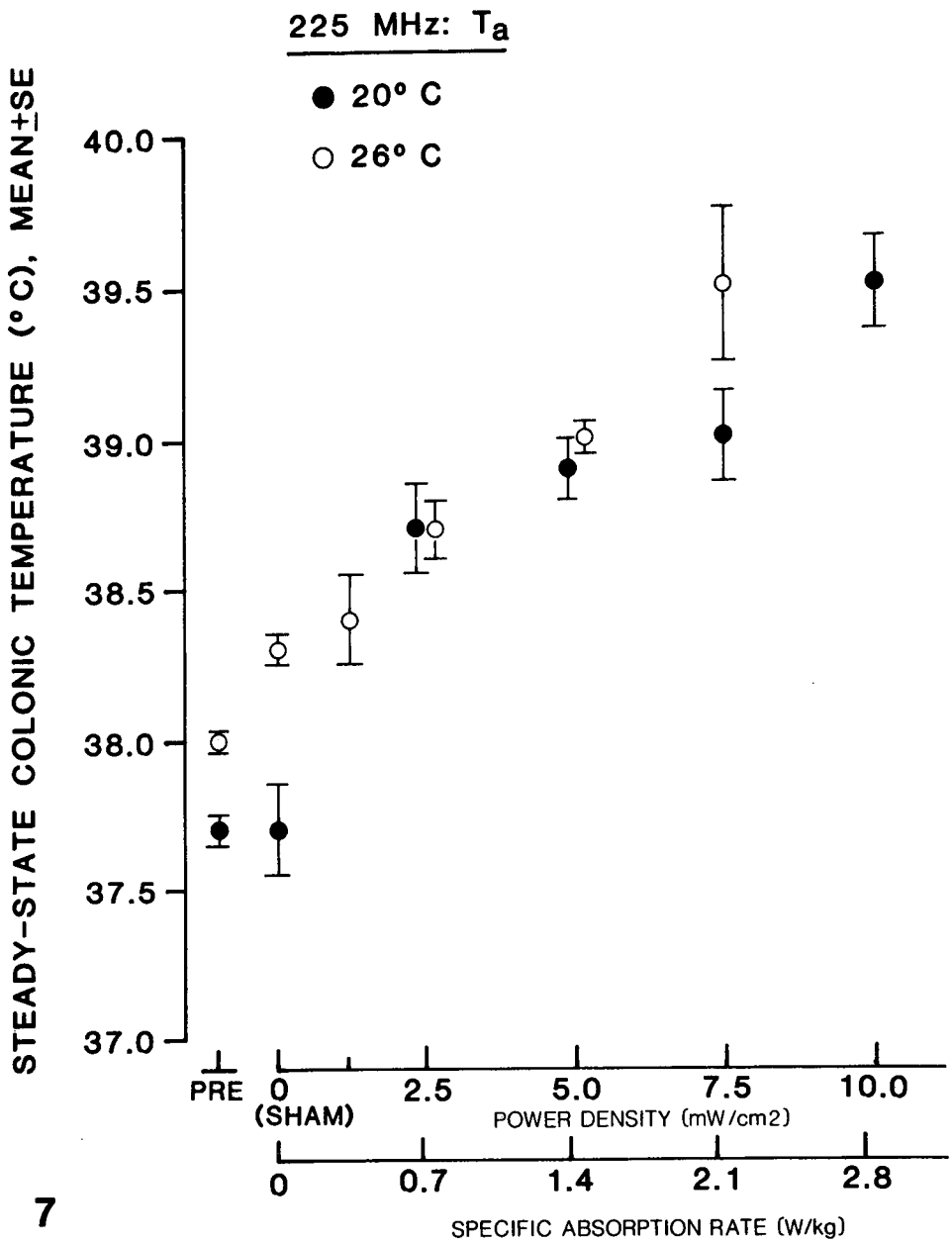

Fig. 7. Mean (± SE) colonic temperature of rhesus monkeys (n = 5) exposed to 225 MHz at a T_a of either 20 or 26 °C. Data shown are the mean values of the last 30 min of the exposure period. The values for the last 30 min of the pre-exposure period are indicated above PRE on the abscissa.

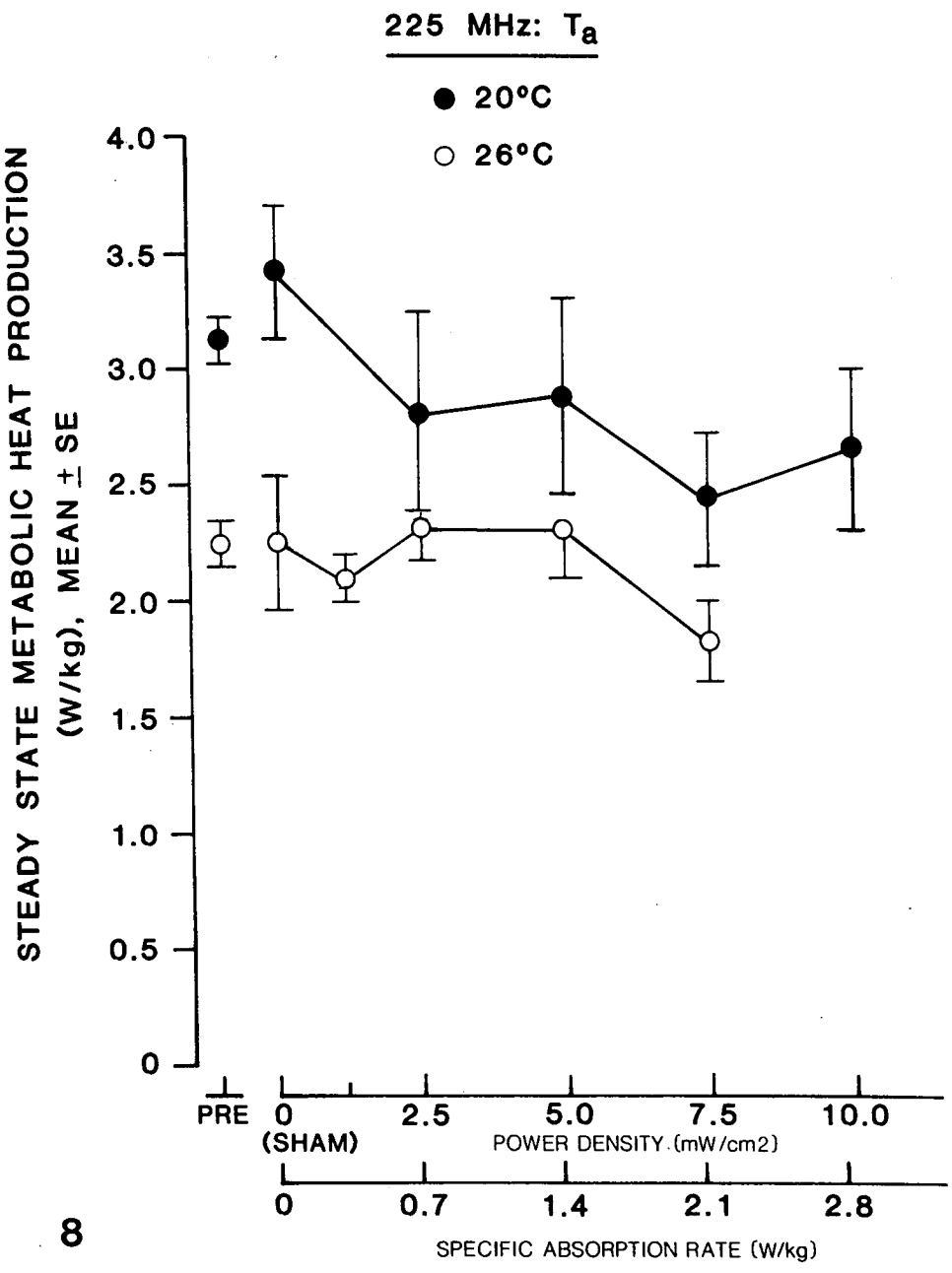

Fig. 8. Mean (± SE) steady-state M of rhesus monkeys (n = 5) exposed to 225 MHz at a T_a of either 20 or 26 °C. Data shown are the mean values of the last 30 min of the exposure and pre-exposure periods as in Figure 7.

during sham-exposures was 32.8 and 34.8 °C at a T_a of 20 and 26 °C, respectively. Johnson and Elizondo [1979] reported group $\bar{T}_{sk}$ (measured as T_{le}) to be 31.7 and 33.6 °C at a T_a of 20 and 25 °C, respectively. The higher results in our work probably reflect the technical problems, and may have resulted from the probe tip pulling back into the sheath (and thus away from the air/skin interface) when the animal moved. The fact that T_{le} in Figure 5 is virtually unchanged by the exposure was unexpected, and is hard to explain, since tail skin temperature is markedly elevated. The experiment shown in Figure 5 is representative, however. Mean steady-state T_{le} was only slightly elevated at a T_a of 26 °C for any of the exposures. Figure 6 also shows a representative result for T_{le} at a T_a of 20 °C. While T_{le} was significantly higher during RF exposure at a T_a of 20 °C, the increases in T_{le} were no greater than the corresponding increases in T_{co} for the same exposures. Thus, our data suggest that T_{co} was elevated as much or more than T_{le} (or possibly $\bar{T}_{sk}$) by exposure to 225 MHz fields. This may be an artifact because of technical problems, or it may represent a key aspect of RF heating with a frequency that penetrates deeply into the body. Further studies of thermoregulatory responses during exposure with penetrating RF frequencies are needed to answer this question.

Our data agree with other studies of the influence of microwave/RF exposure on thermoregulatory function. In the earliest studies of this type, Phillips et al [1975] and Ho and Edwards [1977] observed reductions in M in rats or mice exposed to 2450 MHz. In the most extensive work to date on the subject, Adair and Adams have shown that squirrel monkeys exposed to 2450 MHz exhibit behavioral [1980a], metabolic [1982], vasomotor [1980b], and sudomotor [Adair, 1983] responses that are qualitatively similar to those reported here for the rhesus monkey. One feature of our data, unlike that of Adair and Adams (1982), is that the reduction in M at a T_a of 20 °C is not large enough to be quantitatively comparable to the SAR of most exposures used. In the squirrel monkey exposed to microwaves (T_a = 20 °C), the reduction in M during steady state conditions (90 min) was equal to a SAR of 1–2 W/kg.

A major problem in comparing data from these two species, however, is that M is not sufficiently elevated in the rhesus at a T_a of 20 °C to allow reductions in M during microwave exposure as large as those that were observed for the squirrel monkey. In the squirrel monkey, M increases at a T_a of 20 °C were 3–4 W/kg above M at a T_a of 25 °C [Adair and Adams, 1982]. The mean elevation in M for the rhesus at a T_a of 20 °C was only 0.87 W/kg above M at a T_a of 26 °C. This limited range of adjustment in M of the rhesus monkey, coupled with the inherent variability of M observed, restricts quantitative comparison of these studies. For the squirrel monkey, reductions in M during 2450 MHz exposure at a T_a of 20 °C can fully compensate for the microwave-induced heat at SARs up to about 4.5 W/kg [Candas et al, 1985]. This was not the case for the rhesus exposed to 225 MHz at a T_a of 20 °C. As shown in Figure 8, the reduction in M for rhesus monkeys exposed to 225 MHz (T_a = 20 °C) for 120 min was less than the SAR at power densities above 2.5 mW/cm^2 (0.7 W/kg). At 2.5 mW/cm^2, the mean reduction in M (0.6 W/kg) and the SAR were comparable. Interestingly, only one of five animals showed the secondary vasomotor response during the 120-min exposure to 2.5 mW/cm^2 at 20 °C.

Thus, the rhesus monkey apparently compensated for RF exposure at 2.5 mW/cm^2 by metabolic adjustments alone, even though this did not prevent an increase in T_{co}. At higher power densities, e.g., 7.5. mW/cm^2, the mean reduction in M was

only 25% or less of the SAR, and the vasomotor response was recruited. This recruitment of thermoregulatory effectors is qualitatively identical to that observed in the squirrel monkey exposed to 2450 MHz at a T_a of 20 °C and power densities greater than 35 mW/cm^2 [Candas et al, 1985], even though distinct quantitative differences exist. Both species activate heat loss mechanisms (vasodilation) when the RF load cannot be offset by lowering M, and the steady-state response to RF exposures at a T_a of 20 °C reduced M to a level near that observed in a thermoneutral environment in both species. This reduction in M toward RMR during RF exposure at a T_a of 20 °C can be seen in Figure 6. The mean M for monkey 2 during the last 30 min of the 7.5 mW/cm^2 exposure was 2.46 W/kg, which was close to the 2.39 W/kg for this monkey during sham exposure at a T of 26 °C.

The SAR required (1.4 W/kg at 5 mW/cm^2) to initiate thermoregulatory responses in the rhesus monkey at either T_a is similar to the SAR observed to initiate these responses in the squirrel monkey exposed to 2450 MHz [Adair and Adams, 1982]. However, these SARs represent different heat loads relative to the RMR of the species. For the squirrel monkey, the threshold SAR for thermoregulatory responses to 2450 MHz exposure is of the order of 0.2 MET [Adair and Adams, 1980b; 1982] where MET designates the resting M in a thermoneutral environment [Bligh and Johnson, 1973]. For the rhesus monkey, thermoregulatory responses were initiated during exposures to 225 MHz at a SAR of approximately 0.5 MET. Behavioral thermoregulatory responses have been observed in rats exposed to 2450 MHz fields at a threshold of about of 0.2 MET [Stern et al, 1979]. This difference in exposure thresholds relative to MET may be due to the differences in species, frequencies, or other unidentified factors in the studies.

Another significant finding of the present study is the elevation in T_{co} at low SAR; the T_{co} increases appear to be greater than those observed in a number of other microwave/RF exposure studies. In the work by Adair and her colleagues with squirrel monkeys, microwave exposure at power densities initiating thermoregulatory responses (0.2 MET)) did not increase T_{co} more than 0.2–0.3 °C. For the rhesus monkey exposed to 225 MHz at power densities high enough to initiate thermoregulatory responses (0.5 MET), T_{co} was increased 0.7 and 1.2 °C at a T_a of 26 and 20 °C, respectively. When the rhesus monkey was exposed at a SAR of the order of 0.2 MET (0.35 W/kg) at a T_a of 26 °C, steady-state T_{co} was only 0.3 °C above the sham-exposure value. The SAR required to cause a 1 °C increase in T_{co} of the rhesus monkey exposed to 225 MHz at a T_a of 26 °C was 2.1 W/kg, or about 1 MET. For the squirrel monkey exposed to 2450 MHz at a T_a of 24 °C, a 1 °C increase in T_{co} also occurs at a SAR equal to about 1 MET [de Lorge, 1983]. For the rat, the SAR required to increase T_{co} 1 °C during 2450 MHz exposure at a T_a of 24 °C is about 0.5 MET [Lotz and Michaelson, 1978]. Thus, when viewed in terms of SAR required to produce ΔT_{co} of 1 °C and relative heat load (MET), the T_{co} increases noted in our data are not significantly different from those reported for squirrel monkeys. If the comparison is limited to frequencies above whole-body resonance, however, a trend exists wherein the relative RF induced heat load required (in METs) to raise T_{co} more than 1 °C increases with animal size. At 1.3 [Lotz and Podgorski, 1982] and 2.45 GHz [de Lorge, 1983], the SAR required to raise T_{co} of the rhesus monkey 1 °C is about 2 MET, compared to 1 MET for squirrel monkeys and 0.5 MET for rats. Whether or not this trend would extend to even larger mammals, including man, is not known.

The increases in internal temperature (Fig. 6) caused by exposure to 225 MHz in this study confirm that the T_{co} response to RF heating of the rhesus monkey is frequency dependant, because the changes in T_{co} at 225 MHz are greater than those observed in rhesus monkeys exposed to equivalent SARs at a considerably higher frequency (1290 MHz) [Lotz and Podgorski, 1982; Lotz, 1985]. The changes in T_{co} in this study are similar to those reported for two studies in which the control of T_a was less precise [Lotz, 1985; de Lorge, 1984]. At 1290 MHz, the SAR required to raise T_{co} by 1 °C was equivalent to 2 MET [Lotz and Podgorski, 1982]. At 225 MHz, as noted above, T_{co} was raised 1 °C during exposure to a SAR of only about 1 MET. The data presented here are not sufficient to determine why these changes in T_{co} differ with frequency. The difference could be simply related to depth of penetration of the RF energy, or it could be related to quantitative differences in the sensitivity and responsiveness of the thermoregulatory system to such energy. We favor the hypothesis that the greater internal heating at a frequency near resonance is due to the depth of penetration of the energy. If this is true, then equivalent SARs at frequencies below resonance would also produce the same phenomenon. Adair [1985] has concluded in a recent summary of her work that "...thermal sensors in the skin, rather than those deeper in the body, are probably responsible for most of the response changes observed..." in the squirrel monkey exposed to 2450 MHz. The observation that longer wavelength radiation, which penetrates into deeper tissues, is less effective in stimulating thermoregulatory responses, but more effective in heating internal tissues, is consistent with her conclusions. Additional experiments with monkeys exposed to frequencies above, at, or below resonance should be done to address these questions.

In summary, metabolic and vasomotor adjustments were shown to occur in rhesus monkeys exposed to 225 MHz during brief (10 min) or sustained (120 min) exposures at SARs ranging from 1.4–3.5 W/kg. The responses were effectively coordinated to produce steady-state conditions in body temperatures after about 90 min of exposure at a T_a of either 20 or 26 °C. During steady-state conditons, heat storage within the body caused elevations in T_{co} that reached 1 °C during exposures to about 1–2 W/kg, depending on the T_a. These results show that the thermoregulatory response of the rhesus monkey to a RF exposure at the resonant frequency is qualitatively appropriate to limit storage of heat in the body. However, substantial increases in T_{co} were not prevented by such responses, even in a cool environment.

ACKNOWLEDGMENTS

The technical assistance of ENS Michael Golightly, Mr. Steve Woodson and Mr. Robert Upchurch is gratefully acknowledged. We thank Mr. Chuck Mogensen, Mr. Robert Barrett, and Mrs. Anna Johnson for assistance in manuscript preparation.

Opinions and conclusions contained in this report are those of the authors and do not necessarily reflect the views or the endorsement of the Navy Department. This research was supported by the Naval Medical Research and Development Command under work unit number 62758N MF58524.02C-0009, Accession No. DN277076. The animals used in this study were handled in accordance with the principles stated in the "Guide for the Care and Use of Laboratory Animals," Institute of Laboratory Animal Resources, National Research Council, DHHS, NIH Publication No. 85-23, 1985, and the Animal Welfare Act of 1966, as amended.

REFERENCES

Adair ER (1983): Initiation of thermoregulatory sweating by whole-body 2,450 MHz microwave exposure. Fed Proc 42:746.

Adair ER (1985): "Microwave Radiation and Thermoregulation" USAFSAM-TR-85-3. Brooks Air Force Base, TX: USAF School of Aerospace Medicine.

Adair ER, Adams BW (1980a): Microwaves modify thermoregulatory behavior in squirrel monkey. Bioelectromagnetics 1:1–20.

Adair ER, Adams BW (1980b): Microwaves induce peripheral vasodilation in squirrel monkey. Science 207:1381–1383.

Adair ER, Adams BW (1982): Adjustments in metabolic heat production by squirrel monkeys exposed to microwaves. J Appl Physiol: Respirat Environ Exercise Physiol 52:1049–1058.

Bligh J, Johnson KG (1973): Glossary of terms for thermal physiology. J Appl Physiol 35:941–961.

Bourne GH (1975): Collected anatomical and physiological data from the rhesus monkey. In Bourne GH (ed): "The Rhesus Monkey," Vol 1. New York: Academic Press, p.55.

Candas V, Adair ER, Adams BW (1985): Thermoregulatory adjustments in squirrel monkeys exposed to microwaves at high power densities. Bioelectromagnetics 6:221–234.

de Lorge JO (1983): The thermal basis for disruption of operant behavior by microwaves in three animal species. In Adair ER (ed): "Microwaves and Thermoregulation." New York: Plenum Press, pp 379–399.

de Lorge JO (1984): Operant behavior and colonic temperature of *Macaca mulatta* exposed to radio frequency fields at and above resonant frequencies. Bioelectromagnetics 5:233–246.

Durney CH, Johnson CC, Barker PW, Massoudi H, Iskander MF, Lords JL, Ryser DK, Allen SJ, Mitchell JC (1978): "Radio-frequency Radiation Dosimetry Handbook," 2nd Ed, Sam-TR-78-22. Brooks Air Force Base, TX: USAF School of Aerospace Medicine.

Gandhi OP (1975). Conditions of strongest electromagnetic power deposition in man and animals. IEEE Trans Microwave Theory Tech MTT-23:1021–1029.

Ho HS, Edwards WP (1977): Dose rate and oxygen consumption rate in mice confined in a small holder during exposure to 2450 MHz microwave radiation. Radiat Environ Biophys 14:251–256.

Johnson GS, Elizondo RS (1974): Eccrine sweat gland in *Macaca mulatta*: physiology, histochemistry, and distribution. J Appl Physiol 37:814–820.

Johnson GS, Elizondo RS (1979): Thermoregulation in *Macaca mulatta*: A thermal balance study. J Appl Physiol: Respirat Environ Exercise Physiol 46: 268–277.

Kirk RE (1968): "Experimental Design: Procedures for the Behavioral Sciences." Belmont: Wadsworth.

Lotz WG (1982): "Hyperthermia in Rhesus Monkeys Exposed to A Frequency (225 MHz) Near Whole-Body Resonance," NAMRL-1284. Pensacola, FL: Naval Aerospace Medical Research Laboratory.

Lotz WG (1985): Hyperthermia in radiofrequency exposed rhesus monkeys: A comparison of frequency and orientation effects. Radiat Res 102:59–70.

Lotz WG, Michaelson SM (1978): Temperature and corticosterone relationships in microwave-exposed rats. J Appl Physiol: Respirat Environ Exercise Physiol 44:438–445.

Lotz WG, Podgorski RP (1982): Temperature and adrenocortical responses in rhesus monkeys exposed to microwaves. J Appl Physiol: Respirat Environ Exercise Physiol 53:1565–1571.

Olsen RG, Griner TA (1982): Electromagnetic dosimetry in a sitting rhesus model at 225 MHz. Bioelectromagnetics 3:385–389.

Phillips RD, Hunt El, Castro RD, King NW (1975): Thermoregulatory, metabolic, and cardiovascular responses of rats to microwaves. J Appl Physiol 38:630–635.

Stern S, Margolin L, Weiss B., Lu S-T, Michaelson SM (1979): Microwaves: Effect on thermoregulatory behavior in rats. Science 206:1198–1201.

Bioelectromagnetics 8:91–102 (1987)

Simple Method to Measure Power Density Entering a Plane Biological Sample at Millimeter Wavelengths

Z.-Y. Shen, L. Birenbaum, A. Chu, S. Motzkin, S. Rosenthal, and K.-M. Sheng

Department of Radio Electronics, Zhejiang University, Hangzhou (Z.-Y.S.), Department of Applied Physics, Southwestern Jiaotung University, Emei, Sichuan (K.-M.S.), People's Republic of China; Departments of Electrical Engineering and Computer Science (L.B., A.C., S.R.) and Chemistry/Life Sciences (S.M.), Polytechnic University, Brooklyn, New York

A simple method for measuring microwave power density is described. It is applicable to situations where exposure of samples in the near field of a horn is necessary. A transmitted power method is used to calibrate the power density entering the surface of the sample. Once the calibration is available, the power density is known in terms of the incident and reflected powers within the waveguide. The calibration has been carried out for liquid samples in a quartz cell. Formulas for calculating specific absorption rate (SAR) are derived in terms of the power density and the complex dielectric constant of the sample. An error analysis is also given.

Key words: millimeter waves, near-field measurement, microwave power density

INTRODUCTION

The near field of a horn is complicated and difficult to determine, especially when a biological sample is introduced. For this reason, when use of the near field cannot be avoided, a simple method to measure the microwave power density (PD) entering the surface of the sample is useful. From the PD and the complex dielectric constant, the specific absorption rate (SAR) can be calculated.

Ordinarily, the simplest way to measure PD is by using a conventional radiation meter. But it can only give the PD value of the incident wave in free space. When the sample is introduced, reflection and scattering occur. The situation becomes complicated, and it is difficult to measure the PD by conventional methods.

Most biological samples contain large amounts of water, so they are very lossy for the rf fields. As a result, the skin depth is often very small in the microwave and millimeter wave ranges. If the thickness of a (planar) sample is much greater than the

Received for review June 24, 1985; revision received June 6, 1986.

This work was performed at the Polytechnic University. A portion of this paper was presented by Professor Shen at the IMPI Symposium, July 25–30, 1982, in San Diego, California.

Professor Shen is now at HYPRES, Inc., 500 Executive Blvd., Elmsford, NY 10523.

Address reprint requests to Professor Leo Birenbaum, EE/CS Department, Polytechnic University, 333 Jay Street, Brooklyn, NY 11201.

skin depth, then power will be attenuated very strongly as it goes through the sample. This suggests that, behind the sample, measurements of the transmitted power can be carried out without disturbing the fields in front of the sample.

In the method described here, the latter idea is used as the basis for a calibration procedure that, once completed, permits one to determine the power density entering a sample surface from measurements of the incident and reflected power within the waveguide.

The basic idea may be described by referring to Figure 1(a), which shows a highly dissipative planar sample s (housed within a quartz cell) located in the near field of a transmitting horn H_1. Power P_1' leaves the horn, and a portion enters the surface s_1 closest to the horn. The power density p_1' that enters s_1 is the quantity of principal interest. The power density reaching the sample surface s_2, farthest from the transmitting horn, is assumed to be at least 10dB below that which enters surface s_1.

If a receiving horn H_2 is now positioned so that its aperture nearly coincides with s_2, and a detector is placed at the end of the receiving waveguide, a power reading P_t' will be obtained. However, this reading does not give the power density that enters surface s_1. In addition, the ratio R between the power density p'_1 entering s_1 and the power P'_1 leaving the transmitting horn is unknown.

R may be determined by the following method: First, the sample, together with its receiving horn assembly, is moved so that it covers the transmitting horn aperture, as in Figure 1(b). Then, the incident and reflected powers are measured within the transmitting waveguide. From this data, it is possible to deduce the net power P_1 now entering the surface s_1, and hence to calculate the power density p_1 entering s_1, all

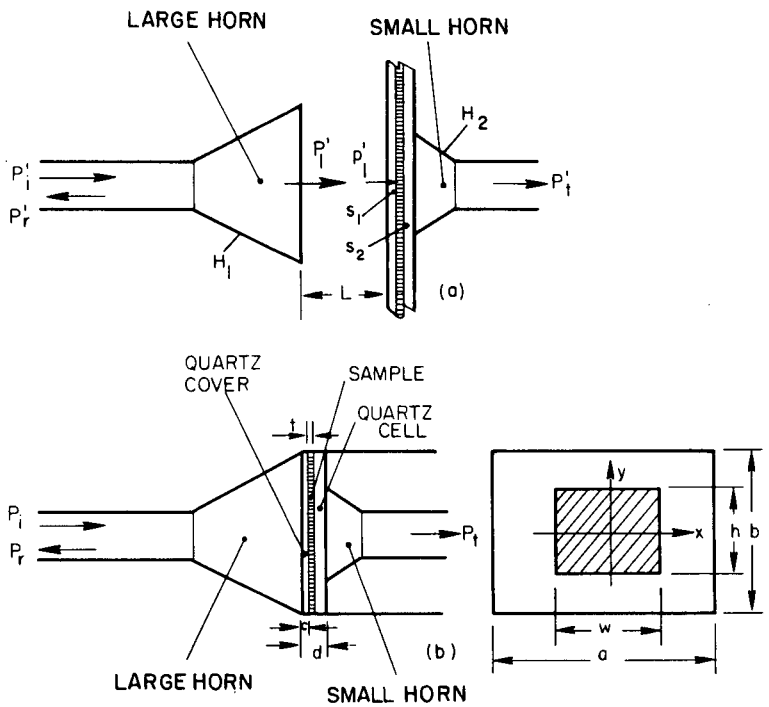

Fig. 1. Sketch showing basic principle of calibration scheme.

for the situation of Figure 1(b). If the receiver power reading is now P_t, and the attenuation of the sample is high, one may write:

$$\frac{p'_1}{P'_t} = \frac{p_1}{P_t}.$$

This relationship expresses the idea that the ratio of the power density entering surface s_1 to the reading on the far-end detector is the same in the two situations because of the high sample attenuation. Hence, in the original position shown in Figure 1(a), the ratio R of the power density entering s_1 to the power P'_1 leaving the transmitting horn may be calculated as:

$$R = \frac{p'_1}{P'_1} = \left(\frac{p_1}{P_t} P'_t\right) \cdot \frac{1}{P'_1} = \frac{p_1}{P_1} \cdot \frac{P'_t}{P_t} \cdot \frac{P_1}{P'_1}.$$

Once the calibration constant R has been determined, the receiving horn is no longer needed; that is, $p'_1 = P'_1 R$. This means that, even though the sample is located in the near field of the horn, it is still possible to determine the power density entering the sample surface from measurements made in the transmitting waveguide alone, once the calibration procedure has been carried out.

In the portions of the paper to follow, this idea is discussed more precisely and in detail.

DETAILS OF THE THEORY AND DEFINITION OF CALIBRATION CONSTANT

For a given sample at a given frequency, the power transmitted through the sample is proportional to the PD entering the front surface, due to the linearity of the system. In order to define the proportionality constant, it is helpful to reconsider the arrangement shown in Figure 1 in more detail. Conceptually, we place the sample into a TE_{10} waveguide, shown at the right in Figure 1(b), whose cross section is the same as that of the sample and also the same as the aperture of the transmitting horn. This creates an idealized configuration for which the PD pattern is known. It is assumed that only the dominant mode is present. For measuring the transmitted power, we put a small horn behind the sample. Here, it is assumed that there is sufficient sample attenuation present so that the PD in the front layers of the sample is unaffected by the receiving horn. It is also assumed that, in the rear layers of the sample, the receiving horn does not appreciably disturb the field distribution within. On the front surface of the sample, PD is a function only of the horizontal distance x from the center of the transmitting horn:

$$PD(x) = PD(0) \cos^2\left(\frac{\pi}{a} x\right) \tag{1}$$

where PD(0) is the PD at center of the horn aperture. The average PD within the

rectangular area (shaded area in Fig. 1(b)), having a width w identical to that of the receiving horn, is given by:

$$PD(w) = F(w)\, PD(0) \tag{2}$$

where

$$F(w) = \frac{1}{w}\int_{-w/2}^{w/2} \cos^2\left(\frac{\pi}{a}x\right) dx = \frac{1}{2}\left[1 + \frac{\sin\left(\pi\frac{w}{a}\right)}{\left(\pi\frac{w}{a}\right)}\right]. \tag{3}$$

The average PD over the whole cross section of the large waveguide can be determined from Equations (2) and (3) as follows:

$$\overline{PD}(a) = F(a)\, PD(0) = \frac{1}{2} PD(0) = \frac{P_i - P_r}{ab}$$

and

$$PD(0) = \frac{2(P_i - P_r)}{ab}.$$

The quantities P_i and P_r are the incident and reflected powers in front of the sample. Substituting into Equation (2), we have:

$$\overline{PD}(w) = \frac{2(P_i - P_r)}{ab} F(w).$$

Now we define

$$C = \overline{PD}(w)/P_t = \frac{2(P_i - P_r)}{abP_t} F(w) \tag{4}$$

as a calibration constant. For a given structure, a, b, w, and F(w) are known; the incident power P_i, the reflected power P_r, and the transmitted power P_t behind the sample can be measured. Consequently, C can be calculated according to Equation (4); $\overline{PD}(w)$ is given by:

$$\overline{PD}(w) = C\, P_t. \tag{5}$$

Therefore, once the calibration has been done and the value of C is known, the PD (average value within the shaded area in front of the sample) can be determined for another location of the sample by measuring P_t with the same small horn behind the sample, provided the surface of the sample is kept perpendicular to the incident wave.

When a real irradiation experiment with a biological sample is performed, the situation corresponds to that shown in Figure 1(a) rather than that of Figure 1(b). It is more convenient to eliminate the small horn and to measure the incident power P_i' and reflected power P_r' in the input waveguide of the large horn rather than to measure

the transmitted power P_t directly. Hence, we need to introduce more calibration constants:

$$M = (P'_i - P'_r)/P'_t \tag{6}$$

and

$$R = C/M. \tag{7}$$

Then

$$PD = R\,(P'_i - P'_r). \tag{8}$$

Thus, once the calibration has been completed, the small horn behind the sample is no longer needed. The separation L between the radiating horn and the sample surface is zero during the calibration procedure for C and is fixed at its normal value during the calibration procedure for M.

EXPERIMENTAL RESULTS

Several calibration experiments were carried out over the 50–64 GHz frequency range using the equipment shown in the block diagram of Figure 2.

Figure 3 shows the normalized calibration constant 1/2 abR as a function of frequency f for two .5-mm thick planar liquid samples contained in a quartz cell. The

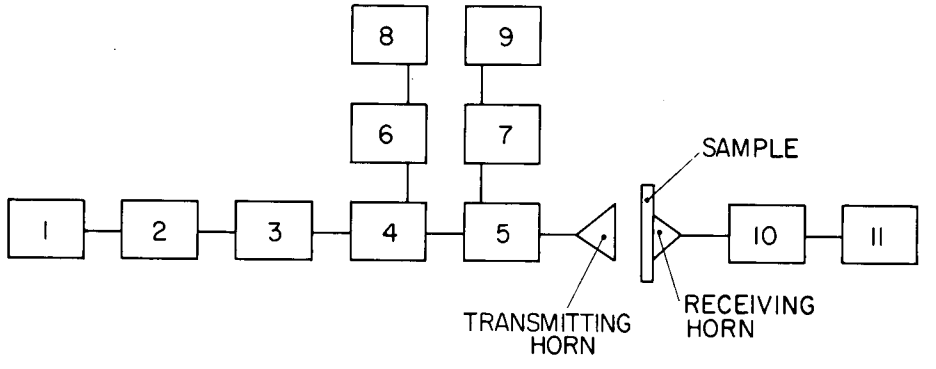

Fig. 2. Block diagram of equipment used for calibration. 1) Millimeter source, Siemens RWO-60; 2) attenuator FXR M164AO; 3) frequency meter, TRG V551; 4) forward sampling directional coupler, Hitachi, 2101, 10dB; 5) backward sampling directional coupler, Hitachi, 2101, 10dB; 6,7) thermistor mounts for measuring incident and reflected powers, Hughes 45774H; 8,9) power meters for measuring incident and reflected powers, HP 432A; 10,11) thermistor mount and power meter for measuring transmitted power, Hughes 45774H and HP 432A.

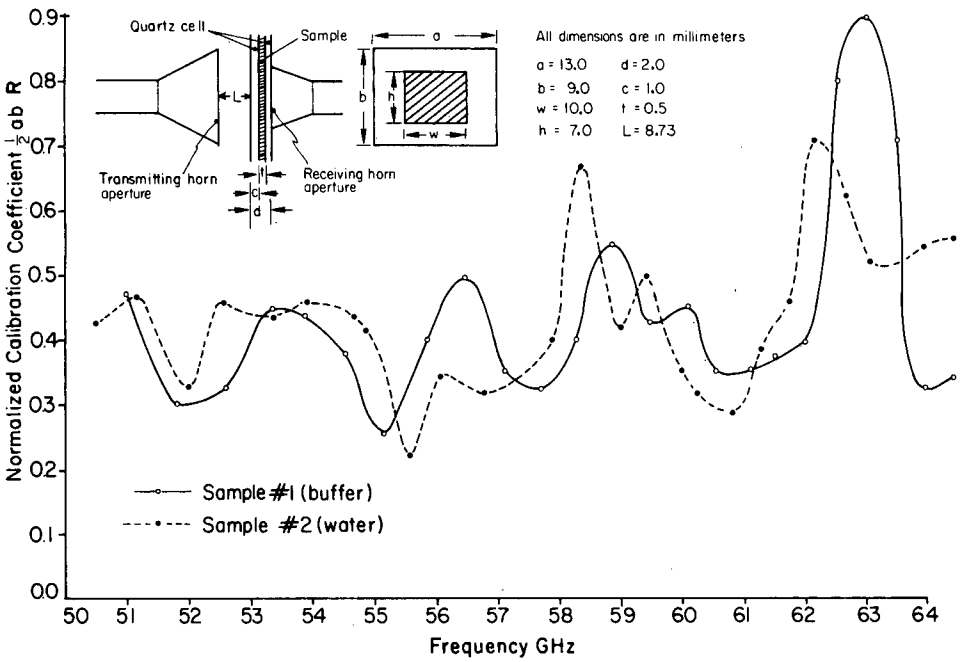

Fig. 3. Calibration constant R vs frequency for two samples.

solid curve represents the result for a sample of buffer (an aqueous solution resistant to changes in pH when small quantities of acidic or basic substances are added; commonly used in biological work). (Our buffer contained the following concentrations of solute: 150 mM KCl, 20 mM Hepes Tris, 0.1 mM DTT, 0.5 mM EDTA.) The dotted curve represents the result obtained for a sample of plain water. R was determined by:

1) Measuring C at each frequency. This was done by recording P_i, P_r, and P_t with the front surface of the quartz cell in contact with the transmitting horn aperture. Then Equation (4) was used to calculate the (normalized) value 1/2 abC.

2) Measuring M at each frequency. This was done by recording P'_i, P'_r, and P'_t with the quartz cell positioned as it would be for an irradiation of the sample, ie, in the near field of the horn. Then Equation (6) was used to calculate M.

3) Calculating the (normalized) value 1/2 abR as 1/2 abC/M.

Figure 4 shows the calibration constants 1/2 abC and M separately for the same sample of buffer as in Figure 3. It is interesting to find that the rapid fluctuations of these two curves, 1/2 abC and M, are almost synchronized. Therefore, in the curve of 1/2 abR = 1/2 abC/M (the solid curve in Figure 3), the rapid fluctuations are almost canceled out, with only the long range variations remaining.

The fact that there is almost precise indexing of the maxima and minima for the two cases suggests that the oscillations are due to interactions between reflections from the rear face of the sample and from the thermistor mount. (The physical separation between the receiving horn aperture and the thermistor mount is about 11 cm.)

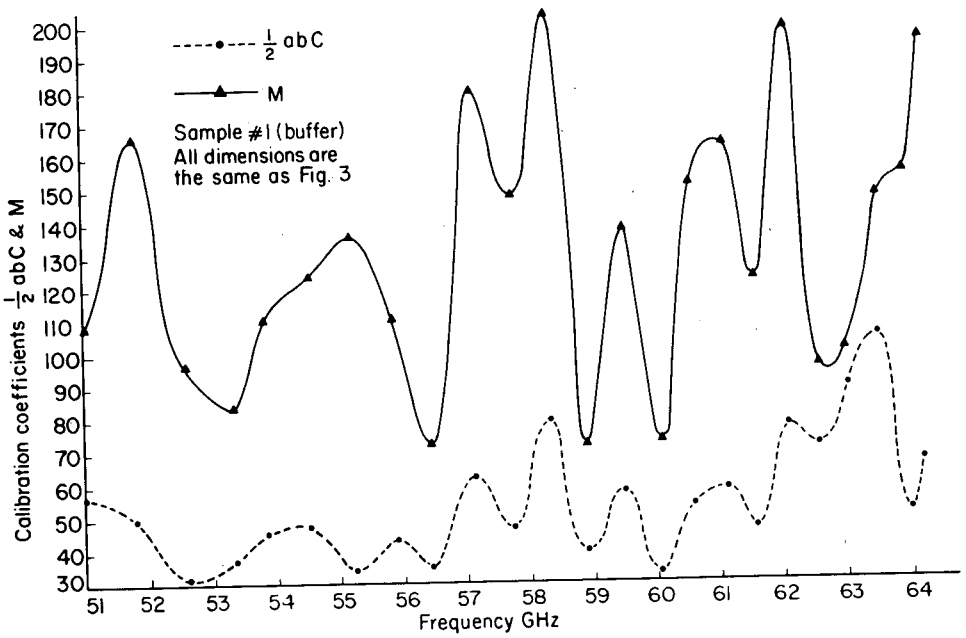

Fig. 4. Calibration constants C and M vs frequency.

Figure 5 shows the normalized calibration constant 1/2 abR as a function of distance L between the aperture of the large horn and the front surface of the sample cell. Those points that have horizontal slopes represent values of L for which the calibration for R is insensitive to separation at the test frequency.

CALCULATION OF SAR FROM THE POWER DENSITY

The definition of SAR can be expressed as follows:

$$\text{SAR} = \frac{\Delta P}{\Delta M} = \frac{1}{\rho}\frac{\Delta P}{\Delta V} = \frac{\sigma}{2\rho}\mathbf{E}^*\cdot\mathbf{E} = \frac{\omega\epsilon\tan\delta}{2\rho}\mathbf{E}^*\cdot\mathbf{E}. \tag{9}$$

Here, ΔV is a small volume in the sample with mass density $\rho = \Delta M/\Delta V$ and absorbed power ΔP. σ and $\tan\delta$ are the electrical conductivity and loss tangent of the sample medium, respectively. $\omega = 2\pi f$ is the angular frequency; $\mathbf{E}$ is the vector electric field amplitude; * signifies complex conjugate. The quantity ϵ is the real part of the dielectric constant $\bar{\epsilon}$, which is complex and given by:

$$\bar{\epsilon} = \epsilon\,(1 - j\tan\delta) = \epsilon_o\,\epsilon_r\,(1 - j\tan\delta).$$

Assume that the rf field inside the sample is an incident wave only. (This is approximately true when the thickness of the sample is much greater than the skin depth.) The PD that is defined at the same point in the sample as the SAR is:

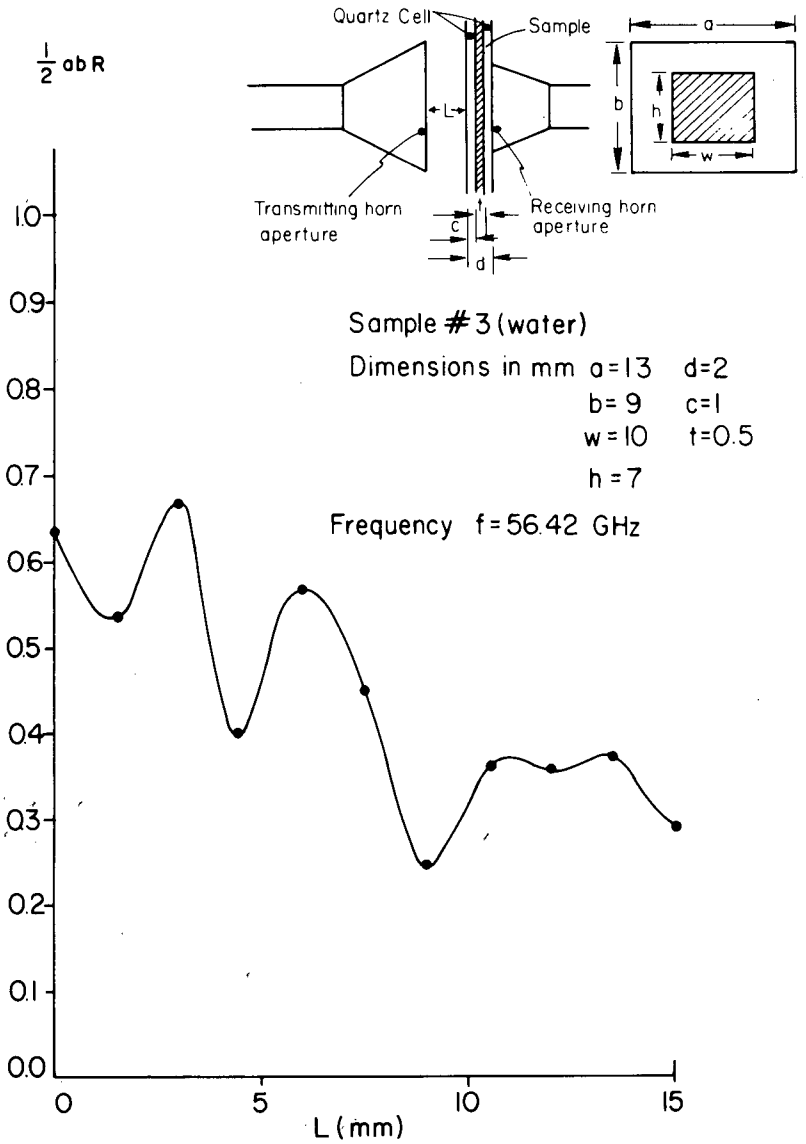

Fig. 5. Normalized calibration constant R as a function distance L.

$$PD = \frac{1}{2}\,\mathrm{Re}[\mathbf{E}^{*}\mathrm{x}\mathbf{H}\cdot\mathbf{i}_z] = \frac{1}{2}\mathrm{Re}\left[\sqrt{\frac{\epsilon(1-\mathrm{j}\tan\delta)}{\mu_o}}\mathbf{E}^{*}\cdot\mathbf{E}\right]$$
$$= \frac{1}{2}\sqrt{\frac{\epsilon}{\mu_o}}\sqrt{\frac{\sqrt{1+\tan^2\delta}+1}{2}}\mathbf{E}^{*}\cdot\mathbf{E} \qquad (10)$$

Here, $\mathbf{H}$ is the magnetic field intensity, μ_o is the magnetic permeability in vacuum, and $\mathbf{i}_z$ is the unit vector in the z direction. From Equations (9) and (10), we have:

$$\text{SAR} = \frac{\omega\epsilon\tan\delta}{\rho}\sqrt{\frac{\mu_o}{\epsilon}}\sqrt{\frac{2}{\sqrt{1+\tan^2\delta}+1}}\,\text{PD}$$

$$= \frac{2\pi\tan\delta}{\lambda\rho}\sqrt{\frac{2\epsilon_r}{\sqrt{1+\tan^2\delta}+1}}\,\text{PD} \tag{11}$$

Here, λ is the wavelength is free space; ϵ_r is the relative dielectric constant.

Equation (11) gives the relation between PD and SAR at the same point in the sample. The PD entering the front surface of the sample can be measured by the transmitted power method described earlier. Inside the sample, both PD and SAR decay exponentially with respect to the longitudinal distance z:

$$\text{PD}(z) = \text{PD}(0)\exp(-2\alpha z) \tag{12a}$$

$$\text{SAR}(z) = \text{SAR}(0)\exp(-2\alpha z) \tag{12b}$$

with the attenuation constant

$$\alpha = \text{Im}\left[\frac{2\pi}{\lambda}\sqrt{\epsilon_r(1-j\tan\delta)}\right] = \frac{2\pi}{\lambda}\sqrt{\frac{\epsilon_r(\sqrt{1+\tan^2\delta}-1)}{2}}. \tag{12c}$$

It is interesting that, when Equations (11) and (12c) are combined, an alternative expression for SAR is obtained:

$$\text{SAR} = \frac{2\alpha}{\rho}\text{PD}. \tag{13}$$

This is really a consequence of Equations (9) and (12a). If A is a cross-sectional area in the sample, then:

$$\text{SAR} = \frac{1}{\rho}\frac{\Delta P}{\Delta V} = \frac{-\Delta(\text{PD}\cdot A)}{\rho\,(\Delta z)A} = -\frac{1}{\rho}\frac{d(\text{PD})}{dz} = -\frac{1}{\rho}\frac{d(\text{PD}(0)\exp(-2\alpha z))}{dz}$$

$$\text{SAR} = \frac{2\alpha}{\rho}\text{PD}(0)\exp(-2\alpha z) = \frac{2\alpha}{\rho}\text{PD}.$$

Hence, the SAR may be calculated either from Equation (11) and the known complex dielectric constant [Franks, 1972; Grant et al, 1978; Szwarnowski and Sheppard, 1977] or from Equation (13) if a direct measurement of the attenuation constant α is available.

ERROR ANALYSIS

It is worthwhile to discuss some of the factors that limit the accuracy of this method. There are several different kinds of errors.

We have assumed before that the thickness of the (lossy) sample is greater than the skin depth. If this assumption is not satisfied, the wave reflected from the rear surface of the sample may affect the calibration. For example, the transmitting horn may be able to "see" the receiving horn or the environment behind the rear sample surface, rather than a uniform planar sample of "infinite" depth. In addition, the receiving horn may see different impedances during the C and M portions of the calibration. To estimate the importance of this error, assume that the "one-way" attenuation of the sample layer is 10 dB. Then the "round-trip" attenuation in the same layer should be at least 20 dB. Hence, at the front surface of the sample, reflections due to the finite thickness of the sample layer will be 20 dB below, ie, less than one-hundredth of the incident wave, which may be considered negligible. In the millimeter wave range, most biological samples are very lossy, so that this error need be considered only when the sample is very thin compared to the skin depth.

It is noted that the sample thickness (0.5 mm) was actually rather small, because the skin depth in water is about 0.4 mm at 70 GHz [Grant et al, 1978]. The use of a 1-mm cell would have been preferable, to completely eliminate effects due to reflections from the rear surfaces of the sample.

The accuracy of this method also depends upon the calibration procedure. We first determine the calibration constant C by using a small horn behind the sample when the latter is located at the plane of the transmitting horn aperture. The electric field within the aperture of the small horn is then determined by the transmitting horn aperture distribution and is termed the "distribution function of the field":

$$\underline{f}(x,y) = \mathbf{i}_y A \cos\left(\frac{\pi}{a}x\right), \quad -\frac{w}{2} \leqslant x \leqslant \frac{w}{2}, \quad -\frac{h}{2} \leqslant y \leqslant \frac{h}{2} \tag{14}$$

where $\mathbf{i}_y$ is the unit vector in the y direction. If the distribution function of the field during the M-portion of the calibration:

$$\underline{g}(x,y), \quad \left(-\frac{w}{2} \leqslant x \leqslant \frac{w}{2}, \quad -\frac{h}{2} \leqslant y \leqslant \frac{h}{2}\right)$$

is different from $\underline{f}(x,y)$, some kind of error is to be expected, as detailed below.

The absorbed power is proportional to the square of the field strength. Hence, the powers absorbed by the portion of the sample within the aperture area of the small horn in the two cases are as follows:

$$\text{C case: } P_a = K_1 \int_{-w/2}^{w/2} dx \int_{-h/2}^{h/2} dy \, |\underline{f}(x,y)|^2 \tag{15a}$$

$$\text{M case: } P'_a = K_1 \int_{-w/2}^{w/2} dx \int_{-h/2}^{h/2} dy \, |\underline{g}(x,y)|^2, \tag{15b}$$

where K_1 is a constant.

The transmitted power received by the small horn is proportional to the square of the coupling coefficient, which is the overlapping integral of two coupling fields over the aperture area. Hence the transmitted power detected by the receiving horn in each of these two cases can be expressed as follows:

$$\text{C case: } P_t = K_2\left[\int_{-w/2}^{w/2} dx \int_{-h/2}^{h/2} dy\, \mathbf{i}_y \cdot \underline{f}(x,y) \cos\left(\frac{\pi}{w} x\right)\right]^2 \tag{16a}$$

$$\text{M case: } P_t' = K_2\left[\int_{-w/2}^{w/2} dx \int_{-h/2}^{h/2} dy\, \mathbf{i}_y \cdot \underline{g}(x,y) \cos\left(\frac{\pi}{w} x\right)\right]^2 \tag{16b}$$

where K_2 is another constant.

In order to estimate the error due to the difference between the two field distributions, we compare P'_a with P_a under the condition:

$$P'_t = P_t. \tag{17}$$

Substituting Equation (16) into Equation (17), we have:

$$\int_{-w/2}^{w/2} dx \int_{-h/2}^{h/2} dy[\underline{g}(x,y) - \underline{f}(x,y)] \cdot \mathbf{i}_y \cos\left(\frac{\pi}{w} x\right) = 0. \tag{18}$$

Under this condition, the relative calibration error for the absorbed power can be written as:

$$(P'_a - P_a)/P_a = \frac{\int_{-w/2}^{w/2} dx \int_{-h/2}^{h/2} dy[|\underline{g}(x,y)|^2 - |\underline{f}(x,y)|^2]}{\int_{-w/2}^{w/2} dx \int_{-h/2}^{h/2} dy\, |\underline{f}(x,y)|^2}. \tag{19}$$

If $\underline{g}(x,y) = \underline{f}(x,y)$, we obviously have no calibration error. But usually $\underline{g}(x,y) \neq \underline{f}(x,y)$. We can estimate the error by means of Equations (18) and (19), in which $\underline{f}(x,y)$ is given by Equation (14), and where $\underline{g}(x,y)$, the distribution function of the M field, can (in principle) be obtained from measurements with a probe.

From the above analysis, we find that the calibration error can be reduced by reducing the aperture area of the small horn. Actually, if the dimensions w and h are much smaller than a and b, $\underline{f}(x,y)$ becomes almost a constant vector over the aperture area of the small horn, and so does $\underline{g}(x,y)$ in general. According to Equations (18) and (19), if both $\underline{f}(x,y)$ and $\underline{g}(x,y)$ are very close to constant vectors, the error should

approach zero. This is the reason why we prefer to use a small horn behind the sample to measure the transmitted powers during the calibration procedure. In principle, the physical size of the receiving horn aperture may be made very small by using high dielectric constant material within the horn volume, and therefore the error will be correspondingly small.

ACKNOWLEDGMENTS

We would like to thank Ms. Liudmila Benes for suggesting and drawing Figure 4. We also would like to thank Mr. Qing Han for assisting us in performing several of the experiments.

This work was supported by ONR contract N00014-77-C-0413 and EPA contract 68-02-3457.

Professor Shen was on leave from the Department of Radio Electronics, Zhejiang University, Hangzhou, People's Republic of China, to the Polytechnic as a Visiting Scholar.

Professor Sheng was on leave from the Departments of Fundamental Science and Electrical Engineering, Southwestern Jiaotung University, Emei, Sichuan, People's Republic of China, to the Polytechnic as a Visiting Scholar.

REFERENCES

Franks F (1972): "Water—A Comprehensive Treatise. Vol.1. The Physics and Physical Chemistry of Water." New York: Plenum Press.

Grant EH et al (1978): "Dielectric Behavior of Biological Molecules in Solution." New York: Oxford University Press.

Szwarnowski S, Sheppard RJ (1977): Precision waveguide cells for the measurement of permittivity of lossy liquids at 70 GHz. J Physics E: Scientific Instruments 10:1163–1167.

Bioelectromagnetics 8:103–106 (1987)

Brief Communication

Specific Absorption Rate in Humans In Vivo at Radio Frequencies

Andrzej Kraszewski, George Hartsgrove, Stanislaw S. Stuchly, and Maria A. Stuchly

Department of Electrical Engineering, University of Ottawa (A.K., G.H., S.S.S.), and Bureau of Radiation Protection and Medical Devices, Health and Welfare (M.A.S.), Ottawa, Ontario, Canada

Specific absorption rates were measured in three locations of humans exposed in the far field at 160, 350, and 915 MHz. Values obtained for six males are compared with data for a full-scale homogeneous model of man.

Key words: energy absorption, local SAR, measurement

A computer-controlled experimental dosimetry system and implantable electric field probes were previously used to investigate distributions of the specific absorption rate (SAR) in a full-scale homogeneous model of man in the far field [Kraszewski et al, 1984; Stuchly et al, 1985a, 1986a] and the near field [Stuchly et al, 1985b, 1986a,b]. These investigations were undertaken because of the need in the field of health protection to determine if there is excessive energy dissipated in physiologically critical locations. Furthermore, an experimental approach was selected in view of the limitations of presently available numerical methods in terms of accuracy in predicting the SAR distribution at radio frequencies [Kraszewski et al, 1984; Stuchly et al, 1986b].

Measurements of the SAR in a few accessible locations in live humans were performed to verify whether the SAR distributions in the homogeneous model are *reasonable* as compared with the actual human body, and to identify some critical parameters of the measurement method that may affect the accuracy of measurements.

All measurements were performed with males in the supine position exposed in the far field with the wave incident from the back. The body was supported by a styrofoam sheet on a plastic bed. A correction for the nonplanar wavefront of the incident radiation was applied as described elsewhere [Stuchly et al, 1985a]. The measurements were performed at 160, 350, and 915 MHz. The incident field was in

Received for review March 10, 1986; revision received June 6, 1986.

Address reprint requests to Dr. S.S. Stuchly, Department of Electrical Engineering, University of Ottawa, 770 King Edward Avenue, Ottawa, Ontario K1N 6N5, Canada.

the E-polarization with an incident power density of less than 5 mW/cm^2 at any point on the irradiated surface of the body at any of the test frequencies. The methods and hardware used are described elsewhere [Stuchly et al, 1985a,b, 1986a].

A triaxial electric field probe with a diameter of 10 mm was used. The probe was designed at the University of Ottawa and manufactured by Filtran Microcircuits Inc., Ottawa. The probe was fully tested and calibrated in a 14-cm sphere filled with different tissue-equivalent materials [Stuchly et al, 1984]. For the tests on humans, the tip of the probe was surrounded by a flexible bolus. Two sizes of the boli were used, 10 cm^3 and 20 cm^3 in volume, of a semiliquid material having the permittivity equal to that of muscle at the test frequencies. The boli were used to eliminate air pockets between the probe and the tissue. This was necessary because air pockets significantly affect the local electric fields. Furthermore, the use of a bolus in the model simulated more closely geometrical configurations for humans. The larger bolus (20-cm^3 volume) was more effective in reducing the scatter between the data obtained for various persons due to placement of the probe at the test location.

Figure 1 shows geometrical coordinates of the test sites for the 175-cm tall (72 kg) model. The average height and weight and their standard deviations for the six male volunteers were 177.5 $\pm$ 5.3 cm and 73.5 $\pm$ 8.5 kg, respectively. The models' and volunteers' arms were positioned along the body during the tests. In the armpit designated A (axillae), the SAR in the model was interpolated from the values measured very close to the surface in the torso and the arm. In the location L (between the legs, crotch), the SAR in the model used for comparisons was measured about 1.5 cm from the body surface. Other coordinates of the test site are shown in Figure 1. Experimental data obtained with a 20-cm^3 bolus for the volunteers and models are shown in Table 1. Three measurements were taken at each site for each volunteer. The uncertainty in the SAR values for the model is about $\pm$15%.

The following qualitative observations were made during the experiment: 1) Position of the head had a strong effect on the SAR in the mouth; for instance, elevation of the head by 2.5 cm (by a styrofoam support) caused about a 30% change in the SAR; 2) The articulation of the arms caused changes in the SAR in the armpit; 3) Handling of the probe by the volunteer affected SARs in all three sites.

The repeatability of measurements at the same site for each volunteer was reasonably good but varied from individual to individual and from site to site as illustrated in Table 2. The standard deviations as well as the SAR variations, depen-

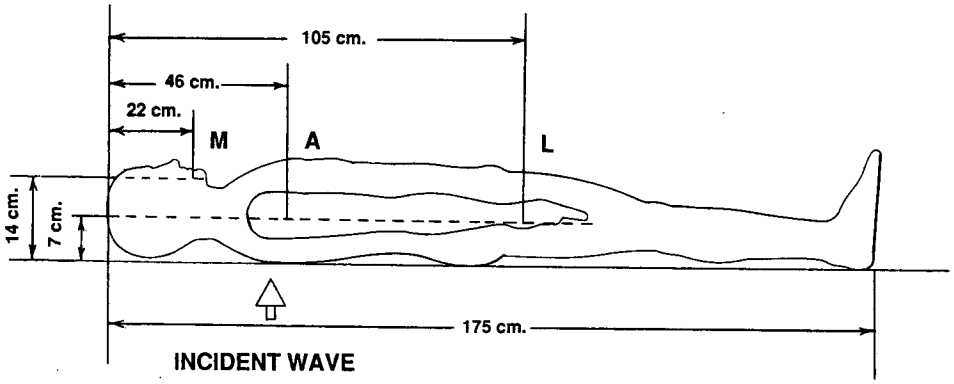

Fig. 1. Geometrical coordinates of the test sites for six male volunteers.

TABLE 1. Specific Absorption Rates (SARs) in mW/kg per 1 mW/cm^2 of the Incident Power Density for Humans and a Fullscale Homogenous Model*

Frequency (MHz)	Site					
	Mouth (M)		Armpits (A)		Legs (l)	
	Humans	Model	Humans	Model	Humans	Model
160	68 (±32)	505	109 (±42)	140	6.5 (±4.3)	11.5
350	25 (±9)	36	25 (±11)	29	2.2 (±0.8)	4.7
915	0.8 (±0.4)	2.6	1.7 (±0.4)	1.5	3.4 (±1.3)	5.5

*Figures given are for mean values; standard deviations are in parentheses.

TABLE 2. Specific Absorption Rates (SARs) in mW/kg per 1 mW/cm^2 of the Incident Power for Six Volunteers at 160 MHz*

Volunteer	Site			
	Mouth	Armpit 1	Armpit 2	Legs
A	92 (±2)	102 (±12)	97 (±8)	0.2 (±0.1)
B	106 (±20)	104 (±3)	145 (±4)	1.8 (±0.4)
C	66 (±2)	24 (±1)	26 (±1)	6.7 (±0.1)
D	22 (±1)	75 (±5)	90 (±5)	3.2 (±0.9)
E	50 (±3)	100 (±6)	36 (±12)	3.4 (±0.3)
F	25 (±5)	165 (±5)	174 (±11)	12.5 (±1)

*Mean values and standard deviations (in parentheses) for three measurements at each site are shown.

dent on the person for a given site, were less at the two higher frequencies. The standard deviation for a given volunteer ranged from less than 5% to 30%, depending on the site and the volunteer.

The variations from individual to individual at 160 MHz (Table 2) were approximately five to seven times for the mouth and the arms, respectively. This depended upon how tightly the probe was held at the measurement site by each person. Furthermore, except for one volunteer, relatively small differences were noted between the SARs measured in the two axillae. However, for the legs, the differences in the SAR varied by a factor of about 60, if all the data are considered. If the data for volunteer A is rejected, the differences are of the order of seven. At 350 MHz, the differences from volunteer to volunteer were approximately three, six, and ten times for the mouth, arms, and legs, respectively; and at 915 MHz, they were about ten, two, and three. It appears that the differences of one order of magnitude are not surprising, in view of variations of the immediate probe surrounding, and depends on both the probe positioning and handling and on anatomical differences.

From Table 1, it can be seen that, apart from relatively large deviations for the mean SAR values for the volunteers, they compare rather favorably with the data for the model, except for the mouth at 160 MHz and 915 MHz. The differences between the SARs for humans (mean values) and the model are within about 50%, except for the mouth at 160 MHz and 915 MHz. Furthermore, at least for the sites and frequencies investigated, the SAR values in humans are *lower* than those in the model.

The main limitation of the data presented here is a small number of locations in which SAR could be measured in humans. The measured SARs for various volunteers differ typically by about one order of magnitude. Because of the use of a bolus (without which the SAR would be affected to a very large extent by the probe

placement), the measured SARs in human volunteers can only be considered as an order-of-magnitude indicator. An inhomogeneous model should provide a much better approximation, as highlighted by large differences in the location (the mouth) in which anatomical differences between humans and the homogeneous model are large.

ACKNOWLEDGMENTS

This work was supported by grants from the Environmental Protection Agency and Health and Welfare Canada.

REFERENCES

Kraszewski A, Stuchly MA, Stuchly SS, Hartsgrove G, Adamski D (1984): Specific absorption rate distribution in a full-scale model of man at 350 MHz. IEEE Trans Microwave Theory Tech 32:779–783.

Stuchly MA, Kraszewski A, Stuchly SS (1984): Implantable electric field probes—some performance characteristics. IEEE Trans Biomed Eng 31:526–531.

Stuchly MA, Kraszewski A, Stuchly SS (1985a): Exposure of human models in the near and far field—a comparison. IEEE Trans Biomed Eng 32:609–916.

Stuchly SS, Kraszewski A, Stuchly MA, Hartsgrove G, Adamski D (1985b): Energy deposition in a model of man in the near field. Bioelectromagnetics 6:115–129.

Stuchly SS, Stuchly MA, Kraszewski A, Hartsgrove G (1986a): Energy deposition in a model of man; frequency effects. IEEE Trans Biomed Eng 33:702–711.

Stuchly MA, Spiegel RJ, Stuchly SS, Kraszewski A (1986b): Exposure of man in the near-field of a resonant dipole, comparison between theory and measurements. IEEE Trans Microwave Theory Tech 34:26–31.

Bioelectromagnetics 8:107–110 (1987)

Brief Communication

Effect of Relative Humidity on the Movement of Rat Vibrissae in a 60-Hz Electric Field

R.J. Weigel and D.L. Lundstrom

Biology and Chemistry Department, Pacific Northwest Laboratory, Richland, Washington

The snouts of rats were placed in a 60-Hz electric field at an unperturbed field strength of 50 kV/m. A count of the number of vibrissae that moved in the field was made on a series of rats over a number of days where the laboratory humidity varied from 25% to 48%. The number observed to vibrate fell from nine to zero or one at relative humidities between 25% and 39%, respectively.

Key words: sensory stimulation, hair vibration, cutaneous mechanoreceptors

Research findings on the biological effects of 60-Hz electric fields have been plagued by a problem of inconsistency of results from one laboratory to another or, indeed, within a laboratory over time. This has aptly been described as a "Cheshire cat phenomenon" [Graves et al, 1979]. The reasons for this inconsistency have not been explained, and it thus creates difficulties for researchers who wish to duplicate findings or construct and test mechanisms to explain the reported results.

The nervous system has been the site of many of the reported effects of electric-field exposure, such as increased excitability in sympathetic synapses [Jaffe et al, 1980], depression of the circadian rhythm of the pineal gland's output of melatonin [Wilson et al, 1981], and behavioral responses to low-strength electric fields [Stern et al, 1983]. One possible mechanism that has been proposed to explain these effects is that chronic stimulation of various sensory receptors by the electric field causes low-level stress that may manifest itself in the wide range of reported effects. A possible site for peripheral stimulation in rats is the vibrissae, a highly innervated receptor system. Due to field enhancement, which occurs near pointed objects, the vibrissae located on a pointed part of the anatomy (the snout) can experience much larger electric fields than the unperturbed levels in an exposure system. An experiment was conducted to verify that the rat's vibrissae do indeed move under the influence of an electric field. During the course of these tests, we noted a dependence on relative humidity, which may explain many of the "Cheshire cat" results.

Received for review June 13, 1986; revision received July 7, 1986.

Address reprint requests to Dr. Richard J. Weigel, Battelle Northwest Laboratories, P.O. Box 999, Richland, WA 99352.

The exposure system (Fig. 1) used a set of parallel plate electrodes, 15 × 15 cm, separated by 10 cm; one electrode was grounded and the other energized to 5 kV, generating a 50-kV/m electric field. Total harmonic distortion of the field was less than .1%. A hole approximating the cross section of a rat's snout (2.5 × 3.0 cm) was cut out of the center of the grounded electrode. The snout of a rat, grounded and anesthetized with sodium pentabarbital was inserted through the hole so that it projected into the field with its eyes just through the hole. There are approximately 25 vibrissae arranged in rows on each side of the rat's face. The configuration of the exposure system allowed observation of the vibrissae only on the right side of the animal. Movement in some of the vibrissae was restricted because they were against the ground electrode. The number of vibrissae that could vibrate in the field and could be observed was thus limited to approximately 20. Vibrations were observed using a strobe lamp, flashing at between 57–59 Hz or 61–63 Hz. Hairs vibrating at 60 Hz then appeared in the strobe lighting to be slowly moving at 1–3 Hz.

Vibration rate of vibrissae in the electric field was at 60 Hz, suggeting that the interaction of the field with the hair was through charge trapped on the hair. If the interaction had been between the field and induced charge in the hair (ie, acting like a conductor), vibration frequency would have been at 120 Hz. A 120-Hz vibration frequency, observed with a strobe at 60 Hz, would not appear different from hairs vibrating at half that rate. To discrimate between the two possibilities, the strobe rate was increased to 120 Hz where the vibrating hair appeared to split into two. Such an effect could occur only if the rate of vibration was half that of the strobe rate.

We found that the number of vibrissae that were observed to move in the electric field depended on the relative humidity. Twelve rats were placed in an unperturbed electric field of 50 kV/m during the course of the study (spring through winter), and the number of vibrissae that moved were counted. The extreme variability in the

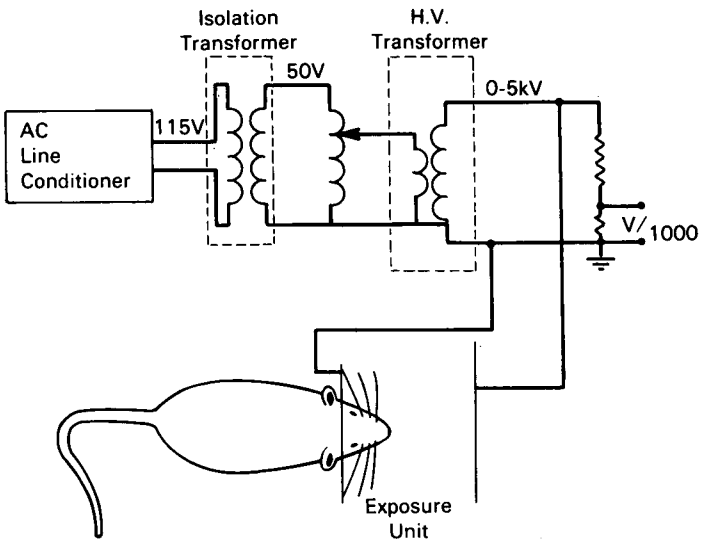

Fig. 1. Drawing of the exposure system and high-voltage equipment. The snout of the rat is inserted between two halves of the ground electrode in which a notch has been cut. The plate separation is 10 cm, generating a maximum unperturbed electric field of 50 kV/m. Some of the vibrissae closest to the ground electrode are in contact with it and cannot move in the field.

number of vibrissae that moved was observed to correlate with relative humidity (Fig. 2). Above 39% relative humidity, it appears unlikely that the field can cause a visible movement of the vibrissae. Seven rats were tested in this range of humidities, and in no case was more than one vibrissa observed to move. Four of the seven showed no movement. As the air became drier, more vibrissae moved in the field. At 25% relative humidity, approximately half of the hairs were observed to vibrate in the field. These observations support the conclusion that charge trapped on the hair interacts with the field. As the water content of the hair increased with humidity, the ability to trap electrical charge on the hair decreased, with a concomitant decrease in its movement in the field. We also observed that vibrissae could be induced to move by exposing them for a short time prior to the onset of the ac field to a small negative-ion generator.

Some important implications for 60-Hz bioeffects research result from these findings. First, electric fields at strengths comparable to many reported laboratory exposure levels can act directly on vibrissae. This is an initial step towards validating the chronic stimulation hypothesis, since it demonstrates that the field interacts with the mechanical input to an important sensory system. With the relatively large excursions observed, stimulation of receptors attached to the vibrissae is likely. Next, the dependence of hair vibration on relative humidity would be extremely significant if some of the observed effects of electric fields are due to chronic stimulation of vibrissae and associated receptors. Much of the variability in observed effects between

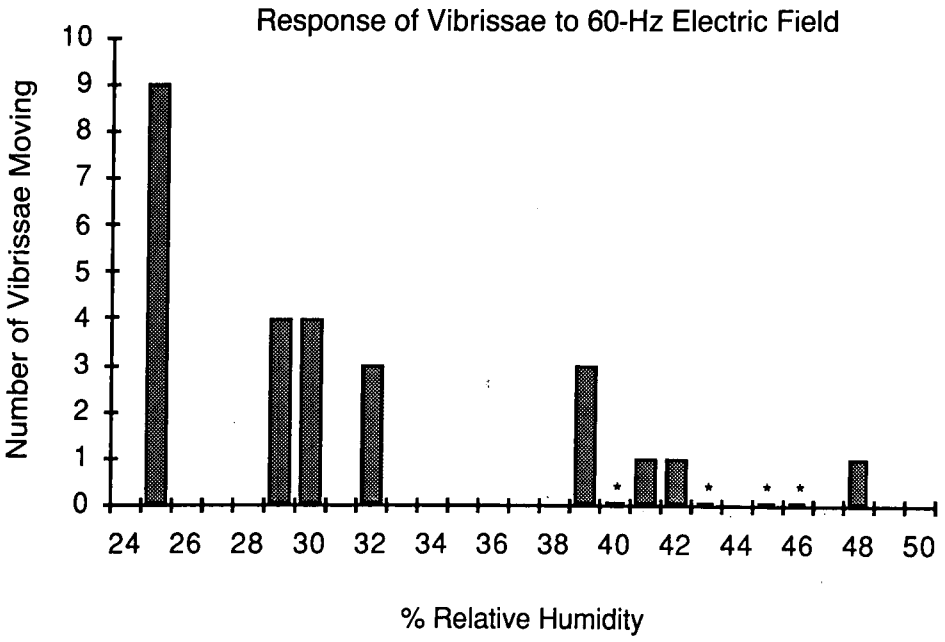

Fig. 2. A count of the number of vibrissae from 12 rats that vibrate in a 50-kV/m unperturbed electric field as a function of room relative humidity. Those rats that had no vibrissae move in the field are indicated by (*) above the appropriate humidity at which they were tested. Approximately 20 vibrissae were eligible to be counted in each test; the remaining vibrissae were obstructed from moving or were not visible.

laboratories and between replicates of experiments could be explained by differences in the relative humidity in the exposure room.

ACKNOWLEDGMENTS

The authors wish to acknowledge the support of the U.S. Department of Energy (contract No. DE-AC06-76RL0-1830) and the technical assistance of Mr. William Forsythe in the construction of the exposure system.

REFERENCES

Graves HB, Long PD, Poznaniak D (1979): Biological effects of 60 Hz alternating current fields: A Cheshire cat phenomenon. In Phillips RD, Gillis MF, Kaune WT, Mahlum DD (eds): "Biological Effects of Extremely Low-Frequency Electromagnetic Fields." Springfield, VA: National Technical Information Service, CONF-781016.

Jaffe RA, Laszewski CA, Carr DB, Phillips RD (1980): Chronic exposure to a 60-Hz electric field: Effects on synaptic transmission and peripheral nerve function in the rat. Bioelectromagnetics 1:131–148.

Kaune WT, Phillips RD (1980): Comparison of the coupling of grounded humans, swine and rats to vertical 60-Hz electric fields. Bioelectromagnetics 1:117–130.

Stern S, Laties VG, Stancampiano CV, Cox C, DeLorge JO (1983): Behavioral detection of 60-Hz electric fields by rats. Bioelectromagnetics 4:215–247.

Wilson, BW, Anderson LE, Hilton DI, Phillips RD (1981): Chronic exposure to 60-Hz electric fields: Effects on pineal function in the rat. Bioelectromagnetics 2:371–380.

UCLA Symposia on Molecular and Cellular Biology, New Series, Volume 33

Yeast Cell Biology

James Hicks, Editor

Yeast, a "small" eukaryote, exhibits nearly all of the cellular structures and functions of "large" eukaryotes such as mammals. Research has shown that yeast proteins often exhibit primary sequence homology with their well-studied counterparts isolated from multicellular organisms. These studies have provided researchers with many useful insights into other cells.

Yeast Cell Biology presents new approaches to understanding the potential of yeast genetics and its application to the study of cell structure and whole-cell processes. The book provides a review of the problems that arise in different areas of yeast research and outlines the various ways that molecular and classical genetic techniques can be used to study these problems.

The volume presents in-depth reviews of various topics, including yeast cytoskeleton and its role in the cell division cycle, structure and replication of yeast chromosomes and the role of the *ras* oncogenes in controlling cell growth. The general traffic pattern of macromolecules through the nucleus and cytoplasm is examined in detail, including articles on mRNA splicing, vacuolar proteases, nuclear structure and the secretory apparatus. Summaries of current strategies used to dissect the mechanisms by which proteins are targeted to the mitochondrion are presented, as well as reviews on pheromones, calcium binding proteins, and endocytosis. The closing chapter highlights the ways that all of the included studies impinge on the complex series of events that make up the mating and sexual cycles of Saccharomyces yeast.

Yeast Cell Biology will be an informative introduction to yeast for the cell biologist as well as a valuable reference source to researchers in the fields of molecular genetics, microbiology, biophysics, industrial chemistry, and pharmacology.

UCLA Symposia on Molecular and Cellular Biology, New Series, Volume 33 • **Yeast Cell Biology** • *Proceedings of a Cetus-UCLA Symposium on Yeast Cell Biology, held in Keystone, Colorado, April 1985* • James Hicks, Editor • ISBN 0-8451-2632-6 • LC 86-10658 • Publication: August 1986 • 694 pages, $125.00

SECTION HEADINGS

In Europe, the United Kingdom, and the countries of East and West Africa order from your bookseller or from: *John Wiley & Sons Limited • Baffins Lane • Chichester • Sussex PO19 1UD • England*

Order from your bookseller or directly from the publisher

Alan R. Liss, Inc., 41 East 11th Street, New York, NY 10003

BIO ELECTRO MAGNETICS

Journal of the Bioelectromagnetics Society

INSTRUCTIONS FOR CONTRIBUTORS

MANUSCRIPTS must be in English. All copies must be typewritten, double spaced, on one side of the paper only, and have 3 cm margins. The first author's surname and the page number should appear in the upper left corner of each page. Manuscripts and all new editorial correspondence should be sent by first-class mail, or by air, to the editor (effective as of Volume 6): Dr. Richard D. Phillips, **BIOELECTROMAGNETICS**, Experimental Biology Division (MD-71), U.S. Environmental Protection Agency, Research Triangle Park, NC 27711, USA. Submit one original and two good quality copies of all elements.

TITLE PAGE: This should contain a brief but informative title, the names and complete institutional affiliations of all authors, the name and address to be used for all correspondence, and a short running title.

ABSTRACT: This must be a factual condensation of the entire work, including a clear description of its major findings, and a concise presentation of the conclusions in 300 words or less.

KEY WORDS: Supply three to eight words or short phrases that will adequately index the subject matter.

TEXT: Full length articles should be organized into sections, follow a format appropriate for the material, eg, Introduction, Materials and Methods, Results, Discussion, Conclusions, and References and should not exceed 20 double-spaced typewritten pages excluding figures and tables. Follow the recommendations in Council of Biology Editors Style Manual: A Guide for Authors, Editors, and Publishers in the Biological Sciences, 5th Edition, published by the Council of Biology Editors, Inc. (Bethesda, MD, 1983). Authors should also follow the recommendations by the IUPAC-IUB Commission for nomenclature and abbreviations. Use of the International System of Units (SI) is strongly preferred for reporting quantitative data.

BRIEF COMMUNICATIONS: Short Reports of novel experimental or theoretical findings should be limited to five double-spaced pages of text with a maximum of two figures and/or tables. Do not include section headings. The abstract should be kept to a few lines and references limited to those essential.

REFERENCES: In the text, cite references by author and year of publication in parentheses (when there are more than two authors, use only the first surname and et al). More than one author reference for the same year of publication must be identified by a letter suffix placed after the year of publication.

Reference to reports that are limited in circulation, eg, laboratory, company, or government agency reports, is discouraged because they are often difficult to obtain. Citations to personal communications or unpublished manuscripts are also discouraged, but, if used, permission must be obtained. These citations are to be incorporated in the text in parentheses. References must be double spaced in alphabetical order. Abbreviate journal names according to Index Medicus. Note the following examples:

Adair EA, Adams BW (1980): Microwaves modify thermoregulatory behavior in squirrel monkey. Bioelectromagnetics 1:1-20.

Linn JC (1978): "Microwave Auditory Effects and Applications." Springfield: Charles C Thomas.

McLee BD, Finch ED (1973): Analysis of reported physiological effects of microwave radiation. In Lawrence, JH, Gofman JW (eds): "Advances in Biological and Medical Physics." Vol 14. New York: Academic, pp 163-223.

TABLES: Type tables, double spaced, on separate sheets. Each table must have a self-explanatory title, be numbered in order of appearance with Arabic numerals, and be keyed into the text.

FIGURES: Figures should be numbered consecutively with Arabic numerals and be keyed into the text. Name of author, figure number and an arrow indicating orientation should be typed on a gummed label and affixed to the back of each illustration. Line drawings must be of high quality; submit either the original drawing or a high-contrast, glossy print. Photomicrographs and other halftone photographs should be high-contrast glossy prints. Magnification factors must be provided and should be indicated by a calibration bar in the figure. If color plates are necessary, their cost must be paid by the author.

LEGENDS: A descriptive legend must accompany each illustration so that it can be understood apart from the text. All abbreviations must be defined within the legend. Type legends, double spaced, on a separate sheet.

GENERAL COMMENTS: All manuscripts submitted to **BIOELECTROMAGNETICS** must be submitted solely to this journal and may not have been published in any part or form in another publication, professional or lay. The author's institution will be asked by the Bioelectromagnetics Society to pay a page charge of $50 per page which entitles the institution to 100 free reprints. There will be no discrimination against papers for which page charges are not paid. Additional reprints may be purchased from the publisher.

BIO ELECTRO MAGNETICS

Journal of the Bioelectromagnetics Society

Volume 8, Number 1, 1987

Articles

Brief Communications